12-31-2020

Coordination, adaptation, and complexity indecision fusion

Weiqiang Dong
New Jersey Institute of Technology

ABSTRACT

COORDINATION, ADAPTATION, AND COMPLEXITY IN DECISION FUSION

by
Weiqiang Dong

A parallel decentralized binary decision fusion architecture employs a bank of local detectors (LDs) that access a commonly-observed phenomenon. The system makes a binary decision about the phenomenon, accepting one of two hypotheses (H_0 ("absent") or H_1 ("present")). The k^{th} LD uses a local decision rule to compress its local observations y_k into a binary local decision u_k; $u_k = 0$ if the k^{th} LD accepts H_0 and $u_k = 1$ if it accepts H_1. The k^{th} LD sends its decision u_k over a noiseless dedicated channel to a Data Fusion Center (DFC). The DFC combines the local decisions it receives from n LDs $(u_1, u_2, \ldots, u_n)$ into a single binary global decision u_0 ($u_0 = 0$ for accepting H_0 or $u_0 = 1$ for accepting H_1). If each LD uses a single deterministic local decision rule (calculating u_k from the local observation y_k) and the DFC uses a single deterministic global decision rule (calculating u_0 from the n local decisions), the team receiver operating characteristic (ROC) curve is in general non-concave. The system's performance under a Neyman-Pearson criterion may therefore be suboptimal in the sense that a mixed strategy may yield a higher probability of detection when the probability of false alarm is constrained not to exceed a certain value, $\alpha > 0$. Specifically, a "dependent randomization" detection scheme can be applied in certain circumstances to improve the system's performance by making the ROC curve concave. This scheme requires a coordinated and synchronized action between the DFC and the LDs. This study specifies when dependent randomization is needed, and discusses the proper response of the detection system if synchronization between the LDs and the DFC is temporarily lost. In addition, the complexity of selected

parallel decentralized binary decision fusion algorithms is studied and the state of the art in adaptive decision fusion is assessed.

COORDINATION, ADAPTATION, AND COMPLEXITY IN DECISION FUSION

by
Weiqiang Dong

A Dissertation
Submitted to the Faculty of
New Jersey Institute of Technology
in Partial Fulfillment of the Requirements for the Degree of
Doctor of Philosophy in Electrical Engineering

Helen and John C. Hartmann Department of
Electrical and Computer Engineering

December 2020

APPROVAL PAGE

COORDINATION, ADAPTATION, AND COMPLEXITY IN DECISION FUSION

Weiqiang Dong

Dr. Moshe Kam, Dissertation Advisor — Date
Professor of Electrical and Computer Engineering, NJIT

Dr. Mengchu Zhou, Committee Member — Date
Distinguished Professor of Electrical and Computer Engineering, NJIT

Dr. Nirwan Ansari, Committee Member — Date
Distinguished Professor of Electrical and Computer Engineering, NJIT

Dr. Edwin Hou, Committee Member — Date
Professor of Electrical and Computer Engineering, NJIT

Dr. Xiaobo Li, Committee Member — Date
Associate Professor of Biomedical Engineering, NJIT

BIOGRAPHICAL SKETCH

Author: Weiqiang Dong

Degree: Doctor of Philosophy

Date: December 2020

Undergraduate and Graduate Education:

- Doctor of Philosophy in Electrical and Engineering,
  New Jersey Institute of Technology, Newark, NJ, 2020
- Master of Science in Electrical and Engineering,
  New Jersey Institute of Technology, Newark, NJ, 2013
- Bachelor of Science in Automation,
  South China University of Technology, Guangdong, China, 2011

Major: Electrical and Engineering

Presentations and Publications:

Weiqiang Dong and Moshe Kam, "Dependent Randomization in Parallel Binary Decision Fusion," *IEEE/CAA Journal of Automatica Sinica*, in press.

Weiqiang Dong and Moshe Kam, "Parallel decentralized detection with dependent randomization," *52nd Annual Conference on Information Sciences and Systems*, pp. 1-6, 2018.

Feng Ding, Guopu Zhu, Weiqiang Dong, and Yun-Qing Shi, "An efficient weak sharpening detection method for image forensics," *Journal of Visual Communication and Image Representation*, vol. 50, pp. 93-99.

Weiqiang Dong and Moshe Kam, "Detection performance vs. complexity in parallel decentralized Bayesian decision fusion," *51st Annual Conference on Information Sciences and Systems*, pp. 1-6, 2017.

Weiqiang Dong and Moshe Kam, "Integration of multiple adaptive algorithms for parallel decision fusion," *50th Annual Conference on Information Sciences and Systems*, pp. 355-359, 2016.

Weiqiang Dong and Moshe Kam, "A greedy algorithm for decentralized Bayesian detection with feedback," *37th IEEE Sarnoff Symposium*, pp. 202-207, 2016.

Feng Ding, Weiqiang Dong, Guopu Zhu, and Yun-Qing Shi, "An advanced texture analysis method for image sharpening detection," *International Workshop on Digital Watermarking*, pp. 72-82, 2015.

ACKNOWLEDGMENT

First of all, I would like to show my deepest appreciation to my supervisor, Dr. Moshe Kam, a responsible and respectable professor, for his patience, motivation, and kindness. His support and enlightening guidance help me all the time of my research.

I also like to thank the rest of my dissertation committee: Dr. Mengchu Zhou, Dr. Nirwan Ansari, Dr. Edwin Hou, Dr. Xiaobo Li, for their helpful suggestions and insightful comments.

I wish to show my gratitude to the Department of Electrical and Computer Engineering for the assistance and support. I thank the Office of Naval Research (N00014-13-1-0733, N00014-14-1-0771) and the Naval Air Warfare Center for funding.

I extend my thanks to Ji-won Choi, Chizhong Wang, and Ludvik Alkhoury, bright and obliging doctoral students, for the days we worked together. My sincere thanks also goes to Dr. Durgamadhab Misra, Sheryl Baker, Angela Vega-Irvin, Carolina Yanez, and Kimberly Dripchak, for their help in the last couple years.

Last, but not least, I would like to thank my parents, Maohua Dong and Yumin Mao; my wife, Meng Kong.

TABLE OF CONTENTS

Chapter **Page**

1 INTRODUCTION 1

1.1 Parallel Decentralized Binary Decision Fusion Architecture 1

1.2 Minimizing the Bayesian cost of the Global Decision 2

1.3 Satisfying a Neyman-Pearson Criterion 3

2 PERFORMANCE AND COMPLEXITY OF SELECTED PARALLEL DECENTRALIZED BINARY DECISION FUSION SYSTEMS 6

2.1 Architectures without Feedback 6

2.1.1 Fixed global fusion rule 6

2.1.2 Fixed local decision rule with identical LDs 6

2.1.3 Calculating the local decision rule and the global fusion rule simultaneously 7

2.1.4 Calculating local decision rule and global fusion rule exhaustively (overall “k out of n” schemes) 7

2.2 Architectures with Feedback 7

2.2.1 Fixed local decision rule 8

2.2.2 Calculating local decision rule and global fusion rule simultaneously 9

2.2.3 Calculating local decision rule and global fusion rule by using a greedy scheme 9

2.3 Example - A 5 Local Detectors System 11

3 DETECTION STRATEGY FOR PARALLEL DECENTRALIZED BINARY DECISION FUSION ARCHITECTURE 15

3.1 Deterministic Strategy 15

3.1.1 Local observations contain no point masses of probability . . . 18

3.1.2 Local observations contain point masses of probability 18

3.2 The Potential of Randomization of Decision Rules 19

3.2.1 Randomization at the DFC only 22

TABLE OF CONTENTS
(Continued)

Chapter **Page**

3.2.2 Dependent randomization 22

4 TWO EXAMPLES OF PARALLEL DECISION FUSION 24

4.1 Example 1: A 2-LD System with Continuous Local Observations . . . 24

4.2 Example 2: A 3-LD System with Discrete Local Observations 29

4.2.1 Deterministic strategy (Section 3.1) 29

4.2.2 Strategy with randomization at the DFC only (Section 3.2.1) . 30

4.2.3 Dependent randomization (Section 3.2.2) 32

5 LOSS OF SYNCHRONIZATION BETWEEN THE DFC AND THE GROUP OF LDS 38

5.1 Effect of Synchronization Loss (DFC) 38

5.2 Corrective Action after the Group of LDs Lost Synchronization with the DFC 41

5.3 Numerical Examples 43

5.3.1 2-LD system 43

5.3.2 3-LD system 45

6 PARTIAL LOSS OF SYNCHRONIZATION AMONG THE LDS 48

6.1 Effect of Synchronization Loss (LDs) 48

6.2 Calculating the Local Operating Points after the LDs in $\overline{Y}$ Lost Synchronization 50

6.3 Calculating the ROC Curves of *System A* and *System B* 51

6.4 Satisfying the Probability of False Alarm Constraint and Maximizing the Probability of Detection 53

6.5 Finding A' from Ω^A if $A' \in \Omega^A$ and B' from Ω^B if $B' \in \Omega^B$ (at least one of A' and B' can be Found) 55

6.6 Finding A' if $A' \notin \Omega^A$ and B' if $B' \notin \Omega^B$ (Applying Randomization at the DFC) 56

6.7 Numerical Examples 58

6.7.1 2-LD system 58

TABLE OF CONTENTS
(Continued)

Chapter **Page**

6.7.2 3-LD system 60

7 ADAPTIVE FUSION 66

7.1 Chair - Varshney Rule 66

7.2 Methods for Estimation of Probabilities 67

7.3 Methodology 69

7.3.1 Archival Data Base of Algorithm Performance 70

7.3.2 Selection algorithm 70

7.4 Average performance in simulations 73

8 END NOTES 76

APPENDIX A LOCATING A' AND B' (CHAPTER 6) 78

A.1 Proof: $P_d^{C'}$ (6.4) is the Maximum Probability of Detection when either (i) $A' \in \Omega^A$ or (ii) $B' \in \Omega^B$ or both ($A' \in \Omega^A$ and $B' \in \Omega^B$) 78

A.2 Finding A' from Ω^A if $A' \in \Omega^A$ and B' from Ω^B if $B' \in \Omega^B$ (Improved Version) 83

A.3 Complete Algorithm of the Corrective Action 87

A.3.1 Redesign the 2-LD system shown in Section 4.1 after the 2^{nd} LD lost synchronization 87

A.3.2 Redesign the 3-LD system shown in Section 4.2 after the 3^{rd} LD lost synchronization 91

REFERENCES 98

LIST OF TABLES

Table **Page**

1.1 Summary of each Chapter in the Dissertation 5

2.1 Review of Four Designs of Architectures without Feedback ("k out of n" Rules, [1], [2], and [3]) 10

2.2 Review of Three Designs of Architectures with Feedback ([4], [5], and [6]) 11

3.1 Input and Output of Three Different Designs of a Parallel Decentralized Binary Decision Fusion System of Figure 1.1 under a Neyman-Pearson Criterion 23

4.1 Input and Output of Three Different Designs of a 2-LD System 27

4.2 All Twenty Monotonic Fusion Rules of the 3-LD System in Section 4.2 and the Corresponding P_f, P_d when $\alpha = 0.1708$ 30

4.3 Input and Output of Three Different Designs of a 3-LD System 36

5.1 Conditions on q (Probability that the DFC Selects γ_0^A) to Satisfy the Neyman-Pearson Constraint after the DFC Loses Synchronization with the LDs Group 43

5.2 The Output of the 2-LD System Employing Dependent Randomization when the DFC Lost Synchronization with the LDs Group before and after a Corrective Action is Taken 45

5.3 The Output of the 3-LD System Employing Dependent Randomization when the DFC Lost Synchronization with the LDs Group before and after a Corrective Action is Taken 47

6.1 Input of the Redesigned Algorithm when each LD in $\overline{Y}$ Lost Synchronization with the DFC and each Other 49

6.2 The Output the 2-LD System Employing Dependent Randomization Before and After a Corrective Action is Taken when $Y = \{LD1\}$ and $\overline{Y} = \{LD2\}$ 61

6.3 The Operating Points of the 2-LD System Employing Different Detection Strategies under the Neyman-Pearson Criterion with $\alpha = 0.2009$ (Corresponding to Figure 6.5) 61

6.4 The Output the 3-LD System Employing Dependent Randomization before and after a Corrective Action is Taken when $Y = \{LD1,\ LD2\}$ and $\overline{Y} = \{LD3\}$ 64

LIST OF TABLES
(Continued)

Table **Page**

6.5 The Operating Points of the 3-LD System Employing Different Detection Strategies under the Neyman-Pearson Criterion with (a) $\alpha = 0.1708$ (Corresponding to Figure 6.7) and (b) $\alpha = 0.05$ 65

7.1 Ranking Distribution of each Method for 605 Contested Runs when $n = 5$ 74

7.2 Ranking Distribution of each Method for 443 Contested Runs when $n = 7$ 74

LIST OF FIGURES

Figure		Page
1.1	Parallel decentralized detection network.	2
2.1	Parallel decentralized binary decision fusion with 1-bit memory DFC, network of [4].	8
2.2	Parallel decentralized binary decision fusion with feedback to LDs, architecture of [5][6].	9
2.3	Probabilities of error by majority voting (2.1.1), designing the system with fixed η_k [1] (2.1.2), designing the system simultaneously [2] (2.1.3), and designing the system exhaustively [3] (2.1.4).	12
2.4	ROC curves by seven different designs, $t = 2$.	14
3.1	Deterministic strategy with isolated operating points.	20
3.2	Randomization can improve detection performance by 'connecting' the isolated operating points.	20
4.1	The ROC curves of the 2-LD system when the DFC uses an AND rule (red curve) and when it uses an OR rule (blue curve). The upper boundary of the two curves is the ROC curve of the system with deterministic strategy.	28
4.2	The operating points of the 2-LD system employing different detection strategies ($\alpha = 0.2009$): (a) deterministic strategy (and randomization at the DFC) (blue circle); (b) dependent randomization (black circle).	28
4.3	The conditional probability distributions of the local observations.	29
4.4	All the operating points of the system with deterministic strategy (blue circles).	31
4.5	The team ROC curve of the system with the deterministic strategy.	31
4.6	The operating points (blue circles) and the ROC curve (red curve) of the 3-LD system when all three LDs operates at $(0.1, 0.6)$. When the local operating points are fixed, the ROC curve of the system employing randomization at the DFC is a concave piecewise linear curve.	33
4.7	All the ROC curves of the system when applying the strategies with randomization at the DFC only (each ROC curve connects the operating points if they correspond to the same local operating points).	34
4.8	The team ROC curves of the deterministic strategy (blue) and the strategy with randomization at the DFC only (red).	34

LIST OF FIGURES
(Continued)

Figure **Page**

4.9 The team ROC curves of the systems with (a) dependent randomization (black); (b) randomization at the DFC only (red); (c) deterministic strategy (blue). 35

4.10 The operating points of the 3-LD system employing different detection strategies under the Neyman-Pearson criterion with probability of false alarm constraint $\alpha = 0.1708$: (a) deterministic strategy (blue circle); (b) randomization at the DFC (red circle); (c) dependent randomization (black circle). The ROC curves of the 3-LD system employing different strategies: (a) deterministic strategy (blue); (b) randomization at the DFC (red); (c) dependent randomization (black). 37

5.1 A, B, $M1$ and $M2$, shown by green circles, are the possible operating points of the 2-LD system (Section 4.1) when the synchronization between the LDs and the DFC is lost. The black circle, C, shows the operating point of the synchronized system. The cyan circle, W^*, shows the equivalent operating point of the system when it lost synchronization. C^* is the equivalent operating point after the corrective action is taken. 40

5.2 Zooming in on the ROC curve of the 2-LD system employing dependent randomization. 40

5.3 A, B, $M1$ and $M2$, shown by green circles, are the possible operating points of the 3-LD system (Section 4.2) when the synchronization between the LDs and the DFC is lost. The black circle, C, shows the operating point of the synchronized system. The cyan circle, W^*, shows the equivalent operating point of the system when it lost synchronization. C^* is the equivalent operating point after the corrective action is taken. 47

6.1 *System A* is used with probability p. 50

6.2 *System B* is used with probability $1 - p$. 51

6.3 The ROC curve of the system with dependent randomization is shown by the black curve. For $\alpha \in (P_f^A, P_f^B)$, C is the desired operating point of the system (black circle). A and B (green circles) are the operating points used to generate C through a randomization procedure. When the second LD loses synchronization ($Y = \{LD1\}$, $\overline{Y} = \{LD2\}$), if A is selected the *ROC curve A* is effective (shown in red); if B is selected the *ROC curve B* is effective (shown in blue). 53

LIST OF FIGURES
(Continued)

Figure **Page**

6.4 C is the desired operating point of the system with dependent randomization (black circle). When $Y = \{LD1\}$ and $\overline{Y} = \{LD2\}$, A, B, $M1'$ and $M2'$ are the four possible operating points (green circles). W' is the equivalent operating point (purple circle). The *ROC curve A* is shown as the red curve. The *ROC curve B* is shown as the blue curve. C' is the operating point with maximized probability of detection given $\alpha = 0.2009$, shown by the purple square. 60

6.5 The operating points of the 2-LD system employing different detection strategies under the Neyman-Pearson criterion with $\alpha = 0.2009$. . . . 62

6.6 C is the desired operating point of the system with dependent randomization (black circle). When $Y = \{LD1, LD2\}$ and $\overline{Y} = \{LD3\}$, A, B, $M1'$ and $M2'$ are the four possible operating points (green circles). W' is the equivalent operating point (purple circle). *ROC curve A* and *ROC curve B* are shown as the red curve and the blue curve, respectively. C' is the operating point maximizing the probability of detection given $\alpha = 0.1708$, shown by the purple square. 63

6.7 The operating points of the 3-LD system employing different detection strategies under the Neyman-Pearson criterion with $\alpha = 0.1708$. . . . 65

7.1 The model of proposed algorithm. 69

7.2 A part of graph for $n = 5$. 71

7.3 An example for the proposed algorithm. 73

A.1 The system operates at $a = (P_f^a, P_d^a)$ (cyan circle) with probability p. The system operates at $b = (P_f^b, P_d^b)$ (purple triangle) with probability $1-p$. The resulting operating point is $c = (P_f^c, P_d^c) = (pP_f^a + (1-p)P_f^b = \alpha, pP_d^a + (1-p)P_d^b)$, shown by the purple square. 80

A.2 A graphical illustration of cases (a), (b), and (c) (from left to right). . . 83

A.3 The preliminary of the algorithm of the corrective action after LDs in $\overline{Y}$ lost synchronization. 88

A.4 The algorithm of the corrective action after LDs in $\overline{Y}$ lost synchronization. 89

A.5 The preliminary of the proposed algorithm for redesigning the 2-LD system shown in Section 4.1 after the 2^{nd} LD lost synchronization. . . 91

A.6 Applying the proposed algorithm to redesign the 2-LD system shown in Section 4.1 after the 2^{nd} LD lost synchronization. 93

LIST OF FIGURES (Continued)

Figure **Page**

A.7 The 2-LD system with the 2^{nd} LD loses synchronization. x-marks: all possible deterministic operating points given Φ^A; red circles: all the operating points in Ω^A; red curve: *ROC curve A*. 94

A.8 The 2-LD system with the 2^{nd} LD loses synchronization. x-marks: all possible deterministic operating points given Φ^B; blue circles: all the operating points in Ω^B; blue curve: *ROC curve B*. 94

A.9 The preliminary of the proposed algorithm for redesigning the 3-LD system shown in Section 4.2 after the 3^{rd} LD lost synchronization. . . 95

A.10 Applying the proposed algorithm to redesign the 3-LD system shown in Section 4.2 after the 3^{rd} LD lost synchronization. 96

A.11 The 3-LD system with the 3^{rd} LD loses synchronization. x-marks: all possible deterministic operating points given Φ^A; red circles: all the operating points in Ω^A; red curve: *ROC curve A*. 97

A.12 The 3-LD system with the 3^{rd} LD loses synchronization. x-marks: all possible deterministic operating points given Φ^B; blue circles: all the operating points in Ω^B; blue curve: *ROC curve B*. 97

LIST OF SYMBOLS

P_d	Probability of detection by the DFC, $P(u_0 = 1 \mid H_1)$
P_d^i	Probability of detection by the DFC when the assignment i (typically $i = A$ or $i = B$) is used in randomization, $P(u_0 = 1 \mid H_1)$
P_f	Probability of false alarm by the DFC, $P(u_0 = 1 \mid H_0)$
P_f^i	Probability of false alarm by the DFC when the assignment i (typically $i = A$ or $i = B$) is used in randomization, $P(u_0 = 1 \mid H_0)$
P_0	A priori probability of hypothesis H_0
P_1	A priori probability of hypothesis H_1
P_{dk}	Probability of detection by the k^{th} local detector, $P(u_k = 1 \mid H_1)$
P_{fk}	Probability of false alarm by the k^{th} local detector, $P(u_k = 1 \mid H_0)$
U	Local decision vector, $U = \{u_1, u_2, \ldots, u_n\}$
Y	The set of synchronized LDs
$\overline{Y}$	The set of non-synchronized LDs
n	Number of local detectors in the parallel fusion architecture
u_0	Global decision of the data fusion center ($u_0 = 1$ or 0)
u_0^t	Global decision of the data fusion center at time step t ($u_0^t = 1$ or 0)
u_k	Local decision of the k^{th} detector ($u_k = 1$ or 0)
y_k	Local observations of the k^{th} detector
y_k^t	Local observation of the k^{th} detector at time step t

Ω^i The sequence containing $(0,0),(1,1)$, and all corner points on the ROC curve i, $i = A, B$, sorted in the ascending order according to the value of probability of false alarm

Φ^i The set of local operating points when the assignment i is used by all the elements in Y, $i = A, B$

η_0 The threshold in the global decision rule

η_k The threshold in the local decision rule at the k^{th} LD

γ The deterministic strategy, including the global decision rule and the local decision rules, $\gamma = (\gamma_0, \gamma_{LD})$

γ^i The i^{th} strategy in randomization, $i = 1, 2, \ldots$

γ_k The local decision rule of local detector k

γ_0 The global decision rule of the DFC

γ_0^i The i^{th} global decision rule in randomization, $i = 1, \ldots, M$

γ_{LD} The local decision rules of all the LDs, $\gamma_{LD} = \{\gamma_1, \ldots, \gamma_n\}$

γ_k^i The i^{th} local decision rules of the k^{th} LD in randomization, $i = 1, \ldots, N$

CHAPTER 1

INTRODUCTION

In this chapter, the parallel binary decision fusion architecture is introduced, along with and the two principal performance criteria used for its design.

1.1 Parallel Decentralized Binary Decision Fusion Architecture

A parallel decentralized binary decision fusion architecture is shown in Figure 1.1. The system uses n local detectors (LDs) to observe a binary phenomenon ("target/no target"). The objective is to decide if a target is present (hypothesis H_1) or absent (hypothesis H_0). P_1 is the a priori probability that a target is present (hypothesis H_1) and $P_0 = 1 - P_1$ is the a priori probability that a target is absent (hypothesis H_0). The local observations collected by the k^{th} LD are denoted y_k. All the local observations are assumed to be statistically independent, conditioned on the hypothesis, therefore, $Pr(y_1, \ldots, y_n|H_j) = \prod_k Pr(y_k|H_j), k \in \{1, \ldots, n\}, j \in \{0, 1\}$. Each LD compresses its local observations into a local decision; the local decision of the k^{th} LD is $u_k = \gamma_k(y_k)$, $u_k \in \{0, 1\}$ and $U = \{u_1, u_2, \ldots, u_n\}$. Here $u_k = 0$ means that the k^{th} LD prefers hypothesis H_0, and $u_k = 1$ means that the k^{th} LD prefers hypothesis H_1. A Data Fusion Center (DFC) combines all the local decisions to generate a global decision $u_0 = \gamma_0(U)$, $u_0 \in \{0, 1\}$, where $u_0 = 0$ indicates preference for hypothesis H_0, and $u_0 = 1$ indicates preference for hypothesis H_1. The probability of false alarm of the DFC is $P_f = Pr(u_0 = 1|H_0)$. The probability of detection of the DFC is $P_d = Pr(u_0 = 1|H_1)$. The tuple (P_f, P_d) is considered the *operating point* of the detection system. Similarly, the local operating point of the k^{th} LD is (P_{fk}, P_{dk}), where $P_{fk} = Pr(u_k = 1|H_0)$ and $P_{dk} = Pr(u_k = 1|H_1)$. (P_f^A, P_d^A) is referred as "point A".

This dissertation studies the design of the parallel decentralized binary decision fusion architecture in Figure 1.1 aiming at either minimizing the Bayesian cost of the global decision u_0 or satisfying a Neyman-Pearson criterion.

To achieve this objective, the implementation tasks are to determine the local decision rules (mapping γ_k from y_k to u_k, $k = 1, \ldots, n$) and the global decision rule (mapping γ_0 from U to u_0). The local decision rule of the k^{th} LD, $\gamma_k(.)$, determines how the k^{th} LD compresses its local observations y_k into its local decision u_k as $u_k = \gamma_k(y_k)$. The global decision rule, γ_0, represents how the DFC integrates all the local decisions into the global decision u_0 as $u_0 = \gamma_0(U)$. The combination of all the local decision rules is $\gamma_{LD} = \{\gamma_1, \ldots, \gamma_n\}$. The combination of the global decision rule and all the local decision rules is the *detection strategy*, $\gamma = \{\gamma_0, \gamma_{LD}\} = \{\gamma_0, \ldots, \gamma_n\}$.

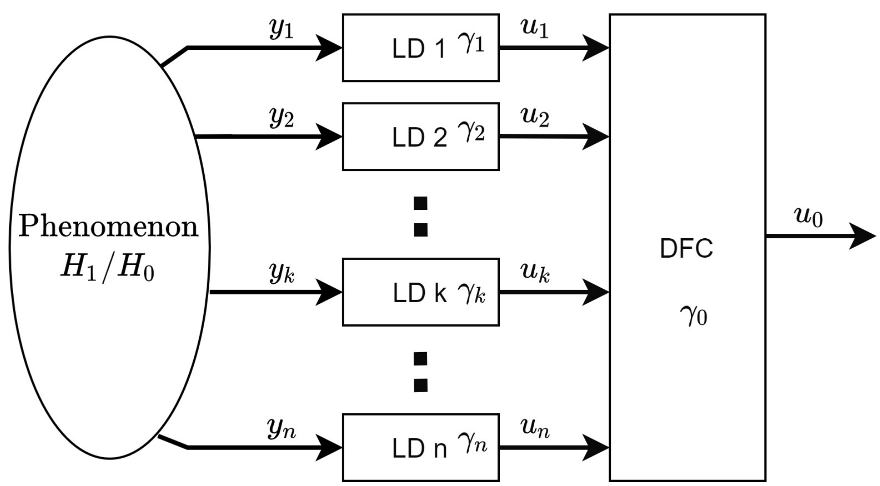

Figure 1.1 Parallel decentralized detection network.

1.2 Minimizing the Bayesian cost of the Global Decision

One performance index often used to design the architecture in Figure 1.1 is the Bayesian criterion. The design of the system aims at minimizing the Bayesian cost of the global decision J, where

$$J = C_{00} P(u_0 = 0|H_0) P_0 + C_{01} P(u_0 = 0|H_1) P_1 + C_{10} P(u_0 = 1|H_0) P_0 + C_{11} P(u_0 = 1|H_1) P_1. \tag{1.1}$$

C_{ij} is the cost for the DFC to accept H_i when the true hypothesis is H_j. P_i is the a priori probability of H_i.

Chapter 2 investigates several existing approaches for minimizing the Bayesian cost of the global decision in parallel decentralized binary decision fusion. Among these studies, the design in [1] fixes the local decision rule and calculates the optimal global decision fusion rule. In [2], Hoballah and Varshney proposed a PBPO procedure to calculate the local decision rule and the global decision rule simultaneously ([2]). In [3], a design of the system with identical LDs was presented. In [4][5][6], variants of the architecture in Figure 1.1 were studied which employ feedback. In these variants, the system uses its previous global decision u_0^{t-1} (at time $t-1$) to improve current global decision u_0^t (at time t). These designs vary in performance and complexity, depending on the selection of objective functions and on compromises made between global optimality and computability.

1.3 Satisfying a Neyman-Pearson Criterion

When satisfying a Neyman-Pearson criterion, the system maximizes the probability of detection P_d while keeping the global probability of false alarm P_f no larger than a specified value α ($0 < \alpha < 1$).

Chapter 3 presents three detection strategies for the system in Figure 1.1, under the Neyman-Pearson criterion.

(a) A deterministic strategy: each LD uses a deterministic local decision rule and the DFC uses a deterministic global decision rule [7].

(b) A strategy with randomization at the DFC only: each LD uses a deterministic local decision rule and the DFC uses a randomized global decision rule [8][9].

(c) Dependent randomization: all the LDs and the DFC use randomized decision rules. The randomization between the LDs and the DFC is coordinated and synchronized [10].

When the DFC employs a single deterministic global decision rule and each LD employs a single deterministic local decision rule (strategy (a)), the resulting ROC curve is generally non-concave. If the local observations are discrete, the resulting ROC curve may be discontinuous. The non-concavity or discontinuity of the ROC curve imply the suboptimality of the design under a Neyman-Pearson criterion. The introduction of the randomization makes the resulting ROC curve continuous (strategy (b) and (c)). Meanwhile, dependent randomization promises the concavity of the resulting ROC curve. It is shown in [11][12] that randomization is not necessary when minimizing the Bayesian cost in (1.1). Therefore, this dissertation focuses on deterministic strategy when the performance index is the Bayesian cost in (1.1).

Chapter 4 offers two examples (with continuous and discrete local observations) of the parallel decentralized binary decision fusion architecture. These two cases are used to exemplify different operating conditions and decision performance throughout the dissertation.

Chapters 5 and 6 study the impact of the loss of synchronization between the LDs and the DFC when dependent randomization is employed (strategy (c)). When using dependent randomization, the LDs and the DFC are coordinated and synchronized. When the synchronization is lost, system performance usually deteriorates. chapters 5 and 6 analyze the following cases:

(d) Dependent randomization (unsynchronized DFC) (studied in Chapter 5): all the LDs and the DFC use randomized decision rules. The LDs are coordinated and synchronized with each other. The DFC uses a randomized global decision rule but is not synchronized with the LDs.

(e) Dependent randomization (unsynchronized LDs) (studied in Chapter 6) : all the LDs and the DFC use randomized decision rules. The randomization between some LDs and the DFC is coordinated and synchronized. Other LDs use randomized local decision rules independently of the other LDs and the DFC.

Chapter 7 studies what happens when some of the probabilities needed for the design are not available. This chapter starts with the work of Chair and Varshney [1]. Their design requires prior knowledge of the probabilities of each hypothesis and the performance probabilities of each sensor. When these probabilities are not available, several adaptive fusion techniques [13][14][15][16] can be applied to estimate them from data. An algorithm that integrates the decisions of these algorithms is proposed, demonstrating superior performance over each algorithm acting alone.

Table 1.1 summarizes the content of the dissertation.

Table 1.1 Summary of each Chapter in the Dissertation

Chapter	Problem/Subject	Outcome
2	Review of designs approaches for parallel decentralized binary decision fusion architecture	Understanding the tradeoff between performance and computational complexity
3	Summary of three detection strategies studied in the existing literature	Comparing three detection strategies, finding conditions under which dependent randomization is beneficial
4	Two examples of parallel decentralized binary decision fusion	-
5	The impact of the loss of synchronization between the DFC and the LDs group	Quantifying the effect of synchronization loss and demonstrating how to recover (partially) from synchronization loss
6	The impact of the partial loss of synchronization among the LDs	Quantifying the effect of synchronization loss and demonstrating how to recover (partially) from synchronization loss
7	Integration of multiple adaptive fusion approaches	A procedure for fusing several adaptive algorithms
8	End notes	-

CHAPTER 2

PERFORMANCE AND COMPLEXITY OF SELECTED PARALLEL DECENTRALIZED BINARY DECISION FUSION SYSTEMS

The performance and design complexity of several parallel decentralized binary decision fusion architecture variants are calculated and compared.

There are several existing design techniques for parallel decentralized binary decision fusion architectures of Figure 1.1, with and without feedback. The designs vary in performance and complexity, depending on the selection of objective functions and on compromises between global optimality and computability. In this chapter, the tradeoff is studied between the performance (when minimizing a Bayesian cost (e.g., (1.1))) and the computational complexity of the design (also see [17]).

2.1 Architectures without Feedback

2.1.1 Fixed global fusion rule

When the LDs in the system are identical, each LD has the same weight, in terms of its influence on the DFC's final decision. In this situation, the fusion rule becomes one of the k out of n rules, where $k = 1, 2, \ldots, n$, and n is the number of LDs in the system. For each "k out of n rule", finding the local decision rule requires solving one non-linear equation ((9) in[3]).

2.1.2 Fixed local decision rule with identical LDs

The design in [1] fixes the local decision rule and calculates the optimal global fusion rule. The global fusion rule employs a threshold which depends on the a priori probability of the hypothesis H_0 and the parameters of the Bayesian cost C_{ij} ((8) in [1]).

2.1.3 Calculating the local decision rule and the global fusion rule simultaneously

The authors of [2] proposed a PBPO procedure to calculate the local decision rule and the global fusion rule simultaneously. This design entails a high computational cost. For non-identical LDs, 2^n non-linear global threshold equations and n non-linear local threshold equations need to be solved at the same time ((19, 20) in [2]).

2.1.4 Calculating local decision rule and global fusion rule exhaustively (overall "k out of n" schemes)

The idea in [3] is to evaluate the performance of the system for every combinations of γ_k and γ_0 (each corresponding to a different k in the "k out of n" scheme). The authors study each fusion rule of the "k out of n" form and develop the local decision rule resulting for the fusion rule. When applied to a system with identical local detectors, the exhaustive design [3] and the simultaneous design [2] have close performance. However, the exhaustive design of [3] has significantly smaller computational complexity. The authors launch an exhaustive search for $n+1$ "k out of n" rules twice. Hence finding the global fusion rule require the solution of $2n+2$ non-linear equations.

2.2 Architectures with Feedback

When the hypothesis remains the same during a certain time epoch, the system can use its previous global decision u_0^{t-1} (at time $t-1$) to improve current global decision u_0^t (at time t). The local observations by each LD are assumed to be statistically independent in time, conditioned on the hypothesis, i.e., $y_k^1, y_k^2, \ldots, y_k^t$ are statistically independent, conditioned on the hypothesis. The previous global decision u_0^{t-1} and current global decision u_0^t are therefore also independent, conditioned on the hypothesis.

A variation of the parallel architecture of Figure 1.1 is offered in Figure 2.1. The DFC remembers and uses its most recent decision to generate the next decision. Kam et al. [4] developed the optimal fusion rule for this architecture with identical LDs and a fixed local decision rule (this is an extension of [1]).

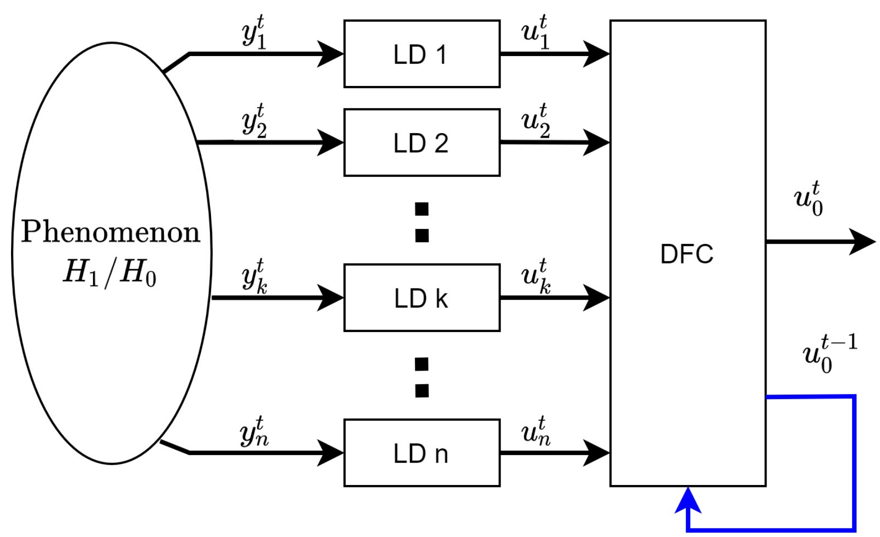

Figure 2.1 Parallel decentralized binary decision fusion with 1-bit memory DFC, network of [4].

Another architecture with feedback is shown in Figure 2.2. At each time step t, the inputs of each LD are not only the local observations but also the previous global decision, u_0^{t-1}. Alhakeem and Varshney [5] proposed a PBPO procedure for designing the local decision rules and the fusion rule for this scheme simultaneously.

2.2.1 Fixed local decision rule

In [4], the LDs are assumed to be identical. The introduction of the feedback updates the value of η_0. In each time step, given the performance of the LDs and the performance of the previous global decision, the η_0 has two different possible values since the previous global decision had two different values, each corresponding to a different accepted hypothesis. These two values are dependent on P_0 and the previous global decision ((2) in [4]).

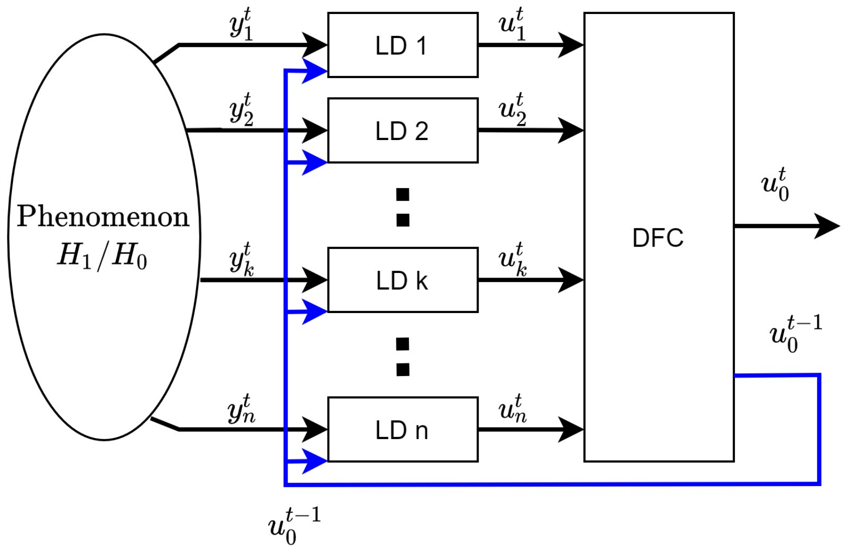

Figure 2.2 Parallel decentralized binary decision fusion with feedback to LDs, architecture of [5][6].

2.2.2 Calculating local decision rule and global fusion rule simultaneously

In [5], the feedback is introduced to all LDs, hence the local decision rule and global fusion are coupled. When the system employs n non-identical LDs, there are 2^n non-linear global threshold equations and $2n$ non-linear local threshold equations which need to be solved at the same time for each step ((2.3, 2.5) in [5]).

2.2.3 Calculating local decision rule and global fusion rule by using a greedy scheme

The authors of [6] propose a greedy scheme to calculate the local decision rule and the global fusion rule. Each LD minimizes the Bayesian cost of its own local decision. In each time step, there are $2n$ non-linear local threshold equations and 1 non-linear global threshold equation that need to be solved ((9, 22) in [6]).

The design of architectures with feedback requires knowledge of the performance of previous global decision at the beginning of each time step. For architectures with identical local detectors acquiring this knowledge means that the complexity of the design is linear in the number of local detectors. For architectures with non-identical local detectors, the complexity is exponential in the number of local detectors [18].

Table 5.1 and Table 2.2 summarize the basic schemes. In Table 5.1 the schemes have no feedback. In Table 2.2 feedback is employed.

Table 2.1 Review of Four Designs of Architectures without Feedback ("k out of n" Rules, [1], [2], and [3])

Method	"k out of n" rule (identical LDs)	Fixed local decision rule (Chair and Varshney [1]) (identical LDs)	Calculating the whole system simultaneously (Hoballah and Varshney [2])	Exhaustive search for every pairs of η_k and η_0 (Acharya et al. [3]) (identical LDs)
η_k	Need to be calculated	Fixed, depends on P_0	Local and global thresholds are coupled, need to be calculated	Local threshold is calculated for each "k out of n" rule
η_0	Fixed, depends on k and n	Need to be calculated		
Equations to be solved	1 non-linear equation ((9) in [3])	Constant ((8) in [1])	$2^n + n$ non-linear coupled equations ((19,20) in [2])	$2n + 2$ non-linear coupled equations (Table 1 in [3])
Key properties	1. Fix $\gamma_0(.)$, design $\gamma_k(.)$ 2.Fix the weight of the LDs	Fix $\gamma_k(.)$, design $\gamma_0(.)$	1. Design $\gamma_k(.)$ and $\gamma_0(.)$ simultaneously 2. The best detection performance and the most complex computation	1. Design $\gamma_k(.)$ and $\gamma_0(.)$ exhaustively 2. Efficient when using identical LDs

Table 2.2 Review of Three Designs of Architectures with Feedback ([4], [5], and [6])

Method	Fixed local decision rule (Kam et al. [4]) (identical LDs)	Calculating the whole system simultaneously (Alhakeem and Varshney [5])	Designing the system with a greedy scheme (Dong and Kam [6])
η_k	Fixed, depends on P_0	Local and global thresholds are coupled, need to be calculated	Local and global thresholds are uncoupled
η_0	Need to be calculated		
Equations to be solved at each step	Constant, depends on P_0 ((2) in [4])	$2^n + 2n$ non-linear coupled equations ((2.3, 2.5) in [5])	$2n + 1$ non-linear coupled equations ((9,22) in [6])
Key properties	Fixed $\gamma_k(.)$, design $\gamma_0(.)$	1.Design $\gamma_k(.)$ and $\gamma_0(.)$ simultaneously 2. The best detection performance and the most complex computation	1. Design $\gamma_k(.)$ and $\gamma_0(.)$ by a greedy scheme 2. Computationally simpler than [5] and shows improvement over the system without feedback

2.3 Example - A 5 Local Detectors System

The performance of the reviewed methods is simulated using a 5 LDs system. The Bayesian criterion is used with $C_{00} = C_{11} = 0$ and $C_{01} = C_{10} = 1$, thus the cost in (1.1) becomes the probability of error,

$$P_e = P_0 P_f + P_1(1 - P_d). \tag{2.1}$$

The local observations conditioned on the hypothesis are normally distributed. In the examples, under H_0 the mean is 0 and variance is 1. Under H_1 the mean is 1 and variance is 0.8.

The system employs five identical LDs. Figure 2.3 shows the probabilities of error by four different designs for architectures with no feedback. The red curve shows the probability of error by the method designing the whole system "simultaneously" (Hoballah and Varshney [2]). The black curve shows the probability of error by designing the system "exhaustively" (Acharya et al. [3]). For an architecture with identical LDs, [2] and [3] have nearly the same performance. The blue curve shows the probability of error when designing the system with $\eta_k = P_0/P_1$ (Chair and Varshney [1]). The green curve shows the probability of error by using majority voting ("k out of n" rule with k = n/2).

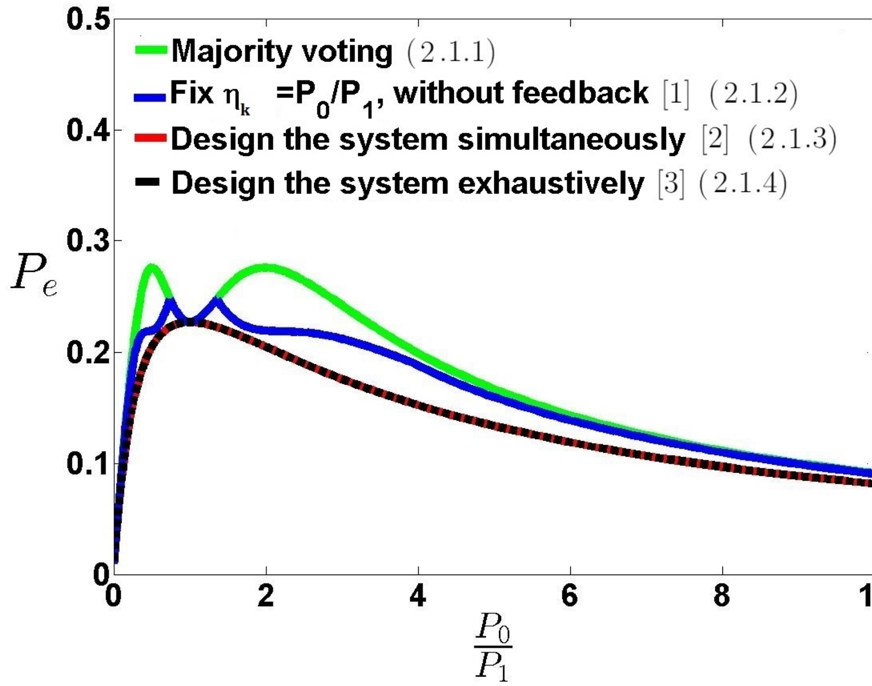

Figure 2.3 Probabilities of error by majority voting (2.1.1), designing the system with fixed η_k [1] (2.1.2), designing the system simultaneously [2] (2.1.3), and designing the system exhaustively [3] (2.1.4).

In Figure 2.3, the green curve shows the probability of error for majority voting, the blue curve shows the probability error using the Chair and Varshney's method (fixed local detection). The red curve shows the probability of error using the Hoballah and Varshney's method (designing the whole system "simultaneously"). The black curve shows the probability of error using the method by Acharya et al. [3] (exhaustive search for every pair of the (finite) possible η_k and η_0).

Figure 2.4 shows the ROC curves of the parallel decentralized binary fusion architecture with several different designs. The designs that use feedback are shown at their second time step (in other words the previous global decision was fed back once into the system). The blue graph and the brown graph show the ROC curve by designing the system with fixed η_k (Chair and Varshney [1]) (η_k=0.5 in the system shown by the blue curve, η_k=P_0/P_1 in the system shown by the brown curve). The black graph shows the ROC curve by designing the whole system simultaneously (Hoballah and Varshney [2]). The cyan graph shows the ROC curve by the design of Acharya et al. [3]. The pink graph shows the ROC curve by designing the system with fixed η_k and feedback (η_k=0.5) (Kam et al. [4]). The red graph shows the ROC curve by designing the whole system simultaneously with feedback (Alhakeem and Varshney [5]). The green curve shows the ROC curve by designing the system with the greedy scheme of Dong and Kam [6].

As Figure 2.3 shows, the blue graph, showing the probability of error by the design with fixed η_k (Chair and Varshney [1]), lies above the black graph (probability of error by the design of Acharya et al. [3]) and the red graph (probability of error by the design of Hoballah and Varshney [2]). However, the computational complexity of the design with fixed η_k (Chair and Varshney [1]) is much lower than the computational complexity of the design of Acharya et al. [3] and the design of Hoballah and Varshney [2].

As Figure 2.4 shows, the introduction of feedback improves the performance of the system (compare the design with feedback by Alhakeem and Varshney [5] to the corresponding design without feedback by Hoballah and Varshney [2], and compare the design with fixed η_k and feedback by Kam et al. [4] to the corresponding design with fixed η_k and no feedback by Chair and Varshney [1]). The curves showing the performance by the design that attempt global optimality lie above the curves corresponding to other designs (compare the design with feedback that attempt global optimality [5] to the corresponding design with feedback by using a greedy scheme [6], and to the corresponding design with fixed η_k and feedback [4]; compare the design without feedback that attempt global optimality [2] to the corresponding design with fixed η_k and no feedback [1]).

The graph showing the performance of the design by Acharya et al. [3] and the graph showing the performance of the design by Hoballah and Varshney [2] almost overlap in Figures 2.3 and 2.4. Still, the computation complexity of the "exhaustive" design (Acharya et al. [3]) is simpler than the computational complexity of the "simultaneous" design (Hoballah and Varshney [2]). However, the "exhaustive" design (Acharya et al. [3]) becomes computationally inefficient when applied to a system with non-identical LDs.

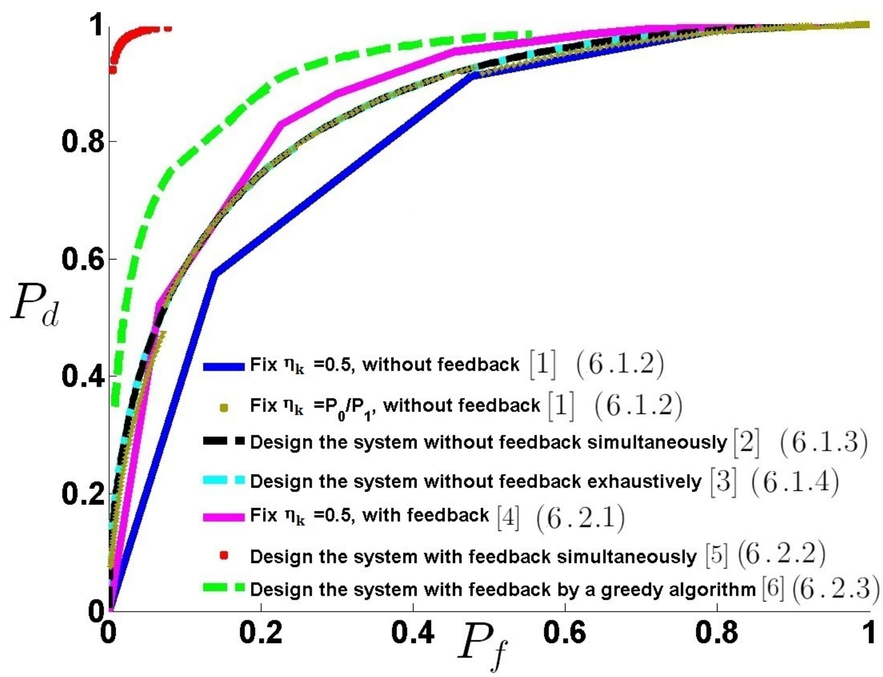

Figure 2.4 ROC curves by seven different designs, $t = 2$.

CHAPTER 3

DETECTION STRATEGY FOR PARALLEL DECENTRALIZED BINARY DECISION FUSION ARCHITECTURE

Design approaches for parallel decentralized binary decision fusion architectures are reviewed. The concept of dependent randomization in the design is explained and illustrated.

3.1 Deterministic Strategy

A detection strategy is deterministic if each LD uses a single deterministic local decision rule and the DFC uses a single deterministic global decision rule. The operating point of the system $A = (P_f^A, P_d^A)$ is determined by the deterministic strategy $\gamma^A = \{\gamma_0^A, \ldots, \gamma_n^A\}$. The corresponding operating point of the k^{th} LD in the system, determined by γ_k^A, is (P_{fk}^A, P_{dk}^A).

It is shown in [10] that under the assumption that the local observations $y_1, \ldots, y_n$ are conditionally independent given the hypothesis H_0 or H_1, for satisfying a Neyman-Pearson criterion, both γ_0 and γ_k are likelihood ratio tests of the form

$$u_0 = \gamma_0(U) = \begin{cases} 0 & \Lambda(U) < \eta_0 \\ 1 & \Lambda(U) \geq \eta_0, \end{cases} \tag{3.1}$$

$$u_k = \gamma_k(y_k) = \begin{cases} 0 & \Lambda(y_k) < \eta_k \\ 1 & \Lambda(y_k) \geq \eta_k, \end{cases} \tag{3.2}$$

where

$$\Lambda(x) = \frac{P(x|H_1)}{P(x|H_0)}. \tag{3.3}$$

η_0 is the threshold of the global decision rule and η_k is the threshold of the local decision rule of the k^{th} LD. Under a Neyman-Pearson criterion, $\eta_0, \eta_1, \ldots \eta_n$ are designed to maximize the probability of detection while keeping the probability of false alarm not greater than $\alpha \in (0, 1)$.

For a parallel decentralized binary decision fusion system with n LDs, the local decision vector U has 2^n possible values, which translates into 2^{2^n} possible global decision rules. However, not every global decision rules is eligible for consideration as a potentially optimal decision rule. According to (3.1), the global decision rule is a likelihood ratio test and u_0 is a non-decreasing function of $\Lambda(U)$. Thomopoulos *et al.* [8] showed that the optimal deterministic global decision rule that satisfies the Neyman-Pearson criterion (3.1) must be a monotonic fusion rule (per Lemma 1 of [8], function d). A fusion rule is monotonic if, for every combination of local decisions $U = \{u_1, \ldots, u_n\}$, switching one of the local decision from 0 to 1 can only cause the global decision u_0 to switch from $u_0 = 0$ to $u_0 = 1$ and not from $u_0 = 1$ to $u_0 = 0$. An algorithm that calculates all the monotonic fusion rules of a system with n LDs is provided in [19]. Since some monotonic fusion rules dominate others (would always result in better performance than others), the eligible optimal deterministic global decision rules would be a subset of all the monotonic fusion rules.

The probability of false alarm and the probability of detection of the architecture shown in Figure 1.1 are:

$$\begin{aligned} P_f &= Pr(u_0 = 1|H_0) = \sum_{\Lambda(U) \geq \eta_0} P(\Lambda(U)|H_0), \\ P_d &= Pr(u_0 = 1|H_1) = \sum_{\Lambda(U) \geq \eta_0} P(\Lambda(U)|H_1). \end{aligned} \tag{3.4}$$

The probability of false alarm and the probability of detection at the k^{th} LD are:

$$\begin{aligned} P_{fk} &= \Pr(u_k = 1|H_0) = \int_{y_k|\Lambda(y_k)\geq\eta_k} P(y_k|H_0)dy_k, \\ P_{dk} &= \Pr(u_k = 1|H_0) = \int_{y_k|\Lambda(y_k)\geq\eta_k} P(y_k|H_1)dy_k. \end{aligned} \tag{3.5}$$

When all the local operating points $(P_{fk}, P_{dk}), k = 1, \ldots, n$ are known, then (3.4) can be written as ([18, pp. 567–568]):

$$\begin{aligned} P_f &= \sum_{u_1=0}^{1} \cdots \sum_{u_n=0}^{1} \prod_{k=1}^{n} P_{fk}^{u_k}(1-P_{fk})^{(1-u_k)} \quad \times \mathbf{U_{-1}}(\prod_{k=1}^{n}(\frac{P_{dk}}{P_{fk}})^{u_k}(\frac{1-P_{dk}}{1-P_{fk}})^{(1-u_k)} - \eta_0), \\ P_d &= \sum_{u_1=0}^{1} \cdots \sum_{u_n=0}^{1} \prod_{k=1}^{n} P_{dk}^{u_k}(1-P_{dk})^{(1-u_k)} \quad \times \mathbf{U_{-1}}(\prod_{k=1}^{n}(\frac{P_{dk}}{P_{fk}})^{u_k}(\frac{1-P_{dk}}{1-P_{fk}})^{(1-u_k)} - \eta_0), \end{aligned} \tag{3.6}$$

where $\mathbf{U_{-1}}(.)$ is the unit step function:

$$\mathbf{U_{-1}}(x) = \begin{cases} 0 & x < 0 \\ 1 & x \geq 0 \end{cases}. \tag{3.7}$$

In (3.6), the unit step function provides the global decision u_0 for a given local decision set $U = \{u_1, \ldots, u_n\}$.

If the local operating points are identical, $(P_{fk}, P_{dk}) = (pf, pd), k = 1, \ldots, n$, the global decision rule (3.1) becomes a "k out of n" rule, which means if k or more LDs in the system decide '1', then $u_0 = 1$; otherwise, $u_0 = 0$. In this circumstance, the probability of false alarm and the probability of detection at the DFC are:

$$\begin{aligned} P_f &= \sum_{k}^{n} \binom{n}{k} pf^k (1-pf)^{(n-k)} \\ P_d &= \sum_{k}^{n} \binom{n}{k} pd^k (1-pd)^{(n-k)}. \end{aligned} \tag{3.8}$$

There are two cases of finding a deterministic strategy, depending on the local observation.

3.1.1 Local observations contain no point masses of probability

Hoballah and Varshney [7] studied this case, using a Person-by-Person optimization (PBPO) approach to synthesize γ_0 and γ_k in (3.1) and (3.2). Acharya *et al.* [3] proposed a method for solving for the optimal γ_0 and γ_k simultaneously when the LDs are identical.

3.1.2 Local observations contain point masses of probability

if the local observations are discrete and finite, the probability distribution of the local observations contain point masses of probability. In this case a finite set of local operating points $\{(P_{f1}, P_{d1}), \ldots, (P_{fn}, P_{dn})\}$ corresponds to the finite set of local decision rules $\{\gamma_1, \ldots, \gamma_n\}$. For each combination of a monotonic global fusion rule and local operating points, the operating point of the system (P_f, P_d) can be calculated by using (3.6). Then all the operating points of the system can be calculated by running a search on all the combinations of a monotonic global fusion rule and local operating points and find the optimal deterministic strategy satisfying the Neyman-Pearson criterion.

3.2 The Potential of Randomization of Decision Rules

Since the vector U is finite-dimensional (and binary), $\Lambda(U)$ in (3.4) has a finite number of values, each with a corresponding probability of false alarm. The value of U that corresponds to the highest probability of false alarm β that satisfies $\beta \leq \alpha$ may have a significant gap $\alpha - \beta$ compared to α.

Figure 3.1 shows the ROC curve of a system with discrete local observations (this curve comes from the system which will be later introduced in Section 4.1). All possible operating points of the system are shown as the blue circles. The probability of false alarm constraint α is shown as the dash line. In this circumstance, the best operating point is ω_3 and $P_f^{\omega_3} < \alpha$.

Performance of the architecture of Figure 1.1 under the circumstance such as the one described in Figure 3.1 can benefit from *randomization*. Randomization means that one or more of the decision makers in the system (an LD or the DFC) is selecting its decision rule (γ_k or γ_0) at each time instant by selecting one rule from a finite set of decision rules. The k^{th} LD selects a rule from among $\{\gamma_k^1, \ldots, \gamma_k^i, \ldots, \gamma_k^N\}$, for some positive integer N. The rule γ_k^i is selected with probability p_k^i and $\sum_{i=1}^N p_k^i = 1$. The DFC selects a rule from among $\{\gamma_0^1, \ldots, \gamma_0^i, \ldots, \gamma_0^M\}$, where γ_0^i is selected with probability p_0^i and $\sum_{i=1}^M p_0^i = 1$. Randomization will be considered when the specified probability of false alarm constraint α is not achievable by a deterministic strategy (such as in Figure 3.1) or when the deterministic strategy achieves the values of false alarm constraint α but the system's ROC curve is not concave.

It is possible that only the DFC employs randomization (e.g., [8][9][20][21]) or that a subset of the of LDs and the DFC employ randomization (independently or dependently). The term "dependent randomization" is used when both the LDs and the DFC employ randomization, and when, in addition, their switching between decision rules is coordinated and synchronized ([10][20][12]).

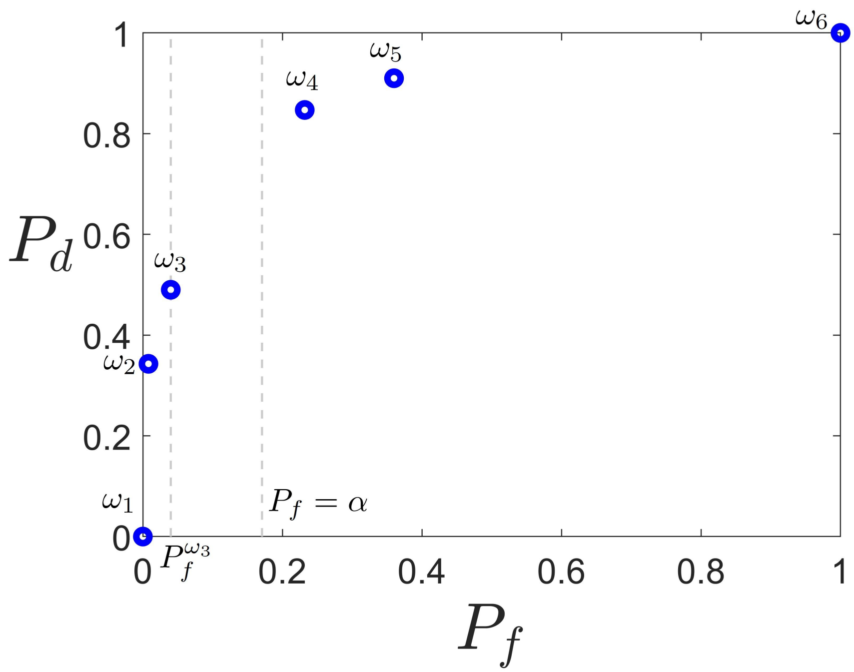

Figure 3.1 Deterministic strategy with isolated operating points.

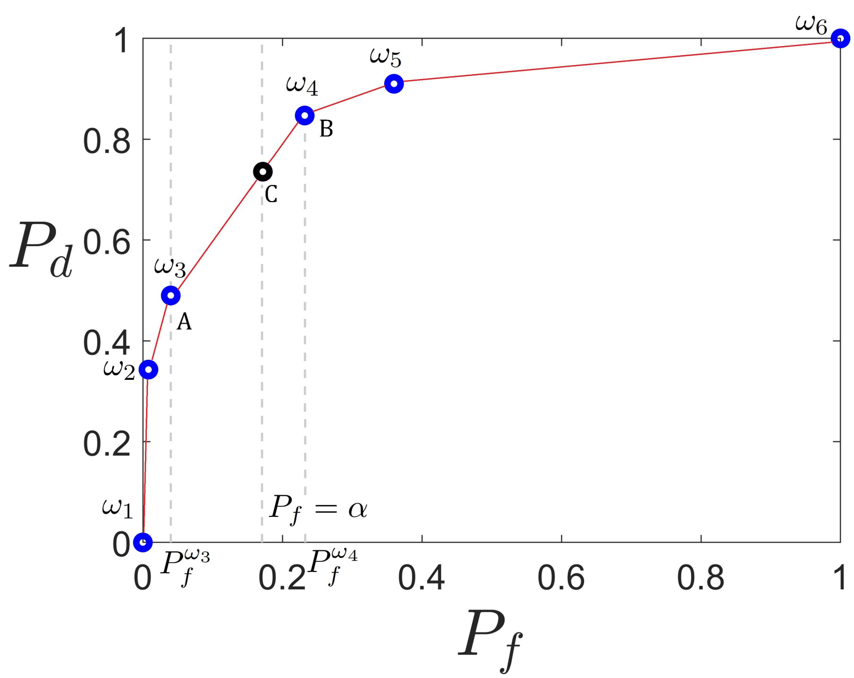

Figure 3.2 Randomization can improve detection performance by 'connecting' the isolated operating points.

One possible design has the system of Figure 1.1 operate at one of two operating points, A and B. At each time step, one of the two is selected (A with probabilities

p and B with probability $1-p$). "Operation at point A" means that the DFC selects γ_0^A and simultaneously each LD ($k = 1, 2, \ldots, n$) selects γ_k^A. "Operation at point B" means that the DFC selects γ_0^B and simultaneously each LD ($k = 1, 2, \ldots, n$) selects γ_k^B. By changing the value of p, the system can effectively operate anywhere along the line segment that connects A and B (every combinations of (P_f, P_d) along this line segment is realizable). The operating point generated by the randomized strategy is denoted as $C = (P_f^C, P_d^C)$, where

$$P_f^C = pP_f^A + (1-p)P_f^B, \tag{3.9}$$

$$P_d^C = pP_d^A + (1-p)P_d^B. \tag{3.10}$$

Satisfying the constraint on the probability of false alarm requires $P_f^C \leq \alpha$. When $P_f^C = \alpha$, the probability of selecting point A, p, is

$$p = \frac{P_f^B - \alpha}{P_f^B - P_f^A}. \tag{3.11}$$

If $\gamma_{LD}^A = \gamma_{LD}^B$ ($\gamma_k^A = \gamma_k^B$ for all k), the randomization occurs only at the DFC. If $\gamma_{LD}^A \neq \gamma_{LD}^B$ and the selection of operating at point A and point B is coordinated and synchronized between the LDs and the DFC, then the scheme is known as dependent randomization.

Figure 3.2 shows how randomization connects the isolated operating points shown in the ROC curve of Figure 3.1. For example, randomization allows the system to operate at point C, rather than at ω_3, thereby achieving a a higher probability of detection while not violating the constraint on probability of false alarm. The red curve is the ROC curve of the system employing randomization, which consists of straight line segments connecting all the previously-isolated operating points (the blue circles). In this example, to achieve the highest probability of detection subject to $P_f \leq \alpha$, $A = \omega_3$ and $B = \omega_4$ are selected. The operating point C achieved by randomization is shown as the black circle. $P_f^C = \alpha = pP_f^{\omega_3} + (1-p)P_f^{\omega_4}$ while p is calculated by (3.11).

3.2.1 Randomization at the DFC only

The authors of [8][9][20][21][22] studied strategies requiring that the DFC implement randomization, when the local decision rules are deterministic ($\gamma_k^A = \gamma_k^B = \gamma_k, \forall k$). Each local decision rule is of the form (3.2). The DFC selects either γ_0^A or γ_0^B at each time step.

Thomopoulos *et al.* ([8]) showed that under a Neyman-Pearson criterion, a desired value of global false alarm α, can always be achieved by a strategy with randomization at the DFC ([8]). In [9] and [22] examples were presented to show that a strategy with randomization at the DFC is able to achieve higher probability of detection than the one achieved by a deterministic detection strategy.

3.2.2 Dependent randomization

In dependent randomization (or “a scheduled test” as it is called in [20]), both the DFC and the LDs participate in the randomization. At each time step, the system makes a selection between two deterministic strategies, $\gamma^A = \{\gamma_0^A, \ldots, \gamma_n^A\}$ and $\gamma^B = \{\gamma_0^B, \ldots, \gamma_n^B\}$ ([10][20][12]). The system can operate on the line segment connecting any two operating points realizable by the deterministic strategy. The ROC curve of the system with dependent randomization is the upper boundary of the convex hull of all the operating points achieved by the deterministic strategy. In other words, dependent randomization can make ROC curve of the system concave.

Dependent randomization requires a coordinated action between the DFC and the LDs. The DFC and the LDs would switch simultaneously together, back and forth, between γ_0^A (for the DFC) and $\gamma_{LD}^A = \{\gamma_1^A, \ldots, \gamma_n^A\}$ (for the LDs); and γ_0^B (for the DFC) and $\gamma_{LD}^B = \{\gamma_1^B, \ldots, \gamma_n^B\}$ (for the LDs). This synchronization challenge is discussed in [10, p. 301][21][12]. Among the means to achieve synchronization between the DFC and the LDs is the use of identical pseudo-code generators (or stored sequences of identical pseudo-code) at the DFC and the LDs simultaneously.

Strategy with *randomization at the DFC only* (Section 3.2.1) can be considered as a special case of dependent randomization, with $\gamma_{LD}^A = \gamma_{LD}^B$. *Randomization at the DFC only* does not require synchronization between the DFC and the LDs but it does not necessarily result in a concave team ROC curve.

Table 3.1 summarizes the input and output of three different designs of a parallel decentralized binary decision fusion system of Figure 1.1.

Table 3.1 Input and Output of Three Different Designs of a Parallel Decentralized Binary Decision Fusion System of Figure 1.1 under a Neyman-Pearson Criterion

<table>
<tr><td colspan="3">Input for the design</td></tr>
<tr><td colspan="3">1. The number of local detectors, n
2. The probability of false alarm constraint, α
3. Conditional probability distributions of the local observations, $P(y_k|H_0)$ and $P(y_k|H_1)$, $k = 1, \ldots, n$</td></tr>
<tr><td colspan="3">Output of a design</td></tr>
<tr><td>Deterministic strategy</td><td colspan="2">1. One global operating point (P_f, P_d)
2. The corresponding local operating points, $(P_{fk}, P_{dk}), k = 1, \ldots, n$</td></tr>
<tr><td>Randomization at the DFC only</td><td rowspan="2">1. Two global operating points $A = (P_f^A, P_d^A)$ and $B = (P_f^B, P_d^B)$
2. The corresponding local operating points of A and B: (P_{fk}^A, P_{dk}^A) and $(P_{fk}^B, P_{dk}^B), k = 1, \ldots, n$
3. The probability of selecting A, p, calculated by (3.11)
4. The operating point $C = (P_f^C, P_d^C)$, calculated by (3.9) and (3.10)</td><td>The local operating points at A and B are identical $(P_{fk}^A, P_{dk}^A) = (P_{fk}^B, P_{dk}^B), k = 1, \ldots, n$</td></tr>
<tr><td>Dependent randomization</td><td>The local operating points at A and B are different $(P_{fk}^A, P_{dk}^A) \neq (P_{fk}^B, P_{dk}^B), k = 1, \ldots, n$</td></tr>
</table>

CHAPTER 4

TWO EXAMPLES OF PARALLEL DECISION FUSION

Two examples, one with two local detectors and one with three local detectors, are provided throughout the study to illustrate performance of the parallel decentralized binary decision fusion architecture under different strategies.

4.1 Example 1: A 2-LD System with Continuous Local Observations

A system with two LDs ($n = 2$) is considered. The local observations are identical logistic random variables (as done in [20]). The conditional probability distribution of the local observations are:

$$\begin{aligned} P(y_k|H_0) &= \frac{1}{4}sech^2(\frac{y_k}{2}), \\ P(y_k|H_1) &= \frac{1}{4}sech^2(\frac{y_k - 2.5}{2}) \end{aligned} \tag{4.1}$$

The operating point (P_{fk}, P_{dk}) of the k^{th} LD ($k = 1, 2$) can be calculated as:

$$\begin{aligned} P_{fk} &= \int_{\tau_k}^{\infty} \frac{1}{4s}sech^2(\frac{y_k}{2})dy_k = \frac{1}{2} - \frac{1}{2}tanh(\frac{\tau_k}{2}), \\ P_{dk} &= \int_{\tau_k}^{\infty} \frac{1}{4s}sech^2(\frac{y_k - 2.5}{2})dy_k = \frac{1}{2} - \frac{1}{2}tanh(\frac{\tau_k - 2.5}{2}), \end{aligned} \tag{4.2}$$

where τ_k is a function of y_k:

$$\tau_k = y_k|_{\Lambda(y_k)=\eta_k}. \tag{4.3}$$

The system is designed under a Neyman-Pearson criterion with $\alpha = 0.2009$. The nontrivial (monotonic) global decision rules are the AND rule ($u_0 = u_1 \& u_2$) and the OR rule ($u_0 = u_1 | u_2$) [20]. For each global decision rule, the operating points of the two LDs are identical, $(P_{f1}, P_{d1}) = (P_{f2}, P_{d2})$. The system operating points can be shown to be: $(P_f, P_d) = ((P_{f1})^2, (P_{d1})^2)$ under the AND rule; and $(P_f, P_d) = ((P_{f1})^2 + 2P_{f1}(1 - P_{f1}), (P_{d1})^2 + 2P_{d1}(1 - P_{d1}))$ under the OR rule.

In Figure 4.1, the ROC curves of this system, using the AND rule and the OR rule, are shown in red and blue, respectively. The ROC curve of the AND rule is given by

$$\begin{aligned} P_d &= \left(\frac{1}{2} - \frac{1}{2} tanh\, \frac{\beta_{AND} - 2.5}{2}\right)^2, \text{where} \\ \beta_{AND} &= ln \frac{\sqrt{P_f} - P_f}{P_f}. \end{aligned} \tag{4.4}$$

The ROC curve of the OR rule is given by

$$\begin{aligned} P_d &= 1 - \left(\frac{1}{2} + \frac{1}{2} tanh\, \frac{\beta_{OR} - 2.5}{2}\right)^2, \text{where} \\ \beta_{OR} &= ln \frac{1 + \sqrt{1 - P_f} - P_f}{P_f}. \end{aligned} \tag{4.5}$$

Although the two individual ROC curves are both concave, the team ROC curve of the system (which is the upper boundary of the two curves) is not. The point of intersection of the two ROC curves is $O = (P_f^O, P_d^O) = (0.1859, 0.8141)$.

Referring to Figure 4.1, if the 2-LD system uses a deterministic strategy to achieve the highest possible P_d, then the DFC employs an AND rule when the desired α is less than or equal to P_f^O and employs an OR rule when the the desired α is greater than P_f^O.

Referring to Figure 4.2 (which shows the ROC curve for $P_f \in [0.14, 0.28]$), let A be the point where the common tangent of the two ROC curves touches the "AND rule ROC curve." let B be the point where the common tangent of the two ROC curves touches the "OR rule ROC curve." If the maximum allowable value of the probability of false alarm, α, satisfies $P_f^A < \alpha < P_f^B$, then dependent randomization would be useful. The ROC curve of the system with dependent randomization as the black curve. In Figure 4.2, for the 2-LD system, the points of tangency are $A = (P_f^A, P_d^A) = (0.1581, 0.7870)$ on the "AND rule ROC curve" and $B = (P_f^B, P_d^B) = (0.2437, 0.8652)$ on the "OR rule ROC curve." The system operates at A when both LDs operate at $(P_{f1}^A, P_{d1}^A) = (P_{f2}^A, P_{d2}^A) = (0.3976, 0.8871)$ and simultaneously the DFC uses the AND rule. The system operates at B when both LDs operate at $(P_{f1}^B, P_{d1}^B) = (P_{f2}^B, P_{d2}^B) = (0.1304, 0.6328)$ and simultaneously the DFC uses the OR rule. To make the team ROC curve concave, dependent randomization is applied whenever the desired probability of false alarm α satisfies $0.1581 = P_f^A < \alpha < P_f^B = 0.2437$. In this range, at each time step the system operates at A with probability p and at B with probability $1 - p$. The equivalent operating point C on the line segment AB is provided by (3.9) and (3.10). Otherwise, if $\alpha < P_f^A$ the AND rule is used, and if $P_f^B < \alpha$ the OR rule is used.

Figure 4.2 shows the operating points of the 2-LD system employing different detection strategies. The blue circle $G = (P_f^G, P_d^G) = (0.2009, 0.8217)$ is the operating point of the system employing deterministic strategy. The system operates at G when both LDs operate at $(P_{f1}^G, P_{d1}^G) = (P_{f2}^G, P_{d2}^G) = (0.4482, 0.9065)$ and the DFC uses the AND fusion rule.

In this case the operating point achieved by the system employing *Randomization at the DFC only* is also G.

The value of α ($\alpha = 0.2009$) in this case satisfies $0.1581 = P_f^A < \alpha < P_f^B = 0.2437$. Therefore, dependent randomization can improve the probability of detection

Table 4.1 Input and Output of Three Different Designs of a 2-LD System

Input for the design	
1. The number of local detectors, $n = 2$ 2. The probability of false alarm constraint, $\alpha = 0.2009$ 3. Conditional probability distributions of the local observations, $P(y_k\|H_0)$ and $P(y_k\|H_1)$, $k = 1, 2$, shown in (4.1)	
Output of a design	
Deterministic strategy	1. System operating point $\boldsymbol{G = (P_f^G, P_d^G) = (0.2009, 0.8217)}$ 2. The system operates at G when both LDs operate at $(P_{f1}^G, P_{d1}^G) = (P_{f2}^G, P_{d2}^G) = (0.4482, 0.9065)$ and the DFC uses the AND fusion rule
Randomization at the DFC	Same as deterministic strategy (Randomization at the DFC does not improve the system performance since the local observations are continuous)
Dependent randomization	1. Two operating points $A = (P_f^A, P_d^A) = (0.1581, 0.7870)$ and $B = (P_f^B, P_d^B) = (0.2437, 0.8652)$ 2. The system operates at A when both LDs operate at $(P_{f1}^A, P_{d1}^A) = (P_{f2}^A, P_{d2}^A) = (0.3976, 0.8871)$ and the DFC uses the AND fusion rule The system operates at B when both LDs operate at $(P_{f1}^B, P_{d1}^B) = (P_{f2}^B, P_{d2}^B) = (0.1304, 0.6328)$ and the DFC uses the OR fusion rule 3. The probability of selecting A is $p = 0.5$ 4. The resulting operating point is $\boldsymbol{C = (P_f^C, P_d^C) = (0.2009, 0.8261)}$

of the system at that value of α. The black circle $C = (P_f^C, P_d^C) = (0.2009, 0.8261)$ is the operating point of the system employing dependent randomization. C is generated by operating at $A = (P_f^A, P_d^A) = (0.1581, 0.7870)$ with probability $p = 0.5$ and at $B = (P_f^B, P_d^B) = (0.2437, 0.8652)$ with probability $1 - p = 0.5$. $p = \frac{0.2437-0.2009}{0.2437-0.1581}$, calculated by (3.11).

Under the Neyman-Pearson criterion with $\alpha = 0.2009$, the input and output of three different designs of the 2-LD system (corresponding to Table 3.1) are shown in Table 4.1. As shown in Table 4.1, dependent randomization is able to increase the probability of detection from $P_d = 0.8217$ to $P_d = 0.8261$ with the same probability of false alarm $P_f = 0.2009$.

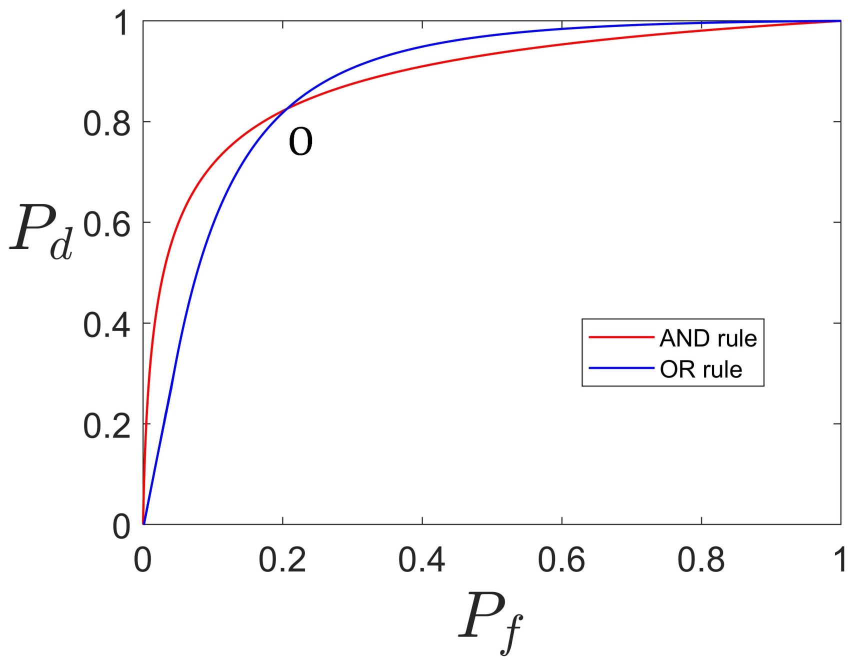

Figure 4.1 The ROC curves of the 2-LD system when the DFC uses an AND rule (red curve) and when it uses an OR rule (blue curve). The upper boundary of the two curves is the ROC curve of the system with deterministic strategy.

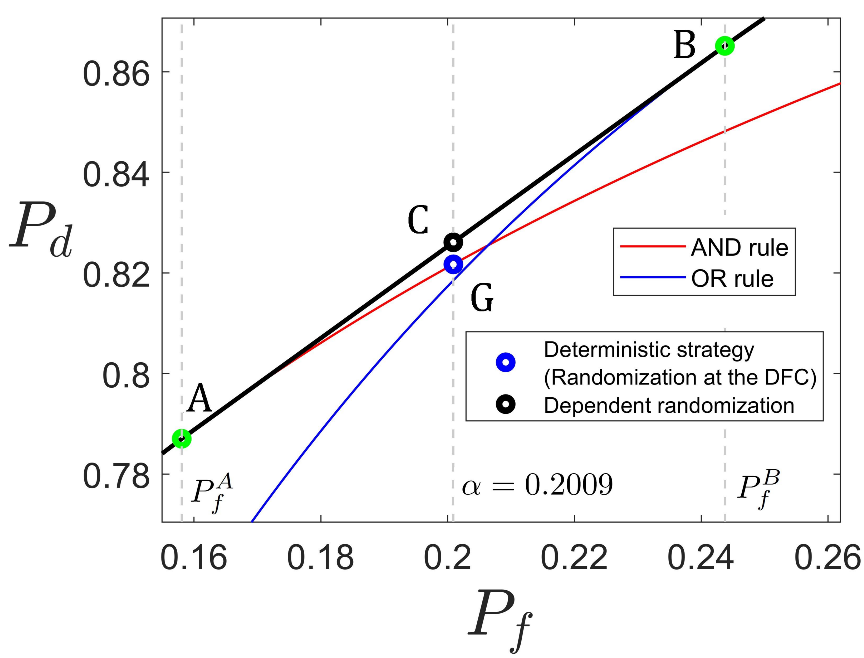

Figure 4.2 The operating points of the 2-LD system employing different detection strategies ($\alpha = 0.2009$): (a) deterministic strategy (and randomization at the DFC) (blue circle); (b) dependent randomization (black circle).

4.2 Example 2: A 3-LD System with Discrete Local Observations

A 3-LD implementation of the structure shown in Figure 1.1 ($n = 3$) is considered. The local observations of the three LDs in the system have identical discrete probability distributions, as shown in Figure 4.3, where the conditional probabilities $P(y_k|H_i)$ are given for $k = 1, 2, 3$ and $i = 0, 1$.

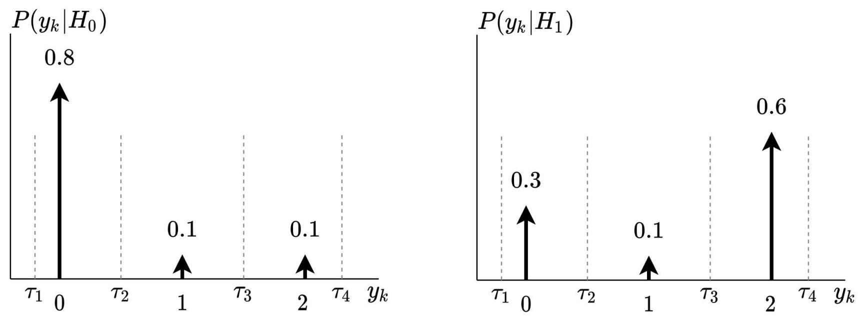

Figure 4.3 The conditional probability distributions of the local observations.

The local observations are assumed to be statistically independent, conditioned on the hypothesis. From Figure 4.3, each LD has four distinct local decision rules, corresponding to four distinct local observation thresholds, τ_1 (anywhere in the range $\tau_1 < 0$), τ_2 ($0 < \tau_2 < 1$), τ_3 ($1 < \tau_3 < 2$), τ_4 ($\tau_4 > 2$). At the k^{th} LD, $k = 1, 2, 3$, if τ_1 is used, $P_{fk} = 1, P_{dk} = 1$; if τ_2 is used, $P_{fk} = 0.2, P_{dk} = 0.7$; if τ_3 is used, $P_{fk} = 0.1, P_{dk} = 0.6$; if τ_4 is used, $P_{fk} = 0, P_{dk} = 0$. Each LD therefore has four possible local operating points (P_{fk}, P_{dk}), which are $(0, 0)$, $(0.1, 0.6)$, $(0.2, 0.7)$, and $(1, 1)$.

4.2.1 Deterministic strategy (Section 3.1)

A 3-LD system has 20 monotonic global decision rules, which are shown in Table 4.2. Since each LD has four (4) possible operating points, there are $4^3 = 64$ combinations of local operating points. Overall, the system has $4^3 \cdot 20 = 1280$ operating points. Since some operating points coincide with others the total number is less than 1280.

Table 4.2 All Twenty Monotonic Fusion Rules of the 3-LD System in Section 4.2 and the Corresponding P_f, P_d when $\alpha = 0.1708$

$\alpha = 0.1708$	γ_0^1	γ_0^2	γ_0^3	γ_0^4	γ_0^5	γ_0^6	γ_0^7	γ_0^8	γ_0^9	γ_0^{10}	γ_0^{11}	γ_0^{12}	γ_0^{13}	γ_0^{14}	γ_0^{15}	γ_0^{16}	γ_0^{17}	γ_0^{18}	γ_0^{19}	γ_0^{20}
(u_1, u_2, u_3)	u_0																			
(0,0,0)	0	0	0	0	0	0	0	0	0	0	0	0	0	0	0	0	0	0	0	1
(0,0,1)	0	0	0	0	0	0	0	0	0	1	0	0	0	0	1	0	1	1	1	1
(0,1,0)	0	0	0	0	0	0	0	0	0	0	1	0	0	1	0	1	1	0	1	1
(1,0,0)	0	0	0	0	0	0	0	0	1	0	0	0	1	0	0	1	0	1	1	1
(0,1,1)	0	0	0	0	1	0	1	1	0	1	1	1	1	1	1	1	1	1	1	1
(1,0,1)	0	0	0	1	0	1	1	0	1	1	0	1	1	1	1	1	1	1	1	1
(1,1,0)	0	0	1	0	0	1	0	1	1	0	1	1	1	1	1	1	1	1	1	1
(1,1,1)	0	1	1	1	1	1	1	1	1	1	1	1	1	1	1	1	1	1	1	1
P_f	0	0.1										0.104	**0.136**			0.1				1
P_d	0	0.6										0.784	**0.796**			0.6				1

Figure 4.4 shows all the distinct operating points of the 3-LD system with deterministic strategy. Since the distribution of the local observations in this example is discrete, the operating points of the system with deterministic strategy are isolated. As a result, in most circumstances the given probability of false alarm constraint α may not be achievable and the system will have to operate at a lower (realizable) rate of probability of false alarm in order not to violate the constraint $P_f \leq \alpha$. The ROC curve of the system has a the staircase form (the blue curve in Figure 4.5). Clearly, this ROC curve is not concave.

4.2.2 Strategy with randomization at the DFC only (Section 3.2.1)

Randomization at the DFC allows the system to operate on the line segments connecting the operating points which are generated by same combination of local operating points. For this 3-LD system, there are overall $4^3 = 64$ combinations of local operating points.

When the local operating points are fixed, since there is finite number of monotonic global decision rules, the operating points of the system would be discrete. The authors of [12] point out that under this circumstance (fixed local operating

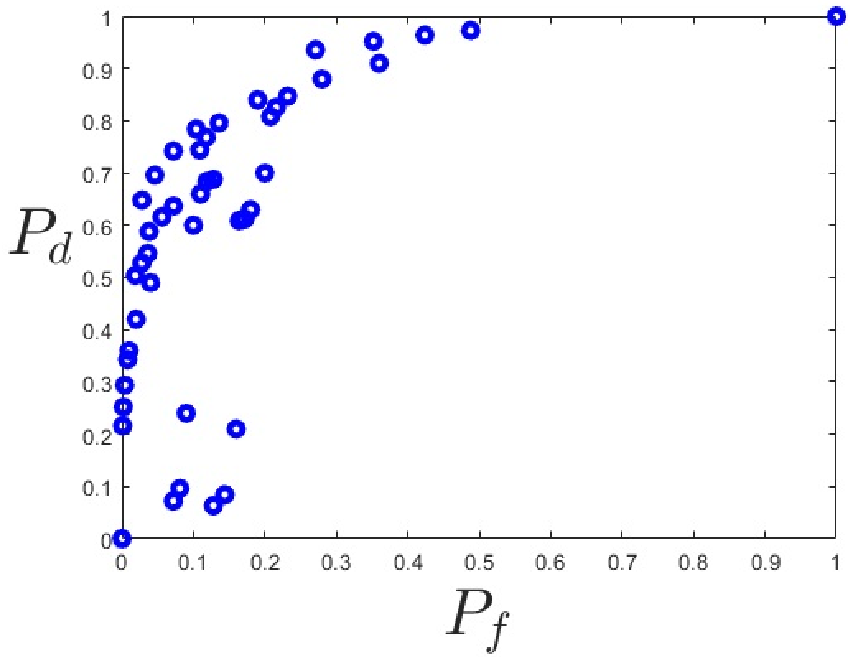

Figure 4.4 All the operating points of the system with deterministic strategy (blue circles).

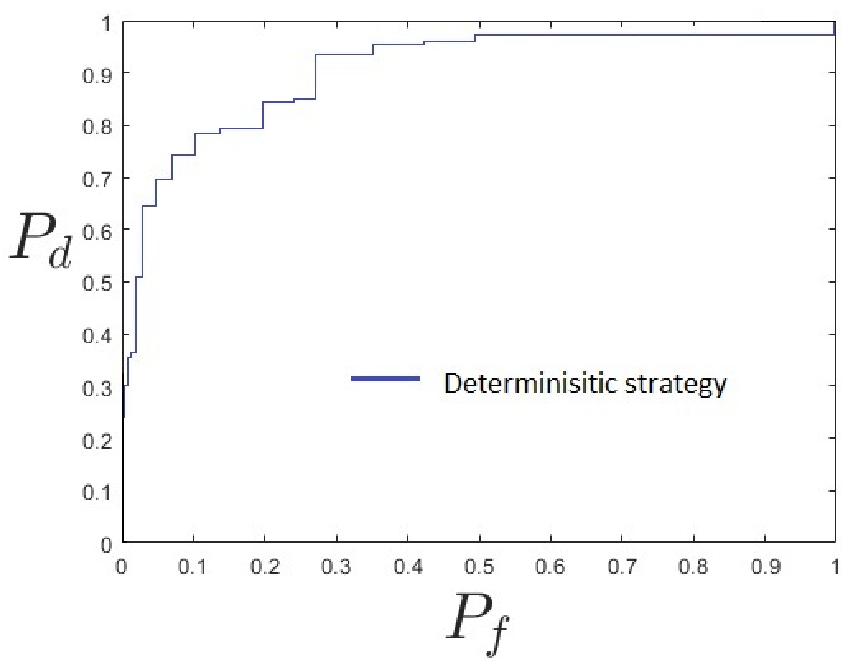

Figure 4.5 The team ROC curve of the system with the deterministic strategy.

points) the ROC curve of the system of Figure 1.1 is a concave piecewise linear curve (i.e., the upper boundary of the convex hull of the discrete operating points is piecewise linear concave). Figure 4.6 shows the ROC curve of the 3-LD system when all three LDs operates at $(0.1, 0.6)$ (which is one of the 64 combinations of local operating points). The blue circles are the operating points of the system employing deterministic fusion rules. The red curve is the concave piecewise linear ROC curve of the 3-LD system when the DFC employs randomization.

Figure 4.7 shows all the ROC curves of the system when the DFC applies randomization at each one of the 64 combinations of the local operating points. Each ROC curve in Figure 4.7, corresponding to one of the 64 combinations of local operating points, is concave piecewise linear (some ROC curves may coincide with others). In Figure 4.7, all the operating points that were used to generate the 64 ROC curves are shown as blue circles. Figure 4.8 shows the team ROC curve of the system with DFC randomization (red piecewise linear curve). It is the upper boundary of all the ROC curves in Figure 4.7. Figure 4.8 also shows the team ROC curve of the system with deterministic strategy (blue). Neither ROC is concave.

4.2.3 Dependent randomization (Section 3.2.2)

Dependent randomization allows the system to operate on the line segment connecting any two operating points generated by deterministic strategy. Therefore the ROC curve of the system with dependent randomization is the upper boundary of the convex hull of all the operating points in Figure 4.4.

Figure 4.9 shows the team ROC curves of the systems with three different detection strategies: (a) deterministic strategy (blue); (b) randomization at the DFC (red); (c) dependent randomization (black). Only the last one is concave. The ROC curve of the strategy with dependent randomization “covers” the ROC curve of the strategy with randomization at the DFC; the ROC curve of the strategy with randomization at the DFC “covers” the ROC curve of the deterministic strategy. As expected, dependent randomization performs at least as well as the strategy with

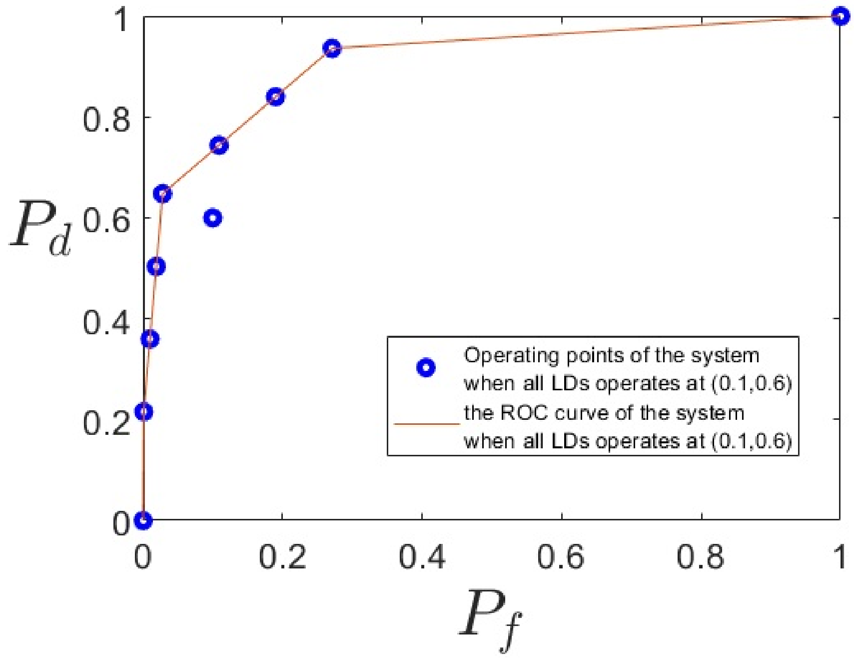

Figure 4.6 The operating points (blue circles) and the ROC curve (red curve) of the 3-LD system when all three LDs operates at $(0.1, 0.6)$. When the local operating points are fixed, the ROC curve of the system employing randomization at the DFC is a concave piecewise linear curve.

randomization at the DFC; the strategy with randomization at the DFC performs at least as well as the deterministic strategy.

Figure 4.10 shows the operating points of the 3-LD system employing three different strategies: (a) deterministic strategy ($G = (0.1360, 0.7960)$, blue circle); (b) randomization at the DFC ($E = (0.1708, 0.8208)$, red circle); (c) deterministic strategy ($C = (0.1708, 0.8448)$, black circle) under a Neyman-Pearson criterion with the probability of false alarm constraint $\alpha = 0.1708$. Table 4.2 shows the probability of false alarm and the probability of detection of the 3-LD system for the 20 applicable monotonic fusion rules (γ_0^1 to γ_0^{20}).

The operating point of the system employing deterministic strategy, G, can be achieved by using three different deterministic strategies: (a) the LDs operate at $\{(0.1, 0.6), (0.2, 0.7), (0.2, 0.7)\}$ while the DFC uses the fusion rule γ_0^{13}; (b) the LDs operate at $\{(0.2, 0.7), (0.1, 0.6), (0.2, 0.7)\}$ while the DFC uses the fusion rule γ_0^{14}; (c)

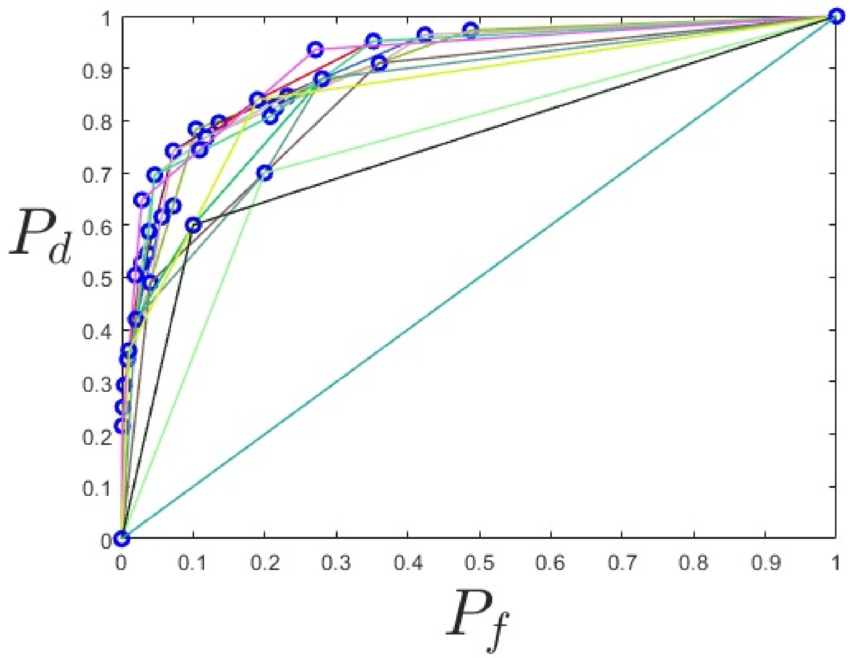

Figure 4.7 All the ROC curves of the system when applying the strategies with randomization at the DFC only (each ROC curve connects the operating points if they correspond to the same local operating points).

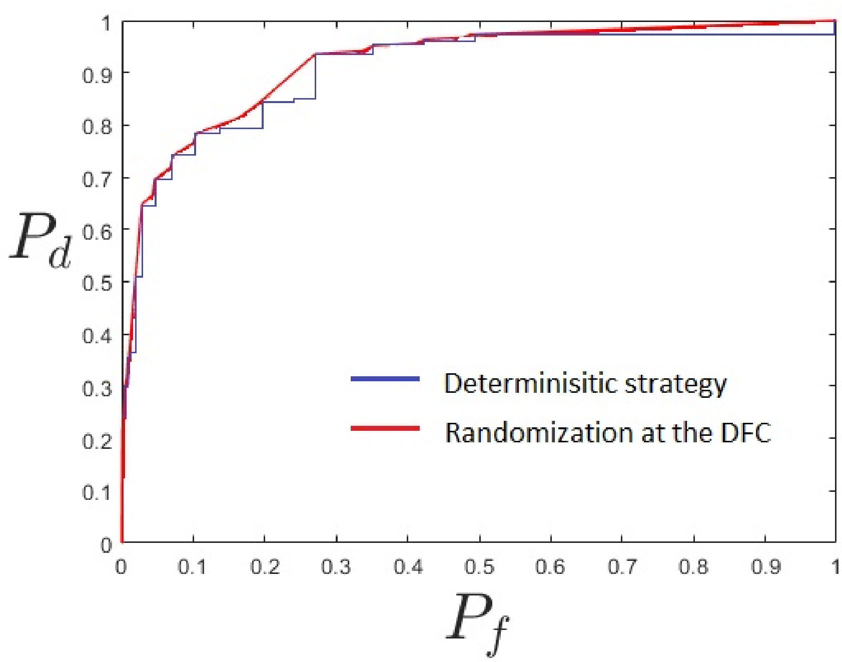

Figure 4.8 The team ROC curves of the deterministic strategy (blue) and the strategy with randomization at the DFC only (red).

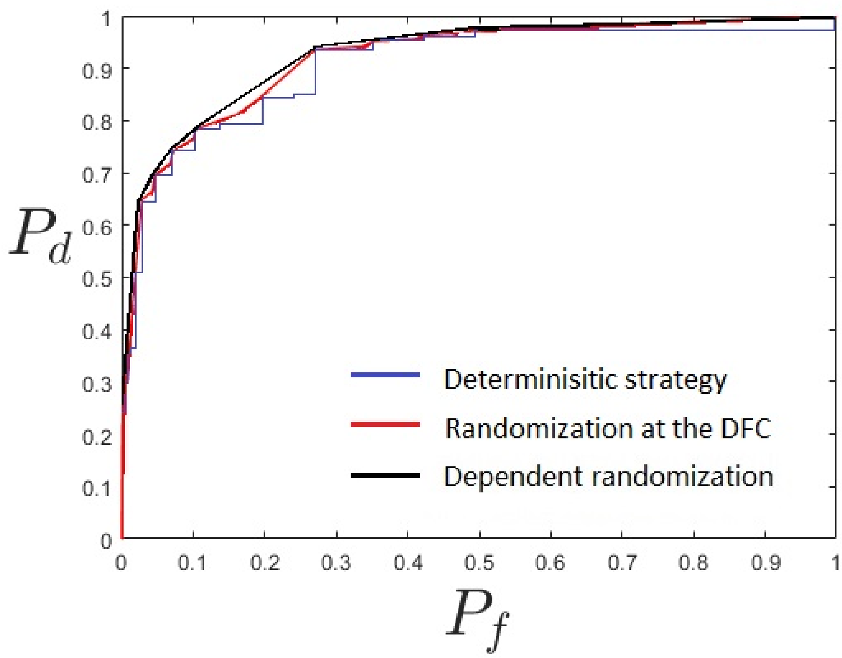

Figure 4.9 The team ROC curves of the systems with (a) dependent randomization (black); (b) randomization at the DFC only (red); (c) deterministic strategy (blue).

the LDs operate at $\{(0.2, 0.7), (0.2, 0.7), (0.1, 0.6)\}$ while the DFC uses the fusion rule γ_0^{15}.

The operating point of the system employing randomization at the DFC, E, can be achieved when the system operates at point $(0.1180, 0.768)$ with probability 0.2667 and operating at point $(0.1900, 0.8400)$ with probability 0.7333. These two points used for achieving E are generated when the LDs operate at $(0.2, 0.7), (0.2, 0.7), (0.1, 0.6)$. The DFC can use the fusion rule γ_0^{14} to achieve point $(0.1180, 0.7680)$ and use the fusion rule γ_0^{16} to achieve point $(0.1900, 0.8400)$.

The operating point of the system employing dependent randomization $C = (0.1708, 0.8448)$ is achieved when the system operates at $A = (0.104, 0.784)$ with probability $p = 0.6$ and at $B = (0.271, 0.936)$ with probability $1-p = 0.4$, respectively. A is achieved when all 3 LDs operate at $(0.2, 0.7)$, i.e. $(P_{fk}, P_{dk}) = (0.2, 0.7), k = 1, 2, 3$, and the DFC uses a "2 out of 3 rule" (γ_0^{12}) (namely, if any two LDs or more decide 1, then $u_0 = 1$; otherwise $u_0 = 0$). B is achieved when all 3 LDs operate at

(0.1, 0.6), i.e. $(P_{fk}, P_{dk}) = (0.1, 0.6), k = 1, 2, 3$, and the DFC uses a "1 out of 3 rule" (γ_0^{19}) (namely, if any one LD or more decides 1, then $u_0 = 1$; otherwise $u_0 = 0$.

Under the Neyman-Pearson criterion with $\alpha = 0.1708$, the input and output of three different designs of the 3-LD system (corresponding to Table 3.1) are shown in Table 4.3.

Table 4.3 Input and Output of Three Different Designs of a 3-LD System

<table>
<tr><td colspan="2">Input for the design</td></tr>
<tr><td colspan="2">1. The number of local detectors, $n = 3$
2. The probability of false alarm constraint, $\alpha = 0.1708$
3. Conditional probability distributions of the local observations,
$P(y_k|H_0)$ and $P(y_k|H_1)$, $k = 1, 2, 3$, shown in Figure 4.3</td></tr>
<tr><td colspan="2">Output of a design</td></tr>
<tr><td>Deterministic strategy</td><td>1. System operating point $\boldsymbol{G = (P_f^G, P_d^G) = (0.1360, 0.7960)}$
2. One way to achieve G is that the LDs operate at $\{(0.1, 0.6), (0.2, 0.7), (0.2, 0.7)\}$
while the DFC uses the fusion rule γ_0^{13}</td></tr>
<tr><td>Randomization at the DFC</td><td>1. Two operating points $A = (P_f^A, P_d^A) = (0.1180, 0.7680)$ and $B = (P_f^B, P_d^B) = (0.1900, 0.8400)$
2. When the LDs operate at $(0.2, 0.7), (0.2, 0.7), (0.1, 0.6)$, the DFC can
use the fusion rule γ_0^{14} to achieve point $A = (0.1180, 0.7680)$ and
use the fusion rule γ_0^{16} to achieve point $B = (0.1900, 0.8400)$.
3. The probability of selecting A is $p = 0.2667$
4. The resulting operating point is $\boldsymbol{E = (P_f^E, P_d^E) = (0.1708, 0.8208)}$</td></tr>
<tr><td>Dependent randomization</td><td>1. Two operating points $A = (P_f^A, P_d^A) = (0.104, 0.784)$ and $B = (P_f^B, P_d^B) = (0.271, 0.936)$
2. A is achieved when $(P_{fk}, P_{dk}) = (0.2, 0.7), k = 1, 2, 3$, and the DFC uses a "2 out of 3 rule" (γ_0^{12})
B is achieved when $(P_{fk}, P_{dk}) = (0.1, 0.6), k = 1, 2, 3$, and the DFC uses a "1 out of 3 rule" (γ_0^{19})
3. The probability of selecting A is $p = 0.6$
4. The resulting operating point is $\boldsymbol{C = (P_f^C, P_d^C) = (0.1708, 0.8448)}$</td></tr>
</table>

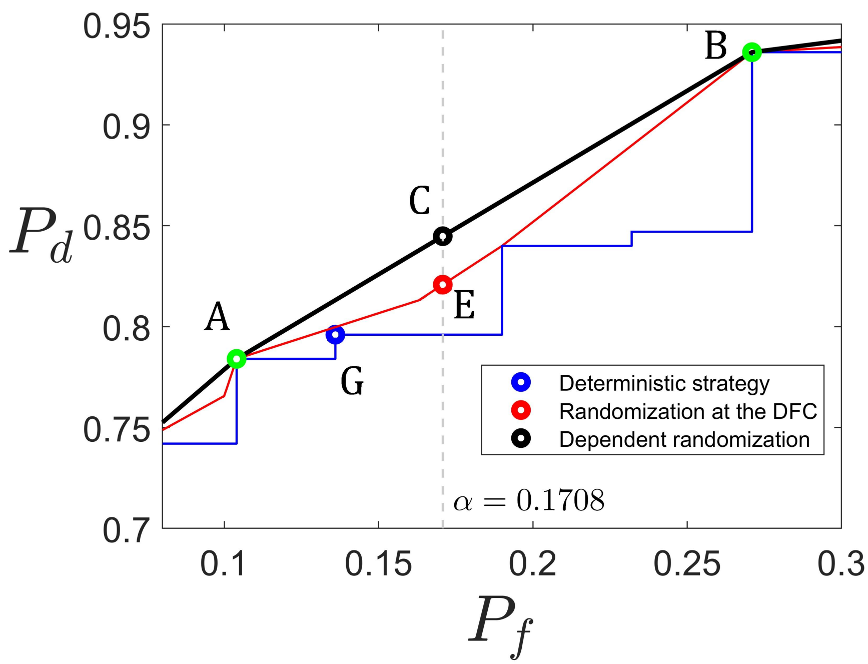

Figure 4.10 The operating points of the 3-LD system employing different detection strategies under the Neyman-Pearson criterion with probability of false alarm constraint $\alpha = 0.1708$: (a) deterministic strategy (blue circle); (b) randomization at the DFC (red circle); (c) dependent randomization (black circle). The ROC curves of the 3-LD system employing different strategies: (a) deterministic strategy (blue); (b) randomization at the DFC (red); (c) dependent randomization (black).

CHAPTER 5

LOSS OF SYNCHRONIZATION BETWEEN THE DFC AND THE GROUP OF LDS

In this chapter, the consequences are studied of the loss of synchronization between the DFC and the group of local detectors in a parallel decentralized binary decision fusion architecture employing dependent randomization.

5.1 Effect of Synchronization Loss (DFC)

Dependent randomization assumes synchronization between all the LDs and the DFC. When this synchronization is lost, unless a corrective action is taken, the system may exceed the allowed probability of false alarm α for which it was designed under a Neyman-Pearson criterion. In this chapter, the corrective action, to be taken upon synchronization loss, is proposed and demonstrated.

The approach to corrective action will be demonstrated on the 2-LD example in Section 4.1 (also looked at in [21]). The ROC curves for the AND rule and the OR rule are shown in Figures 5.1 and 5.2 (also see Figure 4.1). Recall that A and B are, respectively, the points of tangency of the original AND rule and OR rule ROC curves. The two LDs are assumed to be synchronized with each other, while the synchronization between the DFC and the group of LDs was lost. Under these circumstances, the DFC selects γ_0^A with probability p and γ_0^B with probability $1-p$. The group of LDs select $\gamma_1^A, \ldots, \gamma_n^A$ with probability p and $\gamma_1^B, \ldots, \gamma_n^B$ with probability $1-p$. However the DFC selection is not coordinated with the selection of the group of LDs. There are four possible detection strategies: $(\gamma_0^A, \gamma_{LD}^A)$, $(\gamma_0^B, \gamma_{LD}^B)$, $(\gamma_0^B, \gamma_{LD}^A)$, and $(\gamma_0^A, \gamma_{LD}^B)$. They correspond, respectively, to the four operating points A, B, $M1$ and $M2$, shown by green circles in Figure 5.1. Operating point A is selected with probability p^2, operating point B is selected with probability $(1-p)^2$, operating point $M1$ is selected with probability $(1-p)p$, operating point $M2$ is selected with probability $p(1-p)$.

Let W^* represent an equivalent operating point which results from this combination. It is a weighted average of the four points A, B, $M1$ and $M2$. For this operating point W^*, the probability of false alarm $P_f^{W^*}$ and the probability of detection $P_d^{W^*}$ are

$$P_f^{W^*} = p^2 P_f^A + (1-p)^2 P_f^B + (1-p)p P_f^{M1} + p(1-p) P_f^{M2}, \tag{5.1}$$

$$P_d^{W^*} = p^2 P_d^A + (1-p)^2 P_d^B + (1-p)p P_d^{M1} + p(1-p) P_d^{M2}. \tag{5.2}$$

In Figure 5.1, the operating point W^* is shown as a cyan circle. It is possible that $P_f^{W^*} > \alpha$, where α was the upper bound for the system's probability of false alarm.

A special case occurs when the global fusion rules at point A and point B are the same, $\gamma_0^A = \gamma_0^B$. In this case, the DFC does not participate in the randomization. Points A and $M1$ would be the same; points B and $M2$ would be the same. The operating point $W^* = (P_f^{W^*}, P_d^{W^*})$, calculated by (5.1) and (5.2), would be exactly the operating point of the system employing dependent randomization (without losing synchronization), $C = (P_f^C, P_d^C)$, calculated by (3.9) and (3.10). No corrective action is needed in this situation. In all other cases, a corrective action by the DFC may help.

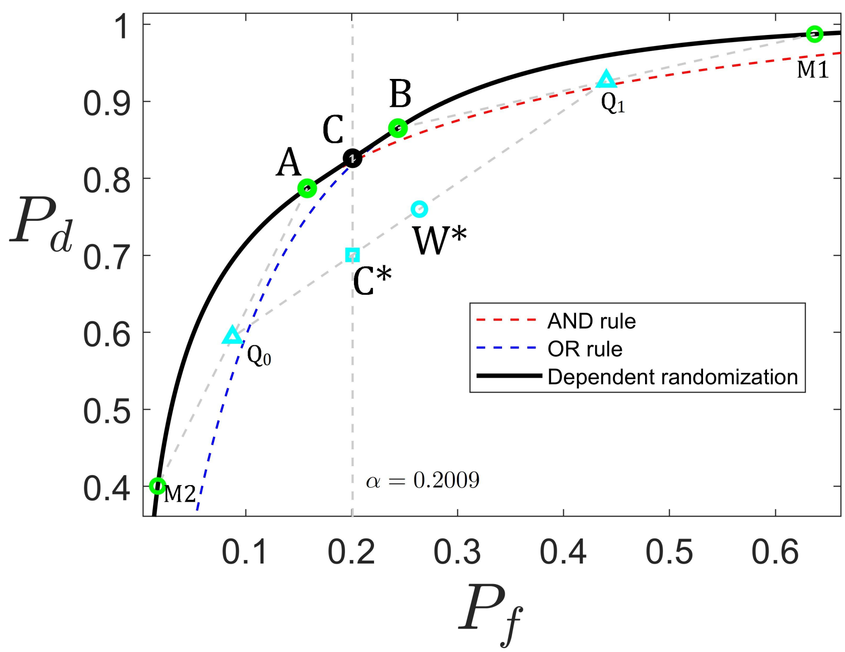

Figure 5.1 A, B, $M1$ and $M2$, shown by green circles, are the possible operating points of the 2-LD system (Section 4.1) when the synchronization between the LDs and the DFC is lost. The black circle, C, shows the operating point of the synchronized system. The cyan circle, W^*, shows the equivalent operating point of the system when it lost synchronization. C^* is the equivalent operating point after the corrective action is taken.

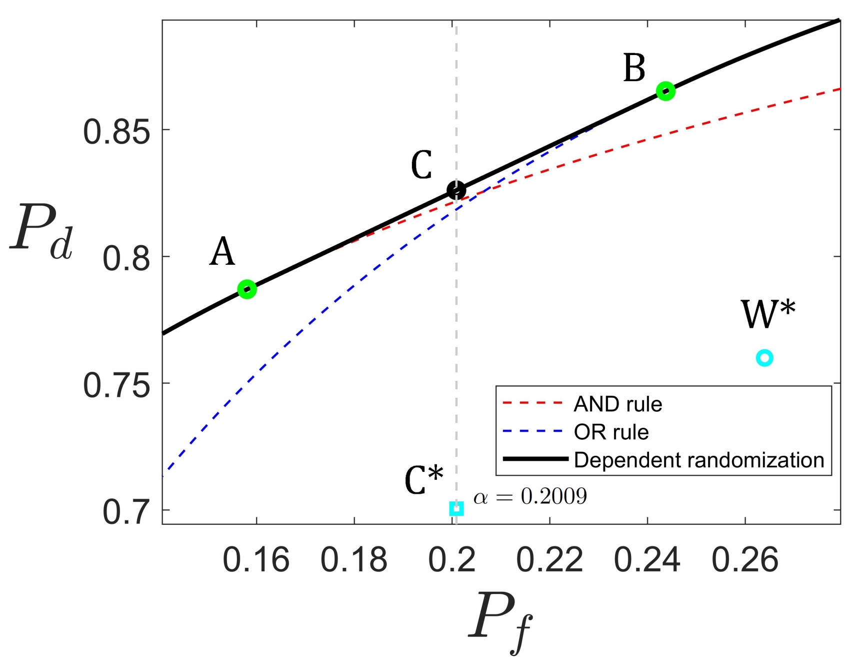

Figure 5.2 Zooming in on the ROC curve of the 2-LD system employing dependent randomization.

5.2 Corrective Action after the Group of LDs Lost Synchronization with the DFC

If the DFC realizes that the synchronization with the group of LDs was lost, it may have the opportunity to take a corrective action to try to satisfy the probability of false alarm constraint $P_f \leq \alpha$. The DFC can do so by changing the probability of selecting point A from p to a certain q, $0 \leq q \leq 1$. Let the DFC choose γ_0^A with probability q (which may be different from p that was used for (5.1) and (5.2)) and γ_0^B with probability $1-q$. A new operating point $C^* = (P_f^{C^*}, P_d^{C^*})$ is created with:

$$P_f^{C^*} = pqP_f^A + (1-p)(1-q)P_f^B + p(1-q)P_f^{M1} + (1-p)qP_f^{M2}, \tag{5.3}$$

$$P_d^{C^*} = pqP_d^A + (1-p)(1-q)P_d^B + p(1-q)P_d^{M1} + (1-p)qP_d^{M2}. \tag{5.4}$$

The role of p in (5.3) and (5.4) is due to the continued use of the probability p (calculated before the loss of synchronization) to select the local decision rules at the operating point A by the LDs. The role of q is due to the selection of the global decision rule at the operating point A by the DFC with probability q (calculated after the loss of synchronization).

Let Q_0 be the operating point when $q = 0$ and Q_1 be the operating point when $q = 1$:

$$P_f^{Q_0}(q=0) = (1-p)P_f^B + pP_f^{M1}. \tag{5.5}$$

$$P_d^{Q_0}(q=0) = (1-p)P_d^B + pP_d^{M1}. \tag{5.6}$$

$$P_f^{Q_1}(q=1) = pP_f^A + (1-p)P_f^{M2}. \tag{5.7}$$

$$P_d^{Q_1}(q=1) = pP_d^A + (1-p)P_d^{M2}. \tag{5.8}$$

Q_0 is located on the line segment connecting B and $M1$; Q_1 is located on the line segment connecting A and $M2$. Both $P_f^{C^*}$ and $P_d^{C^*}$ are affine functions of q (see (5.3) and (5.4)). By changing the value of q from 0 to 1, the system operating point will move from Q_0 to Q_1. Both W^* and C^* are located on the line segment connecting Q_0 and Q_1. By selecting an appropriate value of q to determine C^*, the probability of false alarm constraint $P_f \leq \alpha$ may still be satisfied by point C^* (shown by cyan square in Figure 5.1), but with a lower probability of detection ($P_d^{C^*}$) compared to P_d^C (that was calculated for the synchronized system, see (3.9) and (3.10)).

The value of q, the new probability that determines how the DFC hops between γ_0^A and γ_0^B, can be derived from (5.3) and (5.4):

$$q = \frac{P_f^{Q_0} - \alpha}{P_f^{Q_0} - P_f^{Q_1}} = \frac{[P_f^B - p(P_f^B - P_f^{M1})] - \alpha}{[P_f^B - p(P_f^B - P_f^{M1})] - [P_f^{M2} + p(P_f^A - P_f^{M2})]}. \tag{5.9}$$

It is usable only if $0 \leq q \leq 1$. Otherwise, a corrective action is not possible.

Recall that before the synchronization is lost, dependent randomization would be useful if the probability of false alarm constraint $\alpha \in (P_f^A, P_f^B)$ (assuming $P_f^B > P_f^A$). Satisfying the probability of false alarm constraint after losing synchronization (when the DFC selects γ_0^A with probability q) requires that $\alpha \geq P_f^{Q_0}$ if $P_f^{Q_0} < P_f^{Q_1}$; or $\alpha \geq P_f^{Q_1}$ if $P_f^{Q_1} \leq P_f^{Q_0}$.

Using (5.9), the conditions on the new probability of randomization at the DFC q which satisfies $P_f^{C*} < \alpha$ after the loss of synchronization are summarized in Table 5.1.

Table 5.1 Conditions on q (Probability that the DFC Selects γ_0^A) to Satisfy the Neyman-Pearson Constraint after the DFC Loses Synchronization with the LDs Group

	Value of α	Existence of q	Value of $P_f^{C^*}$
$P_f^{Q_0} < P_f^{Q_1}$	$\alpha \in (-\infty, P_f^{Q_0})$	q does not exist	-
	$\alpha \in [P_f^{Q_0}, P_f^{Q_1}]$	$q \in [0,1]$	$P_f^{C^*} = \alpha$
	$\alpha \in (P_f^{Q_1}, \infty)$	$q = 1$	$P_f^{C^*} = P_f^{Q_1}$
$P_f^{Q_0} \geq P_f^{Q_1}$	$\alpha \in (-\infty, P_f^{Q_1})$	q does not exist	-
	$\alpha \in [P_f^{Q_1}, P_f^{Q_0}]$	$q \in [0,1]$	$P_f^{C^*} = \alpha$
	$\alpha \in (P_f^{Q_0}, \infty)$	$q = 0$	$P_f^{C^*} = P_f^{Q_0}$

So far the 2-LD example in Section 4.1 has been referred. In the general case, points A and B reside on two different ROC curves (each one corresponds to a different decision rule of the DFC). A represents the deterministic operating point of the system with one of the possible deterministic strategy γ^A (the one that corresponds to (P_f^A, P_d^A)). B represents the deterministic operating point of the system with one of the possible deterministic strategy γ^B (the one that corresponds to (P_f^B, P_d^B)). A and B reside on the joint tangent to the two ROC curves, and represent the end points of a line segment on which an operating point resides that satisfies a probability of false alarm constraint α ($P_f^A < \alpha < P_f^B$) while maximizing the probability of the detection using dependent randomization. When the synchronization between the DFC and the LDs is lost, the system can satisfy the probability of false alarm constraint α by assigning a new probability of randomization for the DFC, q (calculated by (5.9)).

5.3 Numerical Examples

5.3.1 2-LD system

The design input and output of the 2-LD system employing dependent randomization with $\alpha = 0.2009$ was shown in Table 4.1. When the DFC lost synchronization with the LDs group in the 2-LD system employing dependent randomization, the input and output of the redesign algorithm are shown in Table 5.2 and Figure 5.1. Before the loss of synchronization the system operated at $C = (0.2009, 0.8261)$ (Table 4.1). After the loss of synchronization the system operates at $C^* = (0.2009, 0.7005)$.

In Figure 5.1, the black curve is the ROC curve of the 2-LD example in Section 4.1 when using dependent randomization. It comprises (from left to right) a segment that corresponds to the AND fusion rule at the DFC (left of point A); a straight line segment AB which is a common tangent of the ROC curves for the AND and OR fusion rules at the DFC; and a segment (to the right of point B) that corresponds to the OR fusion rule at the DFC. When $\alpha = 0.2009$, the operating point of the system is $C = (P_f^C, P_d^C) = (0.2009, 0.8261)$, shown by the black circle. Point C is generated by operating at $A = (P_f^A, P_d^A) = (0.1581, 0.7870)$ with probability $p = 0.5$ and at $B = (P_f^B, P_d^B) = (0.2437, 0.8652)$ with probability $1 - p = 0.5$ (p was calculated using (3.11)). According to Section 4.1, the system operates at A when both LDs operate at $(P_{f1}^A, P_{d1}^A) = (P_{f2}^A, P_{d2}^A) = (0.3976, 0.8871)$ and the DFC uses the AND fusion rule. The system operates at B when both LDs operate at $(P_{f1}^B, P_{d1}^B) = (P_{f2}^B, P_{d2}^B) = (0.1304, 0.6328)$ and the DFC uses the OR fusion rule. When the synchronization between the LDs group and the DFC is lost, the system may also operates (see Figure 5.1) at $M1 = (P_f^{M1}, P_d^{M1}) = (0.6371, 0.9873)$ and $M2 = (P_f^{M2}, P_d^{M2}) = (0.0170, 0.4004)$. The operating point of the non-synchronized system is $W^* = (P_f^{W^*}, P_d^{W^*}) = (0.2640, 0.7600)$, which can be calculated by equations (5.1) and (5.2). The probability of false alarm of the non-synchronized system $P_f^{W^*} = 0.2640$ exceeds the $\alpha = 0.2009$ constraint. When the DFC realizes that synchronization was lost, the DFC can change the probability of randomization from p to q to satisfy the constraint on α. In this situation the system is moved to $C^* = (0.2009, 0.7005)$, calculated by (5.3) and (5.4). The corresponding $q = 0.6787$ is calculated by (5.9). The DFC needs to run a random selection (with probability

Table 5.2 The Output of the 2-LD System Employing Dependent Randomization when the DFC Lost Synchronization with the LDs Group before and after a Corrective Action is Taken

Output of the non-synchronized 2-LD system before the corrective action is taken ($\alpha = 0.2009$)
1. The probability of false alarm constraint, $\alpha = 0.2009$
2. The probability of selecting A, $p = 0.5$, calculated by (3.11)
3. Four possible operating points when the DFC lost synchronization with the LDs group, $A = (0.1581, 0.7870)$, $B = (0.2437, 0.8652)$, $M1 = (0.6371, 0.9873)$, and $M2 = (0.0170, 0.4004)$.
4. The operating point of the non-synchronized system, $W^* = (0.2640, 0.7600)$, calculated by (5.1) and (5.2).
Output of the non-synchronized 2-LD system after the corrective action is taken ($\alpha = 0.2009$)
1. The new probability for the DFC selecting γ_0^A, $q = 0.6787$, calculated by (5.9)
2. The fulfillment of the prerequisite of the correction action, $0 < q < 1$
3. The operating point of the non-synchronized system after the corrective action is taken, $\boldsymbol{C^* = (0.2009, 0.7005)}$, calculated by (5.3) and (5.4).

$q = 0.6787$) between the two global fusion rules (AND and OR) and the LDs run a random selection (with probability $p = 0.5$) between two set of local decision rules, independently of the DFC. Due to the loss of synchronization the probability of detection under the constraint $P_f \leq \alpha = 0.2009$ has been reduced from 0.8261 to 0.7005.

5.3.2 3-LD system

The design input and output of the 3-LD system employing dependent randomization with $\alpha = 0.1708$ was shown in Table 4.3. When the DFC lost synchronization with the LDs group in the 3-LD system employing dependent randomization, the input and output of the redesign algorithm are shown in Table 5.3 and Figure 5.3. Before the loss of synchronization the system operated at $C = (0.1708, 0.8448)$ (Table 4.1). After the loss of synchronization the system operates at $C^* = (0.1708, 0.7974)$.

In Figure 5.3, the black curve is the ROC curve of the 3-LD example in Section 4.2 when using dependent randomization (this is the curve developed in Figures 4.9 and 4.10). $\alpha = 0.1708$ is in the range $0.1040 = P_f^A \leq P_f \leq P_f^B = 0.2710$. When the probability of false alarm $P_f = \alpha = 0.1708$, the operating point of the system is $C = (P_f^C, P_d^C) = (0.1708, 0.8448)$, shown as the black circle. C is generated by operating at $A = (P_f^A, P_d^A) = (0.1040, 0.7840)$ with probability $p = 0.6$ and at $B = (P_f^B, P_d^B) = (0.2710, 0.9360)$ with probability $1 - p = 0.4$, respectively (p was calculated using (3.11). A is achieved when all 3 LDs operate at $(0.2, 0.7)$ and the DFC uses a "2 out of 3 rule". B is achieved when all 3 LDs operate at $(0.1, 0.6)$ and the DFC uses a "1 out of 3 rule". When the synchronization between the LDs group and the DFC is lost, the system may also operate at $M1 = (P_f^{M1}, P_d^{M1}) = (0.4880, 0.9730)$ (all 3 LDs operate at $(0.2, 0.7)$ and the DFC uses "1 out of 3 rule") and $M2 = (P_f^{M2}, P_d^{M2}) = (0.0280, 0.6480)$ (all 3 LDs operate at $(0.1, 0.6)$ and the DFC uses "2 out of 3 rule"). The equivalent operating point of the non-synchronized system is $W^* = (P_f^{W^*}, P_d^{W^*}) = (0.2046, 0.8210)$, which can be calculated by (5.1) and (5.2). The probability of false alarm constraint $P_f \leq \alpha = 0.1708$ is no longer satisfied. When the DFC realizes that synchronization was lost, the DFC can change the probability of randomization from p to q to satisfy the constraint on α. In this situation $C^* = (P_f^{C^*}, P_d^{C^*}) = (0.1708, 0.7974)$, calculated by (5.3) and (5.4). The corresponding probability of randomization at the DFC $q = 0.7033$ can be calculated by (5.9). The DFC needs to run a random selection (with probability $q = 0.7033$) between two global fusion rules and the LDs run a random selection (with probability $p = 0.6$) between two set of local decision rules independently. Due to the loss of synchronization, the probability of detection under the constraint $P_f \leq \alpha = 0.1708$ has been reduced from 0.8448 to 0.7974.

Table 5.3 The Output of the 3-LD System Employing Dependent Randomization when the DFC Lost Synchronization with the LDs Group before and after a Corrective Action is Taken

Output of the non-synchronized 3-LD system before the corrective action is taken ($\alpha = 0.1708$)
1. The probability of false alarm constraint, $\alpha = 0.1708$ 2. The probability of selecting A, $p = 0.6$, calculated by (3.11) 3. Four possible operating points when the DFC lost synchronization with the LDs group, $A = (0.1040, 0.7840)$, $B = (0.2710, 0.9360)$, $M1 = (0.4880, 0.9730)$, and $M2 = (0.0280, 0.6480)$. 4. The operating point of the non-synchronized system, $W^* = (0.2046, 0.8210)$, calculated by (5.1) and (5.2).
Output of the non-synchronized 3-LD system after the corrective action is taken ($\alpha = 0.1708$)
1. The new probability for the DFC selecting γ_0^A, $q = 0.7033$, calculated by (5.9) 2. The fulfillment of the prerequisite of the correction action, $0 < q < 1$ 3. The operating point of the non-synchronized system after the corrective action is taken, $\boldsymbol{C^* = (0.1708, 0.7974)}$, calculated by (5.3) and (5.4).

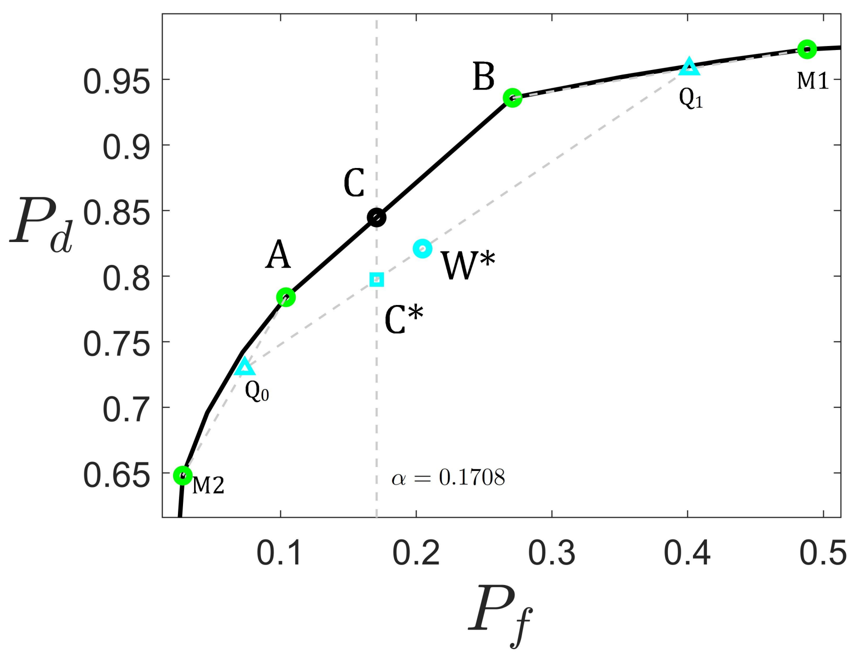

Figure 5.3 A, B, $M1$ and $M2$, shown by green circles, are the possible operating points of the 3-LD system (Section 4.2) when the synchronization between the LDs and the DFC is lost. The black circle, C, shows the operating point of the synchronized system. The cyan circle, W^*, shows the equivalent operating point of the system when it lost synchronization. C^* is the equivalent operating point after the corrective action is taken.

CHAPTER 6

PARTIAL LOSS OF SYNCHRONIZATION AMONG THE LDS

In this chapter, the consequences are studied of the partial loss of synchronization between the local detectors in a parallel decentralized binary decision fusion architecture employing dependent randomization.

6.1 Effect of Synchronization Loss (LDs)

This chapter assumes that a decision fusion architecture was designed per Section 3.2.2 (Dependent randomization) to maximize the probability of detection under a probability of false alarm constraint. This approach means that the LDs and the DFC are designed to operate at any given time at one of two operating points (say A and B). They operate at operating point A (corresponding to deterministic strategy $\gamma^A = \{\gamma_0^A, \gamma_1^A, \ldots, \gamma_n^A\}$) with probability p and at operating point B (corresponding to deterministic strategy $\gamma^B = \{\gamma_0^B, \gamma_1^B, \ldots, \gamma_n^B\}$) with probability $1 - p$. A and B are on the upper boundary of the convex hull of all the operating points which are achievable by deterministic strategies of the system. If a value of p, $0 < p < 1$, exists that would keep the probability of false alarm of the system at the maximal allowable level, α, the resulting operating point of the system $C = (P_f^C = \alpha, P_d^C)$ would be optimal.

In the previous chapter (5: *Loss of Synchronization between the DFC and the LDs Group*), in spite of loss of synchronization between the DFC and the LDs group, all LDs were still synchronized with each other. Under this circumstance, the DFC can in some cases change the probability p of hopping between A and B to satisfy the probability of false alarm constraint, but generally at the expense of reaching a lower probability of detection than P_d^C.

This chapter assumes a synchronization failure of the following characteristics:

(a) Only m $(1 \leq m \leq n-1)$ LDs are synchronized with the DFC and with each other. These synchronized LDs are called group Y.

(b) The remaining $n-m$ LDs are not synchronized with the DFC, nor are they synchronized with each other. These non-synchronized LDs are called group $\overline{Y}$.

(c) The DFC is aware of (a) and (b) and of the identity of members in Y and $\overline{Y}$. The LDs are not.

Each LD of the system (say LD k) flips a coin, and, based on the outcome, it follows the local decision rule γ_k^A or the other local decision rule, γ_k^B (γ_k^A is used with probability p and γ_k^B is used with probability $1-p$). If LD k belongs to Y it uses the "joint coin" flipped simultaneously and synchronously by all the LDs in Y and the DFC. If LD k belongs to $\overline{Y}$ then it flips its own coin, which is not synchronized with either the "joint coin" used by the LDs in Y and the DFC, or the "separate" $n-m-1$ coins of the other members of $\overline{Y}$.

Since $n-m$ LDs are now unsynchronized, the resulting operating point of the system, $W' = (P_f^{W'}, P_d^{W'})$, is a combinations of 2^{n-m+1} possible operating points. If no correction is made, $P_f^{W'}$ is highly likely to exceed the level α which was satisfied (per the constraint $P_f \leq \alpha$) before synchronization was lost. Under these circumstances, the global fusion rules at the DFC is redesigned to satisfy $P_f \leq \alpha$, and the resulting performance cost (the reduction in the probability of detection) is shown.

The input of the redesigned algorithm is shown in Table 6.1.

Table 6.1 Input of the Redesigned Algorithm when each LD in $\overline{Y}$ Lost Synchronization with the DFC and each Other

Input of the redesigned algorithm	
The design input of dependent randomization (Table 3.1)	1. The number of local detectors, n 2. The probability of false alarm constraint, α
The design output of dependent randomization (Table 3.1)	3. The local operating points of A and B: (P_{fk}^A, P_{dk}^A) and $(P_{fk}^B, P_{dk}^B), k = 1, \ldots, n$ 4. The probability of selecting A, p, calculated by (3.11)
Information of synchronized LDs	5. Numbers of synchronized LDs, m ($Y = \{LD1, \ldots, LDm\}$ are synchronized) 6. Identity of all synchronized LDs, $Y = \{LD1, \ldots, LDm\}$

6.2 Calculating the Local Operating Points after the LDs in $\overline{Y}$ Lost Synchronization

The local operating points of the m LDs in Y are $\{(P^i_{f1}, P^i_{d1}), \ldots, (P^i_{fm}, P^i_{dm})\}$, $i \in \{A, B\}$. For the j^{th} LDs in $\overline{Y}$ $(j = m+1, \ldots, n)$, the expected value of the probability of false alarm is $pP^A_{fj} + (1-p)P^B_{fj}$ and the expected value of the probability of detection by the j^{th} LD in $\overline{Y}$ is $pP^A_{dj} + (1-p)P^B_{dj}$. The local operating points of the $n-m$ LDs in $\overline{Y}$ are $\{(pP^A_{fm+1} + (1-p)P^B_{fm+1}, pP^A_{dm+1} + (1-p)P^B_{dm+1}), \ldots, (pP^A_{fn} + (1-p)P^B_{fn}, pP^A_{dn} + (1-p)P^B_{dn})\}$. The equivalent local operating points of the system are $\Phi^i = \{(P^i_{f1}, P^i_{d1}), \ldots, (P^i_{fm}, P^i_{dm}), (pP^A_{fm+1} + (1-p)P^B_{fm+1}, pP^A_{dm+1} + (1-p)P^B_{dm+1}), \ldots, (pP^A_{fn} + (1-p)P^B_{fn}, pP^A_{dn} + (1-p)P^B_{dn})\}$. Therefore, at each time step, *system A* is used, shown in Figure 6.1, with probability p, and *system B* is used, shown in Figure 6.2, with probability $1-p$. The local operating points of $\{LD\ m+1, \ldots, LD\ n\}$ in *system A* and *system B* are the same.

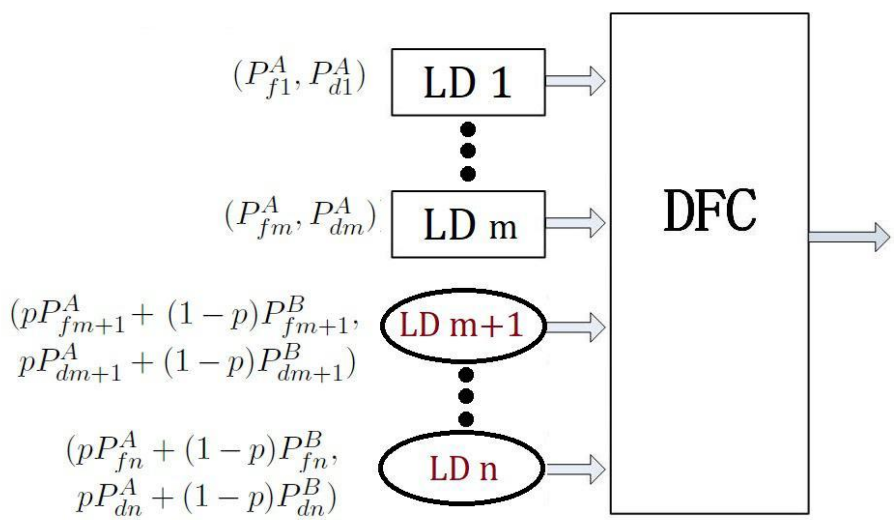

Figure 6.1 *System A* is used with probability p.

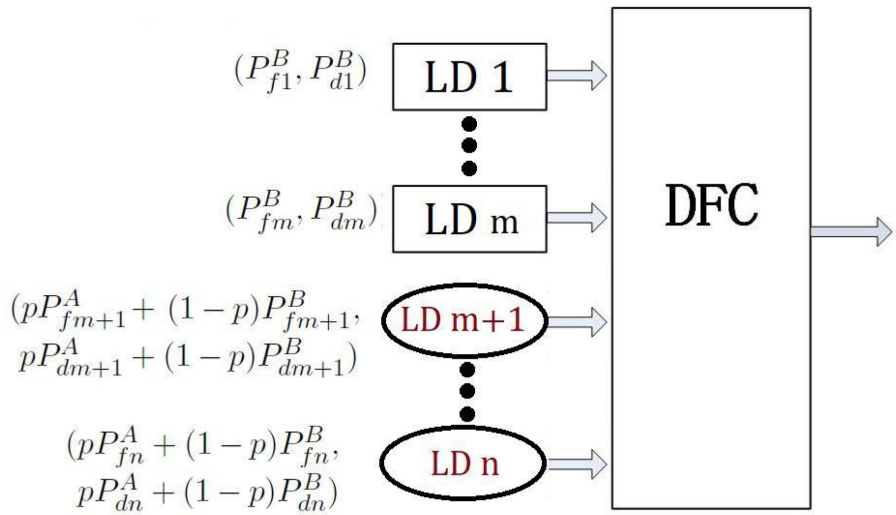

Figure 6.2 *System B* is used with probability $1 - p$.

6.3 Calculating the ROC Curves of *System A* and *System B*

In order to satisfy the Neyman-Pearson criterion, under the new condition the system can try to redesign the global fusion rules at the DFC. At each time step, the DFC will now use $\gamma_0^{A'}$ (was γ_0^A) with probability p and $\gamma_0^{B'}$ (was γ_0^B) with probability $1-p$. Namely, $\gamma_0^{A'}$ will be used by *system A* and $\gamma_0^{B'}$ will be used by *system B*. Unlike γ_0^A and γ_0^B, which are deterministic fusion rules, $\gamma_0^{A'}$ or $\gamma_0^{B'}$ could be a randomized fusion rule. $\gamma_0^{A'}$ and $\gamma_0^{B'}$ are selected from among the monotonic fusion rules ([8]) for both systems. For each one of $\gamma_0^{A'}$ and $\gamma_0^{B'}$, in general two monotonic fusion rules and a randomization scheme to hop between them are needed.

The operating points, corresponding to all the monotonic fusion rules, for both *system A* and *system B*, can be calculated by (3.6). The calculated operating points are isolated in the $P_f - P_d$ plane. *ROC curve A* (*ROC curve B*) is denoted as the ROC curve of *system A* (*system B*). The ROC curve of a system with isolated operating points in the $P_f - P_d$ plane is the upper boundary of the convex hull of those isolated operating points, which is a concave piecewise-linear curve. Therefore both *ROC curve A* and *ROC curve B* are concave piecewise-linear curves. Finding the fusion rule $\gamma_0^{A'}$ for *system A* is equivalent to finding an operating point of *system A* on *ROC* *curve A*. Similarly, finding a fusion rule $\gamma_0^{B'}$ for *system B* is equivalent to finding an operating point of *system B* on *ROC curve B*.

ROC curve A can be drawn as a sequence of straight line segments $\omega_1^A\omega_2^A$, $\omega_2^A\omega_3^A, \ldots, \omega_{mA-1}^A\omega_{mA}^A$, where $\Omega^A = \{\omega_1^A = (0,0), \omega_2^A, \ldots, \omega_{mA-1}^A, \omega_{mA}^A = (1,1)\}$ are points in the $P_f - P_d$ plane. Similarly, $\Omega^B = \{\omega_1^B = (0,0), \omega_2^B, \ldots, \omega_{mB-1}^B, \omega_{mB}^B = (1,1)\}$ for the *ROC curve B*. Each of points in Ω^A and Ω^B is realizable by a deterministic (monotonic) fusion rule. Meanwhile, each one of the other operating points on *ROC curve A* (*ROC curve B*), those that are not in $\Omega^A(\Omega^B)$, can be realized by hopping between two points in Ω^A (Ω^B) by using randomization at the DFC.

In Figure 6.3, the ROC curve of the 2-LD system (Section 4.1) with dependent randomization is shown as the black curve. Recall (Figures 4.1 and 4.2) that to create this curve, two different ROC curves (one corresponding to an AND global decision rule and one corresponding to an OR global decision rule) have been integrated. The points of tangency A and B of the ROC curves for the AND rule and the OR rule have been calculated respectively, and have been connected with a straight line. If $\alpha \in (P_f^A, P_f^B)$ then the highest achievable probability of detection, corresponding to α, was on the straight-line segment that joins points A and B. For α shown in Figure 4.2, the highest probability of detection is denoted P_d^C, achieved at point C, which is the the midpoint of line segment connecting A and B (in this example $p = 0.5$).

Suppose that $LD1$ and the DFC continue to be synchronized with each other ($Y = \{LD1\}$) but $LD2$ lost synchronization with $LD1$ and with the DFC ($\overline{Y} = \{LD2\}$). Figure 6.3 shows two ROC curves for this new situation. *ROC curve A* (red) is obtained when the members of Y (just $LD1$ in this case) select γ_1^A (when this happen $LD2$, oblivious to $LD1$ and the DFC, selects γ_2^A with probability p and γ_2^B with probability $1-p$). *ROC curve B* (blue) is obtained when the members of Y ($LD1$) select γ_1^B ($LD2$ still selects γ_2^A with probability p and γ_2^B with probability $1-p$). In Figure 6.3, Ω^A are shown by the red circles and Ω^B are shown by the blue circles. The next task is to select the points A' (on *ROC curve* A) and B' (on *ROC curve* B) such that the system can hop between them and meet the following objectives: (a) satisfy the probability of false alarm constraint $P_f \leq \alpha$; (b) maximize the probability of detection P_d.

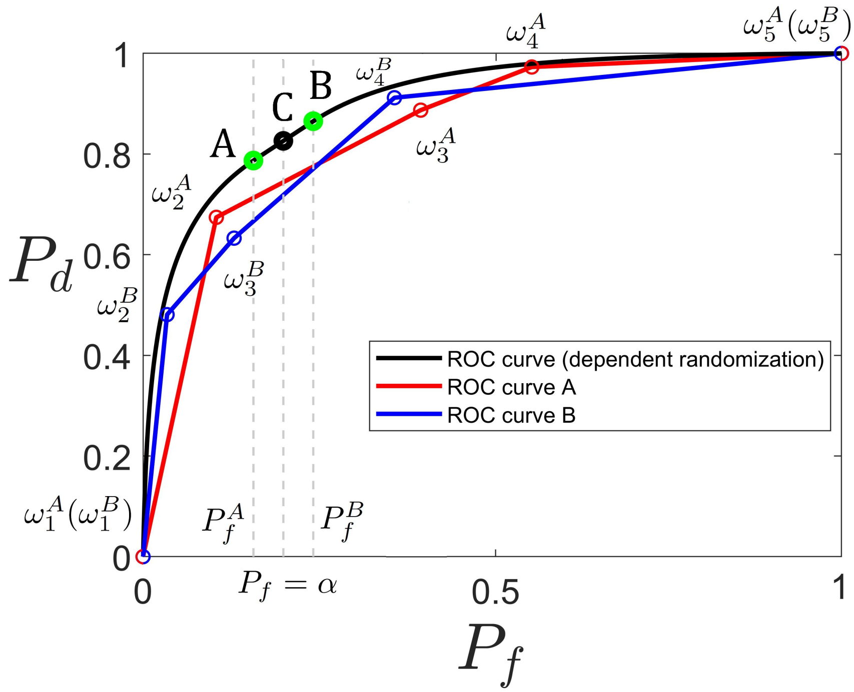

Figure 6.3 The ROC curve of the system with dependent randomization is shown by the black curve. For $\alpha \in (P_f^A, P_f^B)$, C is the desired operating point of the system (black circle). A and B (green circles) are the operating points used to generate C through a randomization procedure. When the second LD loses synchronization ($Y = \{LD1\}$, $\overline{Y} = \{LD2\}$), if A is selected the *ROC curve* A is effective (shown in red); if B is selected the *ROC curve* B is effective (shown in blue).

6.4 Satisfying the Probability of False Alarm Constraint and Maximizing the Probability of Detection

Let $a = (P_f^a, P_d^a)$ be an operating point of *system* A on *ROC curve* A and $b = (P_f^b, P_d^b)$ be an operating point of *system* B on *ROC curve* B. Points a and b are selected such that upper limit of the probability of false alarm of the system, α, satisfies $P_f^a \leq \alpha \leq P_f^b$ or $P_f^b \leq \alpha \leq P_f^a$. In order to meet the probability of false alarm constraint ($P_f = \alpha$), points a and b need to be found such that:

$$\alpha = pP_f^a + (1-p)P_f^b. \tag{6.1}$$

This design would yield the probability of detection

$$P_d = pP_d^a + (1-p)P_d^b. \tag{6.2}$$

The resulting operating point is denoted as $c = (P_f^c, P_d^c) = (\alpha, pP_d^a + (1-p)P_d^b)$. The next step is to locate the specific point on *ROC curve A*, denoted A' (so $a = A'$), and the specific point on *ROC curve B*, denoted as B' (so $b = B'$) that allow the system to maximize the probability of detection while satisfying the probability of false alarm constraint. The optimal resulting system operating point $C' = (P_f^{C'}, P_d^{C'})$ is on the line segment connecting A' and B', where

$$P_f^{C'} = pP_f^{A'} + (1-p)P_f^{B'}, \tag{6.3}$$

$$P_d^{C'} = pP_d^{A'} + (1-p)P_d^{B'}. \tag{6.4}$$

It can be shown that for $P_d^{C'}$ in (6.4) to be the maximum probability of detection either (i) $A' \in \Omega^A$ or (ii) $B' \in \Omega^B$ or both ($A' \in \Omega^A$ and $B' \in \Omega^B$). The proof can be found in Section A.1. Here is an intuitive explanation: The resulting operating point of the system would be on the line segment connecting a point on *ROC curve A* and a point on *ROC curve B*. The line segment can be "lifted" to improve the probability of detection of the resulting operating point. During the process of "lifting", the length of the line segment is adjustable to keep its endpoints on different ROC curves. The resulting probability of detection would stop growing when the line segment is about to "leave" its corresponding ROC curve. The line segment can only "leave" the *ROC curve A* at a point in Ω^A and the *ROC curve B* at a point in Ω^B. Section 6.5 finds A' from Ω^A if $A' \in \Omega^A$ and B' from Ω^B if $B' \in \Omega^B$. Therefore at least one of A' and B' can be found. Occasionally, A' and B' are both realizable by deterministic strategy (both $A' \in \Omega^A$ and $B' \in \Omega^B$ are true) thus both A' and B' can be found by using the procedure in Section 6.5. In most cases, one of A' and B' is realized by randomization at the DFC. In this circumstance, Section 6.6 is needed to find A' if $A' \notin \Omega^A$ and B' from Ω^B if $B' \notin \Omega^B$.

6.5 Finding A' from Ω^A if $A' \in \Omega^A$ and B' from Ω^B if $B' \in \Omega^B$ (at least one of A' and B' can be Found)

A' can be found by examining every points in Ω^A and B' can be found by examining every points in Ω^B. This can be done by using the following steps:

(a) For each operating point $a = (P_f^a, P_d^a) \in \Omega^A$, the probability of the false alarm of the corresponding operating point $b = (P_f^b, P_d^b)$ on *ROC curve B* can be calculated by using (6.1) ($P_f^b = \frac{\alpha - pP_f^a}{1-p}$). Since each probability of detection is paired with exactly one probability of false alarm on *ROC curve B*, P_f^b can be used to locate b on *ROC curve B* and define P_d^b. The resulting probability of detection of the system can be calculated by using (6.2). The resulting probability of detection and the corresponding a and b for each $a \in \Omega^A$ are stored.

(b) For each operating point $b = (P_f^b, P_d^b) \in \Omega^B$, the probability of the false alarm of the corresponding operating point on *ROC curve A* ($P_f^a = \frac{\alpha-(1-p)P_f^b}{p}$) can be calculated by using (6.1). P_f^a can be used to locate a on *ROC curve A* and define P_d^a. The resulting probability of detection of the system can be calculated by using

(6.2). The resulting probability of detection and the corresponding a and b for each $b \in \Omega^B$ are stored.

(c) Let $P_d^{C'}$ be the highest probability of detection found for all the pairs examined in steps (a) and (b). A' and B' are the pair of values of a and b which corresponded to the highest $P_d^{C'}$ for the final design.

Computational complexity: Steps (a) and (b) examine $m_A + m_B$ points (m_A points in Ω^A and m_B points in Ω^B) in order to find A' if $A' \in \Omega^A$ and B' if $B' \in \Omega^B$. An improved procedure which requires the examination of at most $log_2(m_A + m_B)$ points in Ω^A and Ω^B is available in Section A.2.

6.6 Finding A' if $A' \notin \Omega^A$ and B' if $B' \notin \Omega^B$ (Applying Randomization at the DFC)

In most cases, when $P_d^{C'}$ is maximized, one of the points A' and B' is realized by randomization at the DFC and the other is realized by a deterministic strategy (since it is an element of Ω^A or Ω^B). The situation that B' is randomized operating point ($A' \in \Omega^A$ and $B' \notin \Omega^B$) is discussed first. In this circumstance $P_f^{B'} = \frac{\alpha - pP_f^{A'}}{1-p}$ (from (6.1)). B' is on a line segment connecting two operating points in Ω^B, denoted as ω_a^B and ω_b^B.

Let the probabilities needed to redesign B' by hopping between using ω_a^B and ω_b^B be q' and $1-q'$, respectively. Then $P_f^{B'}$ can be expressed as:

$$P_f^{B'} = q'P_f^{\omega_a^B} + (1-q')P_f^{\omega_b^B}. \tag{6.5}$$

Therefore $P_f^{C'}$ is a weighted sum of $P_f^{A'}$, $P_f^{\omega_a^B}$ and $P_f^{\omega_b^B}$:

$$P_f^{C'} = pP_f^{A'} + (1-p)[q'P_f^{\omega_a^B} + (1-q')P_f^{\omega_b^B}]. \tag{6.6}$$

Since $P_f^{C'} = \alpha$, q' can be calculated as:

$$q' = \frac{\alpha - pP_f^{A'} - (1-p)P_f^{\omega_b^B}}{(1-p)(P_f^{\omega_a^B} - P_f^{\omega_b^B})}. \tag{6.7}$$

The probability of detection $P_d^{C'}$ is

$$P_d^{C'} = pP_d^{A'} + p[q'P_d^{\omega_a^B} + (1-q')P_d^{\omega_b^B}]. \tag{6.8}$$

Similarly, when A' is a randomized operating point ($A' \notin \Omega^A$ and $B' \in \Omega^B$), $P_d^{C'}$ becomes:

$$P_d^{C'} = (1-p)P_d^{B'} + p[q''P_d^{\omega_a^A} + (1-q'')P_d^{\omega_b^A}], \tag{6.9}$$

ω_a^A and ω_b^A are the two end points of the line segment on the *ROC curve* A which A' locates on. Let q'' and $1-q''$ be the probabilities of using ω_a^A and ω_b^A respectively. q'' satisfies:

$$\alpha = (1-p)P_f^{B'} + p[q''P_f^{\omega_a^A} + (1-q'')P_f^{\omega_b^A}]. \tag{6.10}$$

q'' is :

$$q'' = \frac{\alpha - (1-p)P_f^{B'} - pP_f^{\omega_b^A}}{p(P_f^{\omega_a^A} - P_f^{\omega_b^A})}. \tag{6.11}$$

In the case $A' \in \Omega^A$ and $B' \in \Omega^B$, both A' and B' are realized by deterministic strategies. The probability of detection can be calculated by (6.4).

6.7 Numerical Examples

The redesign algorithm is implemented to the 2-LD system in Section 4.1 with $\overline{Y} = \{LD2\}$ and the 3-LD system in Section 4.2 with $\overline{Y} = \{LD3\}$. The detail of the implementation can be found in Section A.3.

6.7.1 2-LD system

In Figure 6.4, the black curve is the ROC curve of the 2-LD example in Section 4.1 when using dependent randomization. The design input and output of the 2-LD system employing dependent randomization with $\alpha = 0.2009$ was shown in Table 4.1. The operating point of the system is $C = (0.2009, 0.8261)$, shown by the black circle. C is generated by operating at $A = (0.1581, 0.7870)$ with probability $p = 0.5$ and at $B = (0.2437, 0.8652)$ with probability $1 - p$.

If $Y = \{LD1\}$, $\overline{Y} = \{LD2\}$, there are four possible operating points: A, B, $M1' = (0.0518, 0.5614)$, and $M2' = (0.4761, 0.9586)$, determined by $(\gamma_0^A, \gamma_1^A, \gamma_2^A)$, $(\gamma_0^B, \gamma_1^B, \gamma_2^B)$, $(\gamma_0^A, \gamma_1^A, \gamma_2^B)$, and $(\gamma_0^B, \gamma_1^B, \gamma_2^A)$. A, B, $M1'$, and $M2'$ are shown by the green circles. The resulting operating point $W' = (0.2324, 0.7930)$, shown by the purple circle is calculated as

$$P_f^{W'} = p^2 P_f^A + (1-p)^2 P_f^B + p(1-p) P_f^{M1'} + (1-p)p P_f^{M2'}, \tag{6.12}$$

$$P_d^{W'} = p^2 P_d^A + (1-p)^2 P_d^B + p(1-p) P_d^{M1'} + (1-p)p P_d^{M2'}. \tag{6.13}$$

In this case, $\Phi^A = \{(P_{f1}^A, P_{d1}^A), (pP_{f2}^A + (1-p)P_{f2}^B, pP_{d2}^A + (1-p)P_{d2}^B)\}$. The *ROC curve A* is shown as the red curve; $\Phi^B = \{(P_{f1}^B, P_{d1}^B), (pP_{f2}^A + (1-p)P_{f2}^B, pP_{d2}^A + (1-p)P_{d2}^B)\}$. The *ROC curve B* is shown as the blue curve. Ω^A and Ω^B then can be found, shown in Table 6.2. By using the proposed algorithm, when $A' = (0.1049, 0.6742)$

and $B' = (0.2968, 0.8410)$, the probability of detection is maximized. $A' \in \Omega^A$ and $B' \notin \Omega^B$. A' is shown as the cyan circle. It is achieved when the DFC uses the *AND fusion rule* ($\gamma_0^{A'}(u1, u2) = u_1 \& u_2$). $P_f^{B'}$ can be calculated by (6.1) and B is shown by the purple triangle. B' is generated by the randomized fusion rule $\gamma_0^{B'}$, which requires the system hopping between $\omega_a^B = (0.1304, 0.6328)$ and $\omega_b^B = (0.3599, 0.9199)$. ω_a^B (achieved by the fusion rule such that $u_0 = u_1$) is used with probability q' and ω_b^B (achieved by the *OR fusion rule*) is used with probability $1 - q'$, where $q' = 0.2748$, calculated by (6.7). ω_a^B and ω_b^B are shown as the cyan triangles.

In this example, when the DFC realizes that the $LD2$ loses synchronization, if γ_1^A is selected at the $LD1$ ($p = 0.5$), the system operates at point A'; if γ_1^B is selected at the $LD1$ ($1 - p = 0.5$), the system operates at point ω_a^B with probability $q' = 0.2748$ and operates at point ω_b^B with probability $1 - q' = 0.7252$. The maximized probability of detection is $P_d^{C'} = 0.7547$, calculated from (6.4). $C' = (0.2009, 0.7547)$ is shown by the purple square. Due to the loss of synchronization, the probability of detection drops from $P_d^C = 0.8261$ to $P_d^{C'} = 0.7547$.

Table 6.2 provides a summary of the input and output of the redesign algorithm for the 2-LD system employing dependent randomization when $LD2$ lost synchronization.

Figure 6.5 and Table 6.3 compare the operating points of the 2-LD system under the Neyman-Pearson criterion with $\alpha = 0.2009$ for the following detection strategies:

(a) deterministic strategy and randomization at the DFC (G, blue circle);

(b) dependent randomization (C, black circle);

(c) dependent randomization when the LDs group lost synchronization with the DFC before the redesign algorithm is applied ($W^* = (0.2640, 0.7600)$, cyan circle)/ after the redesign algorithm is applied (C^*, cyan square);

(d) dependent randomization when the $LD2$ lost synchronization with the $LD1$ and the DFC before the redesign algorithm is applied ($W' = (0.2324, 0.7930)$, purple circle)/ after the redesign algorithm is applied (C', purple square); and

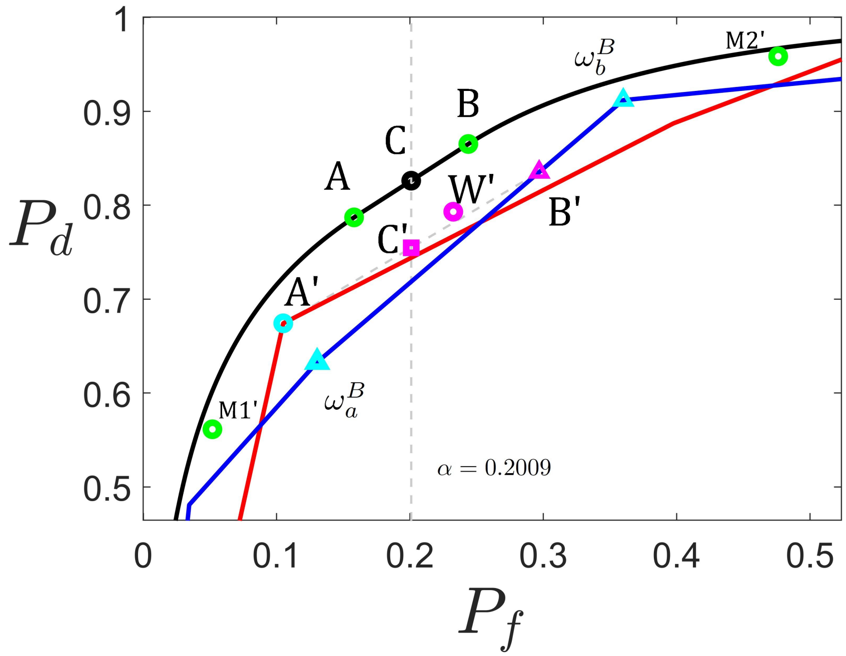

Figure 6.4 C is the desired operating point of the system with dependent randomization (black circle). When $Y = \{LD1\}$ and $\overline{Y} = \{LD2\}$, A, B, $M1'$ and $M2'$ are the four possible operating points (green circles). W' is the equivalent operating point (purple circle). The *ROC curve A* is shown as the red curve. The *ROC curve B* is shown as the blue curve. C' is the operating point with maximized probability of detection given $\alpha = 0.2009$, shown by the purple square.

(e) dependent randomization when two LDs lost synchronization with each other and the DFC before the redesign algorithm is applied ($W'' = (0.2044, 0.6401)$, yellow circle)/ after the redesign algorithm is applied(C'', yellow square).

6.7.2 3-LD system

Returning to the 3-LD system (Section 4.2), Figure 6.6 shows what happen when $Y = \{LD1, LD2\}$ and $\overline{Y} = \{LD3\}$ and when the probability of false alarm constraint is $P_f \leq \alpha = 0.1708$. In Figure 6.6, the black curve is the ROC curve of the 3-LD system with dependent randomization studied in Section 4.2. The specified probability of false alarm $\alpha = 0.1708$. When the entire system is synchronized, it operates at $A = (0.104, 0.784)$ with probability $p = 0.6$ and at $B = (0.271, 0.936)$ with probability $1 - p = 0.4$, respectively, to achieve $C = (0.1708, 0.8448)$. C is shown by the black circle.

Table 6.2 The Output the 2-LD System Employing Dependent Randomization Before and After a Corrective Action is Taken when $Y = \{LD1\}$ and $\overline{Y} = \{LD2\}$

Input of the redesign algorithm for the 2-LD system when $LD2$ lost synchronization	
The design input of dependent randomization (Table 4.1)	1. The number of local detectors, $n = 2$ 2. The probability of false alarm constraint, $\alpha = 0.2009$
The design output of dependent randomization (Table 4.1)	3. The local operating points of A: $(P_{f1}^A, P_{d1}^A) = (P_{f2}^A, P_{d2}^A) = (0.3976, 0.8871)$, The local operating points of B: $(P_{f1}^B, P_{d1}^B) = (P_{f2}^B, P_{d2}^B) = (0.1304, 0.6328)$. 4. The probability of selecting A, $p = 0.5$.
Information at the synchronized LDs	5. Numbers of synchronized LDs, $m = 1$ 6. Identity of all synchronized LDs, $Y = \{LD1\}$
Output of the redesign algorithm for the 2-LD system when $LD2$ lost synchronization	
1. $\Omega^A = \{(0,0), (0.1049, 0.6742), (0.3976, 0.8871), (0.5566, 0.9729), (1,1)\}$, $\Omega^B = \{(0,0), (0.0344, 0.4809), (0.1304, 0.6328), (0.3599, 0.9119), (1,1)\}$	
2. Two operating points $A' = (0.1049, 0.6742) \in \Omega^A$ and $B' = (0.2968, 0.8410) \notin \Omega^B$, which allow $P_f^{C'}$ from (6.3) satisfying the probability of false alarm constraint α and achieving the highest probability of detection	
3. The deterministic fusion rule $\gamma_0^{A'}$ (*AND fusion rule*) used to achieve A'	
4. The randomized fusion rule $\gamma_0^{B'}$ used to achieve B', which requires the system operating at $\omega_a^B = (0.1304, 0.6328)$ (achieved by the fusion rule such that $u_0 = u_1$) with probability q' and $\omega_b^B = (0.3599, 0.9199)$ (achieved by the *OR fusion rule*) with probability $1 - q'$, where $q' = 0.2748$, calculated by (6.7)	
5. The operating point of the non-synchronized system after the corrective action is taken, $\boldsymbol{C' = (0.2009, 0.7547)}$, calculated by (6.6) and (6.8), which is achieved by operating at A' with probability p and B' with probability $1 - p$	

Table 6.3 The Operating Points of the 2-LD System Employing Different Detection Strategies under the Neyman-Pearson Criterion with $\alpha = 0.2009$ (Corresponding to Figure 6.5)

		$\alpha = 0.2009$
1	Deterministic strategy	$G = (0.2009, 0.8217)$
2	Randomization at the DFC	$G = (0.2009, 0.8217)$
3	Dependent randomization (synchronized)	$C = (0.2009, 0.8261)$
4	Dependent randomization (the DFC is unsynchronized with the LDs group)	$C^* = (0.2009, 0.7005)$
5	Dependent randomization (the 2^{nd} LD is unsynchronized with the DFC and other LDs)	$C' = (0.2009, 0.7547)$
6	Dependent randomization (all LDs and the DFC are unsynchronized)	$C'' = (0.2009, 0.7008)$

A is achieved when all 3 LDs operate at $(0.2, 0.7)$, i.e. $(P_{fk}, P_{dk}) = (0.2, 0.7), k = 1, 2, 3$, and the DFC uses a “2 out of 3 rule”, i.e., if there exists two LDs decide

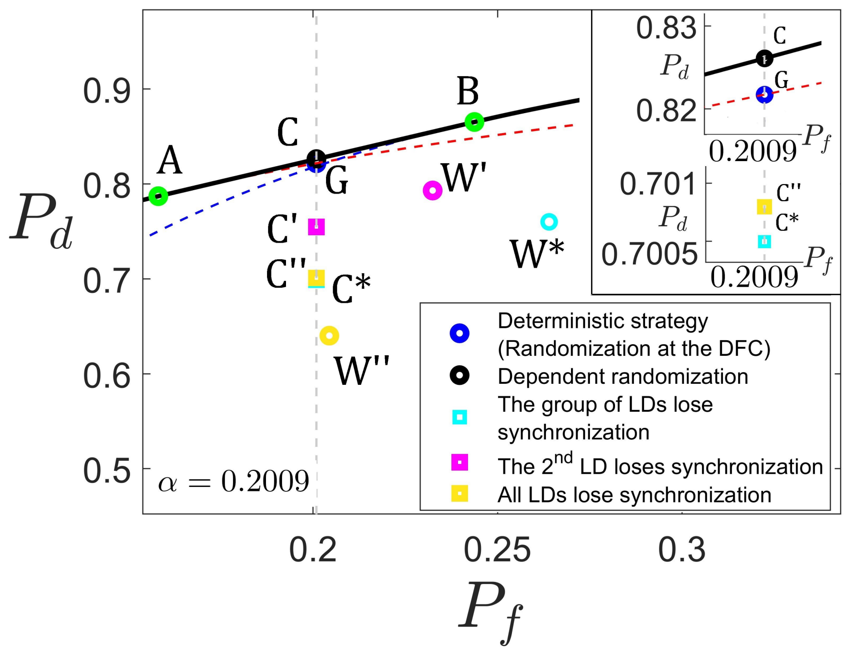

Figure 6.5 The operating points of the 2-LD system employing different detection strategies under the Neyman-Pearson criterion with $\alpha = 0.2009$.

1, $u_0 = 1$; otherwise $u_0 = 0$. B is achieved when all 3 LDs operate at $(0.1, 0.6)$, i.e. $(P_{fk}, P_{dk}) = (0.1, 0.6), k = 1, 2, 3$, and the DFC uses a "1 out of 3 rule", i.e., if there exists one LD decides 1, $u_0 = 1$; otherwise $u_0 = 0$. When the 3^{rd} LD loses synchronization ($Y = \{LD1, LD2\}$ and $\overline{Y} = \{LD3\}$), the four possible operating points are A, B, $M1'$, and $M2'$, shown by green circles. The equivalent operating point is $W' = (0.1826, 0.8386)$, shown by the purple circle. Table 6.4 summarizes the input and output of the redesign algorithm for the 3-LD system employing dependent randomization when $LD3$ lost synchronization.

Figure 6.7 compares the operating points of the 3-LD system under the Neyman-Pearson criterion with $\alpha = 0.1708$ for the following detection strategies:

(a) deterministic strategy (G, blue circle);

(b) randomization at the DFC (E, red circle);

(c) dependent randomization (C, black circle);

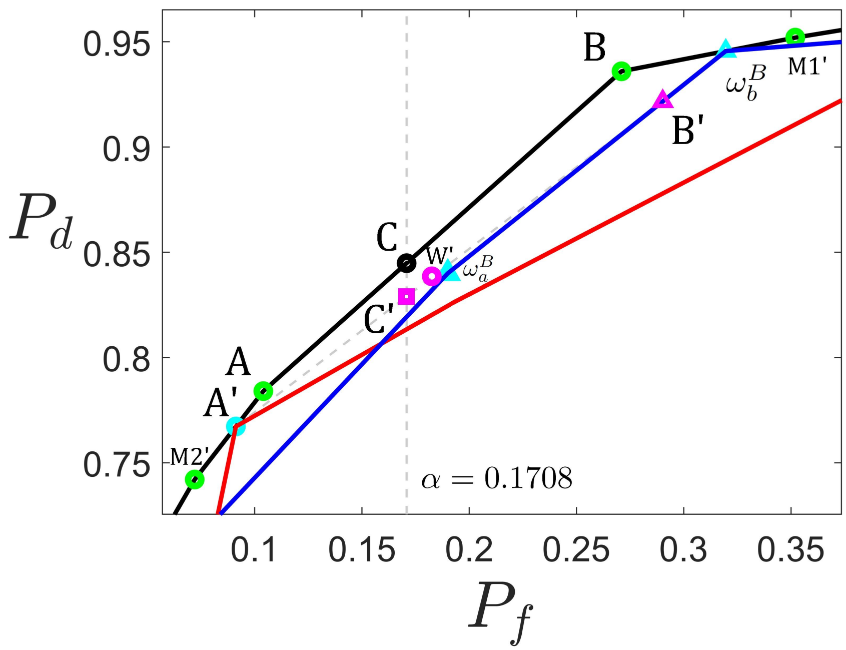

Figure 6.6 C is the desired operating point of the system with dependent randomization (black circle). When $Y = \{LD1, LD2\}$ and $\overline{Y} = \{LD3\}$, A, B, $M1'$ and $M2'$ are the four possible operating points (green circles). W' is the equivalent operating point (purple circle). *ROC curve A* and *ROC curve B* are shown as the red curve and the blue curve, respectively. C' is the operating point maximizing the probability of detection given $\alpha = 0.1708$, shown by the purple square.

(d) dependent randomization when the LDs group lost synchronization with the DFC before the redesign algorithm is applied ($W^* = (0.2046, 0.8210)$, cyan circle)/ after the redesign algorithm is applied (C^*, cyan square);

(e) dependent randomization when the $LD2$ lost synchronization with the $LD1$ and the DFC before the redesign algorithm is applied ($W' = (0.1826, 0.8386)$, purple circle)/ after the redesign algorithm is applied (C', purple square); and

(f) dependent randomization when two LDs lost synchronization with each other and the DFC before the redesign algorithm is applied ($W'' = (0.2223, 0.8380)$, yellow circle)/ after the redesign algorithm is applied (C'', yellow square).

Table 6.5 shows the operating points of the 3-LD system employing different detection strategies under the Neyman-Pearson criterion with (a) $\alpha = 0.1708$ and (b) $\alpha = 0.05$. In line 4 of the third column (corresponding to $\alpha = 0.05$). Although the DFC lost synchronization with the LDs group in dependent randomization, the performance of the system has not been affected. The reason is that when

Table 6.4 The Output the 3-LD System Employing Dependent Randomization before and after a Corrective Action is Taken when $Y = \{LD1,\ LD2\}$ and $\overline{Y} = \{LD3\}$

Input of the redesign algorithm for the 3-LD system when $LD3$ lost synchronization	
The design input of dependent randomization (Table 4.3)	1. The number of local detectors, $n = 3$ 2. The probability of false alarm constraint, $\alpha = 0.1708$
The design output of dependent randomization (Table 4.3)	3. The local operating points of A: $(P_{fk}, P_{dk}) = (0.2, 0.7), k = 1, 2, 3,$ The local operating points of B: $(P_{fk}, P_{dk}) = (0.1, 0.6), k = 1, 2, 3.$ 4. The probability of selecting A, $p = 0.6$.
Information of synchronized LDs	5. Numbers of synchronized LDs, $m = 2$ 6. Identity of all synchronized LDs, $Y = \{LD1, LD2\}$
Output of the redesign algorithm for the 3-LD system when $LD3$ lost synchronization	
1. $\Omega^A = \{(0,0), (0.0064, 0.3234), (0.0576, 0.6006), (0.0912, 0.7672), (0.1936, 0.8266), (0.4624, 0.9694), (1,1)\}$, $\Omega^B = \{(0,0), (0.0016, 0.2376), (0.0100, 0.3600), (0.0388, 0.6768), (0.1900, 0.8400), (0.3196, 0.9456), (1,1)\}$	
2. Two operating points $A' = (0.0912, 0.7672) \in \Omega^A$ and $B' = (0.2902, 0.9216) \notin \Omega^B$, which allow $P_f^{C'}$ from (6.3) satisfying the probability of false alarm constraint α and achieving the highest probability of detection	
3. The deterministic fusion rule $\gamma_0^{A'}$ (*2 out of 3 rule*) used to achieve A'	
4. The randomized fusion rule $\gamma_0^{B'}$ used to achieve B', which requires the system operating at $\omega_a^B = (0.1900, 0.8400)$ (achieved by the fusion rule such that $u_0 = u_1 \vert u_2$) with probability q' and $\omega_b^B = (0.3196, 0.9456)$ (achieved by the *1 out of 3 rule*) with probability $1 - q'$, where $q' = 0.2748$, calculated by (6.7)	
5. The operating point of the non-synchronized system after the corrective action is taken, $\boldsymbol{C' = (0.1708, 0.8290)}$, calculated by (6.6) and (6.8), which is achieved by operating at A' with probability p and B' with probability $1 - p$	

$\alpha = 0.05$, dependent randomization requires the 3-LD system hopping between two operating points with the same global fusion rule. In this circumstance, dependent randomization is "randomization at the LDs only" and the DFC does not participate in the randomization. Therefore, the loss of synchronization between the LDs group and the DFC has no influence to the system performance.

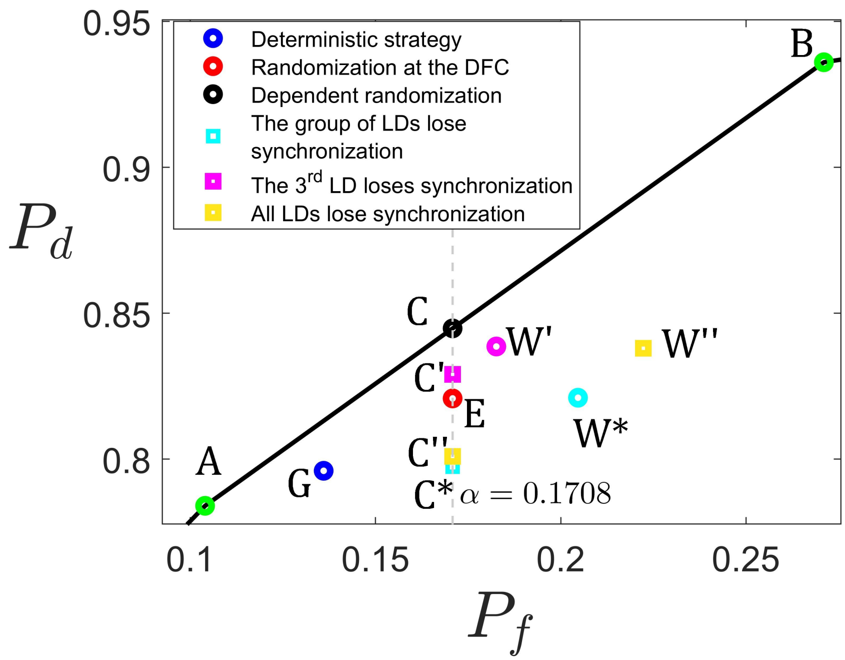

Figure 6.7 The operating points of the 3-LD system employing different detection strategies under the Neyman-Pearson criterion with $\alpha = 0.1708$.

Table 6.5 The Operating Points of the 3-LD System Employing Different Detection Strategies under the Neyman-Pearson Criterion with (a) $\alpha = 0.1708$ (Corresponding to Figure 6.7) and (b) $\alpha = 0.05$

		$\alpha = 0.1708$	$\alpha = 0.05$
1	Deterministic strategy	$G = (0.1360, 0.7960)$	$(0.0460, 0.6960)$
2	Randomization at the DFC	$E = (0.1708, 0.8208)$	$(0.0500, 0.7000)$
3	Dependent randomization (synchronized)	$C = (0.1708, 0.8448)$	$(0.0500, 0.7031)$
4	Dependent randomization (the DFC is unsynchronized with the LDs group)	$C^* = (0.1708, 0.7974)$	$(0.0500, 0.7031)$
5	Dependent randomization (the 3^{rd} LD is unsynchronized with the DFC and other LDs)	$C' = (0.1708, 0.8290)$	$(0.0500, 0.5704)$
6	Dependent randomization (all LDs and the DFC are unsynchronized)	$C'' = (0.1708, 0.8009)$	$(0.0500, 0.5534)$

CHAPTER 7

ADAPTIVE FUSION

Some of the probabilities needed for the designs of parallel decentralized binary decision fusion architecture may not be immediately available. These probabilities can sometimes be estimated from the data. In this chapter, several adaptive fusion approaches are discussed and compared. An algorithm that integrates the decisions of these algorithms is proposed, demonstrating superior performance over each individual algorithm acting alone.

7.1 Chair - Varshney Rule

In [1], an optimal data fusion rule for this architecture in Figure 1.1 is developed by Chair and Varshney. They assume that the LDs use fixed decision rules and that their observations are statistically independent conditioned on the hypothesis. Let $P_{mk} = Prob(u_k = 0|H_1)$ be the probability of missed detection by the k^{th} LD ($P_{mk} = 1 - P_{dk}$) and $P_m = Prob(u_0 = 0|H_1)$ be the probability of missed detection by the DFC ($P_m = 1 - P_d$). To implement the optimal data fusion rule, the DFC needs to know the probabilities of false alarm and missed detection of each LD. The probability of error (Bayes cost in (1.1) with $C_{01} = C_{10} = 1$ and $C_{00} = C_{11} = 0$) by the global decision u_0 can be expressed as:

$$P_e = P_f P_0 + (1 - P_m)P_1 \tag{7.1}$$

The global decision u_0 has the minimum probability of error if:

$$u_0 = U_{-1}\{\sum_{k=1}^{n}[log(\frac{1-P_{mk}}{P_{fk}})u_k + log(\frac{1-P_{fk}}{P_{mk}})(1-u_k)] - log\ w_0\} \tag{7.2}$$

where w_0 is the decision threshold (7.3), U_{-1} is the unit step function (7.4).

$$w_0 = log(\frac{1-P_0}{P_0}) \tag{7.3}$$

$$U_{-1}(x) = \begin{cases} 0 & if\ x \leq 0 \\ 1 & if\ x > 0 \end{cases} \tag{7.4}$$

The weight of the k^{th} local decision is

$$w_k = \begin{cases} log(\frac{1-P_{mk}}{P_{fk}}) & for\ u_k = 1 \\ \\ log(\frac{1-P_{fk}}{P_{mk}}) & for\ u_k = -1 \end{cases} \tag{7.5}$$

where w_k is the weight of k^{th} LD.

7.2 Methods for Estimation of Probabilities

In practice, P_0, P_{fk}, and P_{mk} in Equation (7.2), (7.3) are often unknown, requiring estimates and approximations to complete the design. Several methods were introduced for estimating these probabilities.

- The original version of the method by Kam & Naim (oK) [13]

- The original version of the method by Ansari *et al.* (oA) [15][14]

- The modified version of the method by Kam & Naim (mK) [16]

- The modified version of the method by Ansari *et al.* (mA) [16]

- The original method by Mirjalily *et al.* (M) [16]

Kam & Naim propose an on-line estimation method (oK) to evaluate the P_0, P_{fk}, P_{mk} for distributed Bayesian detection [13]. The method tunes P_{fk}, P_{mk} according to whether u_k agrees with u_0. Since the reference decision u_0 is not consistently correct, the estimates are biased. The oK algorithm uses the global values of P_m and P_f [23] to address the problem in part.

Ansari *et al.* come up with an estimation approach(oA) for w_k and w_0 in equations (7.3) and (7.5) [15][14]. This approach provides good estimates in some scenarios but suffers from some of the same bias-related shortcomings of the oK method. To reduce the bias, instead of using u_0, the reference decision of one LD is the fused decisions of the other $n-1$ LDs. The oA method modifies the estimation of the LD's probabilities only when it believes the reference decision is reliable. Decisions believed to be unreliable are ignored. However, ignoring part of the decision-set also results in bias.

A blind adaptive decision fusion rule (M), which takes advantage of the relation between the unknown probabilities and the joint probabilities of the decisions of three reference LDs, is presented by Mirjalily *et al.* [16]. When the system is comprised of a small number of LDs, this method could achieve high quality performance. However, since the estimates of the reference LDs determine the estimates of the other LDs, the M method becomes less effective as the number of LDs increases.

Modified versions of both oK and oA are proposed in [16]. The modified version of Kam & Naim's method (mK) ensures that the probabilities remain in a reasonable range and hence gains a substantial improvement in reliability. The tradeoff is that the method needs a longer convergence time compared with oK. The modified version of Ansari *et al.*'s method (mA) greatly reduces the number of failures by adopting a reliable initialization.

Extensive simulation shows that any one of these five methods could outperforms the others for some effecting points of P_0, P_{fk}, P_{mk}, and n. A selection algorithm that behaves on average better than each one of the five algorithms operating alone (under a Bayesian objective function) is desired [24]. The purpose of the sought algorithm is to discover which of the five methods is best near the estimated effecting point.

For simplicity, the LDs in the distributed detection system discussed in this chapter are assumed to be identical, i.e., $P_{fk} = P_f$, $P_{mk} = P_m$, $\forall k$.

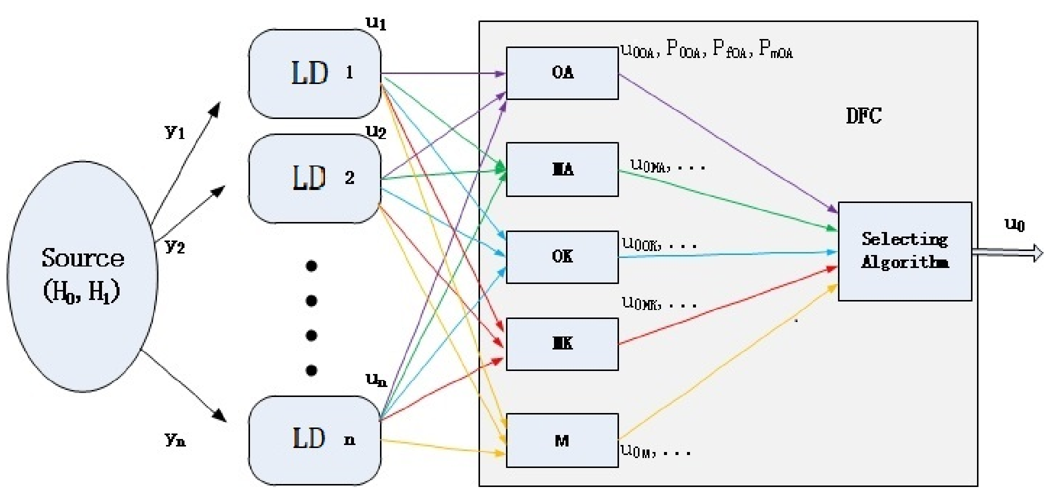

Figure 7.1 The model of proposed algorithm.

7.3 Methodology

The model of proposed algorithm is shown in Figure 7.1. The five adaptive algorithms are run in parallel and a selection algorithm integrates their decisions.

The five methods used in this chapter provide their estimations of P_0, P_f, P_m. Each method also produces a decision by using the Chair-Varshney rule [1]. The output of method i is therefore these probabilities, P_{0i}, P_{fi}, P_{mi}, and the decision u_{0i}, $i \in \{oA, oK, mA, mK, M\}$. The criterion to evaluate the performance of each method in simulation is the fraction of correct decisions it makes from a sequence of observed inputs. The best method is the one which exhibits the highest fraction of correct decisions.

7.3.1 Archival Data Base of Algorithm Performance

A data base of archival data records which method possessed the best performance in each recorded reference point (combinations of different P_0, P_f, and P_m). The data base could be compiled off-line or "on the fly." An excerpt from such data base for $n = 5$ is shown in Figure 7.2. The archival "winners" in each reference point are marked on the graph with their symbols, e.g., for point $(P_0, P_f, P_m) = (0.1, 0.15, 0.15)$, mA is the "winner." If there are multiple winners in a reference point, all their symbols are included, e.g., both mK and M are "winners" in point $(0.1, 0.15, 0.17)$. A reference point is blank if all five methods have identical performance there, e.g., point $(0.2, 0.12, 0.18)$.

The data base provides rough information for figuring out which methods should be considered. For example, in Figure 7.2, the estimated effecting point P_0, P_f, P_m of a certain system is shown as the black dot. Intuitively, it is reasonable to look at the decisions of the mA, M and mK methods in order to decide what to do at the black-dot location. The reason is that these methods outperform the others around this 'black-dot' location.

7.3.2 Selection algorithm

The proposed algorithm operates at two stages.

In the first stage, the less-reliable methods are eliminated from further consideration according to their performance at the effecting point. After that, the probabilities obtained from the more-reliable methods are averaged to create the estimate, P_{0r}, P_{fr}, P_{mr}.

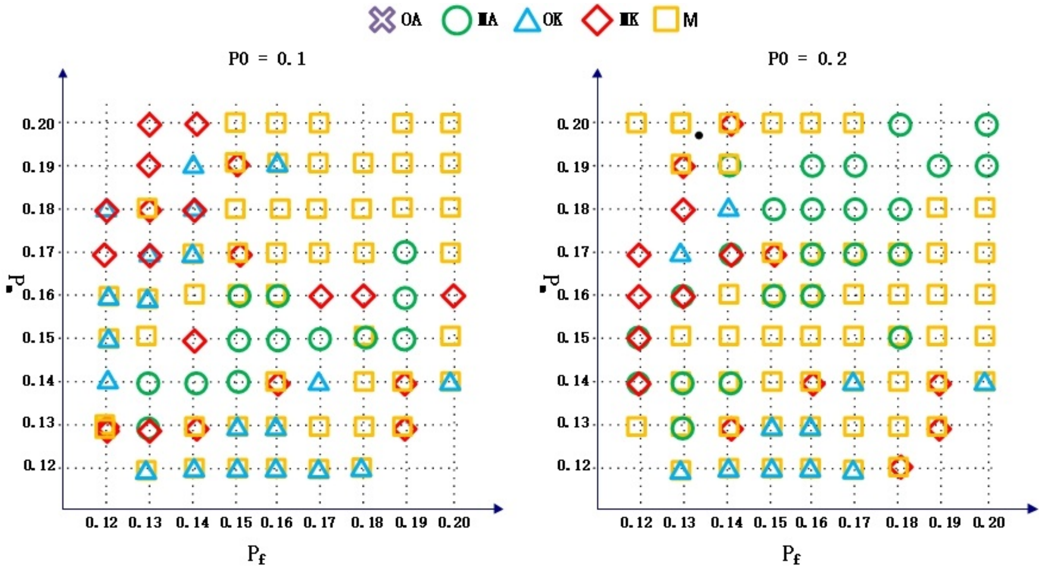

Figure 7.2 A part of graph for $n = 5$.

R is the set of reliable methods. N_R is the number of elements in R. P_{0i}, P_{fi}, P_{mi} are the estimated P_0, P_f, P_m by method i. a, b, c serve as thresholds for checking the reliabilities of some methods.

The estimates obtained by the mK and M algorithms were found to be more reliable than those of other methods over a significant subset of the space $\{P_0,\ P_f,\ P_m,\ n\}$. Therefore, these two methods are in the set R initially. mA is usually more reliable when P_0 is close to P_1. oK is considered reliable when its estimation is close to that of mK. oA is considered reliable when its estimation is close to mA when mA is reliable.

Selection Algorithm

Step 1:

Initialization: $R = \{mK, M\}$ %R includes mK,M at the beginning

If $\frac{1}{N_R}\sum(P_0 - 0.5) < a$, $i \in R$, **then**

$R = R\bigcup\{mA\}$ %R includes mA if P_0 is close to P_1

If $(|P_{0_{oK}} - P_{0_{mK}} < b|\ \&\ |P_{f_{oK}} - P_{f_{mK}} < c|\ \&\ |P_{m_{oK}} - P_{m_{mK}} < c|)$, **then**

$R = R \bigcup \{oK\}$ %R includes oK if oK's estimate is close to mK

If $(|P_{0_{oA}} - P_{0_{mA}} < b|$ & $|P_{f_{oA}} - P_{f_{mA}} < c|$ & $|P_{m_{oA}} - P_{m_{mA}} < c|$ & $(mA \in R))$, **then**

$R = R \bigcup \{oA\}$ %R includes oA if oA's estimate is close to mA and $mA \in R$

$P_{0r} = \frac{1}{N_R} \sum P_{0_i}$, $P_{fr} = \frac{1}{N_R} \sum (P_{f_i})$

$P_{mr} = \frac{1}{N_R} \sum (P_{m_i})$, $i \in R$

The current estimate of P_{0r}, P_{fr}, P_{mr} is referred as the "effecting point." The proposed algorithm consults the 4 reference points closest to the effecting point in the data base and then determines which one represents the best method to process the available information. Each neighboring reference point contains two pieces of information, namely, the best method at this reference point (based on past simulations or calculations (per [23])) and the distance between the point and the effecting point. Method i gains a score, C_{ij}, from the neighbor reference point j. If a certain method was historically the best method at the reference point, $C_{ij} = 1$; else, $C_{ij} = 0$. D_j is the distance between the effecting point and the neighboring reference point j. The total score obtained by any one method is a weighted sum of the score assigned to it by the 4 neighboring reference points closest to the effecting point. The algorithm seeks the method with the highest score.

Step 2:

$S_i = \sum_j^4 (C_{ij} \cdot \frac{1}{D_j}), i \in R,$

$Find\ i = arg\ max(S_i)$

An example is shown in Figure 7.3. The estimated P_{0r}, P_{fr}, and P_{mr} (the effecting point) is shown as the black dot on the graph. $P_{0r} = 0.21$, $P_{fr} = 0.112$, $P_{mr} = 0.198$. The 4 nearest neighbors are denoted $N1, N2, N3$, and $N4$. $D_1 =$

$\sqrt{(P_{0r}-0.2)^2+(P_{fr}-0.11)^2+(P_{mr}-0.20)^2} = 0.0104$. Similarly, $D_2 = 0.0130$, $D_3 = 0.0130$, $D_4 = 0.0151$. $S_{mA} = 1/D4 = 66.23$. $S_{mK} = 1/D2 + 1/D3 = 154.30$. $S_M = 1/D1 + 1/D2 + 1/D3 + 1/D4 = 316.76$. S_{oA} and S_{oK} are 0. Therefore the algorithm picks M, the method in [16], as the most appropriate method in this case.

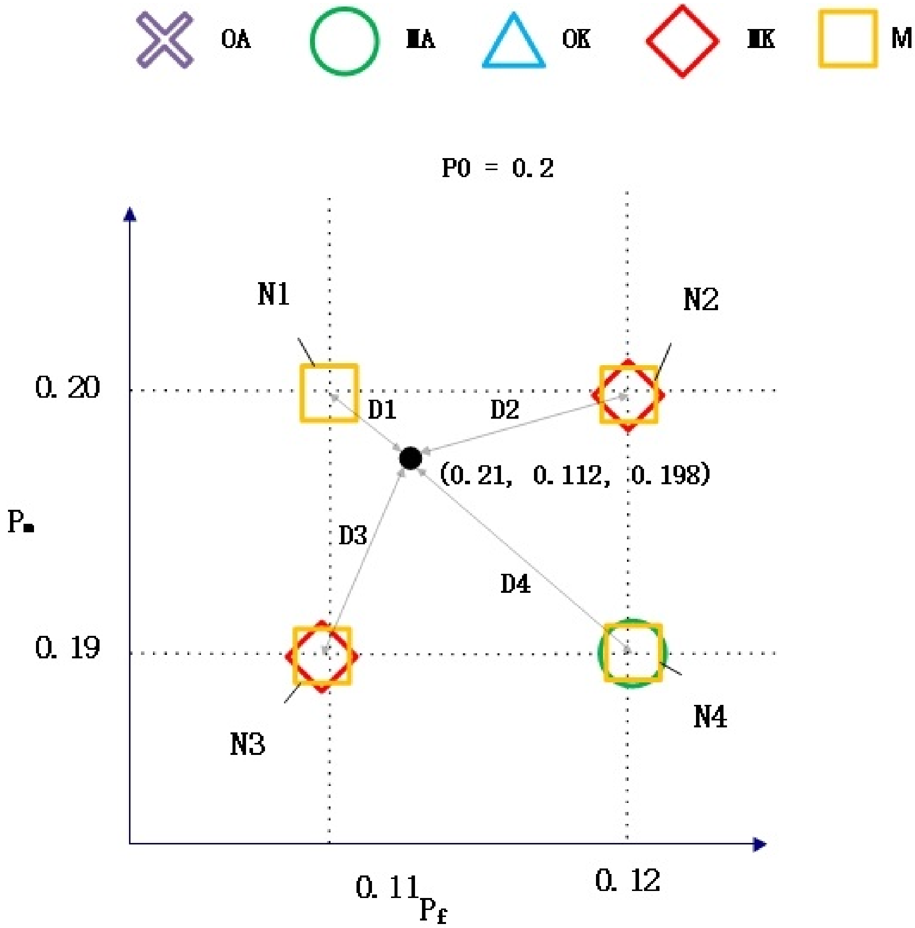

Figure 7.3 An example for the proposed algorithm.

7.4 Average performance in simulations

The selection algorithm per Figure 7.1 is tested multiple times with the following setting: $P_0 \in rand(0,1)$ (P_0 is a random number uniformly distributed between 0 and 1). $P_f \in rand(0,0.2)$, $P_m \in rand(0,0.2)$. In step 1 of the proposed algorithm, $a = 0.3, b = 0.1, c = 0.02$. Each one of the five algorithm is applied, as well as the new selection algorithm 2,000 times, using 10,000 inputs for each run. The experiments during which all methods had the same fraction of the $10,000$ decisions made correctly are discarded. The comparative results are studied when the techniques differed in performance (these are "contested runs").

Table 7.1 Ranking Distribution of each Method for 605 Contested Runs when $n = 5$

$n = 5$	1^{st}	2^{nd}	3^{rd}	4^{th}	5^{th}	err
oA	59	62	191	187	106	5.21%
mA	108	155	212	117	3	2.30%
oK	92	139	138	163	73	4.14%
mK	191	237	119	60	8	1.06%
M	362	172	48	23	0	0.99%
New algorithm	391	173	39	2	0	0.97%
CV	529	33	43	0	0	0.97%

Table 7.2 Ranking Distribution of each Method for 443 Contested Runs when $n = 7$

$n = 7$	1^{st}	2^{nd}	3^{rd}	4^{th}	5^{th}	err
oA	31	35	142	136	99	5.36%
mA	57	55	115	212	4	3.10%
oK	104	82	78	116	63	0.68%
mK	178	111	90	64	0	0.39%
M	137	121	166	19	0	0.40%
New algorithm	206	166	69	2	0	0.40%
CV	441	0	2	0	0	0.36%

Table 7.1 compares the performance of 7 methods, i.e., the five existing adaptive methods, the proposed selection algorithm, and the Chair-Varshney rule. In Table 7.1, $n = 5$, and 605 contested runs were available. Table 7.1 shows the error rate for each method (err) as well as the number of runs when the method was the most accurate(1^{st}); second most accurate(2^{nd}); etc. The sum of each column is not 605 since different methods may have the same rank. CV is the Chair-Varshney rule with complete knowledge of the performance probabilities. In Table 7.1, the result of the oA algorithm was the least satisfactory. It was superior to other methods in only 59 experiments out of 605. Algorithm mA was better than algorithm oA and algorithm mK was better than algorithm oK, which indicated that the modification in [16] did

improve the performance of oA and oK in these simulations. Algorithm M was the best of the existing five methods. It had the leading position in more than half of the experiments. The proposed selection algorithm took the 1^{st} and 2^{nd} places more times than algorithm M, and seldom dropped out of the top three algorithms. Table 7.1 also showed that given the full information on LD performance, the Chair-Varshney fusion rule was (of course) the best. In Table 7.2, the best existing adaptive method was mK, while the proposed algorithm still maintained better performance than all existing adaptive methods.

CHAPTER 8

END NOTES

In parallel decentralized binary decision fusion, dependent randomization can sometimes make the team's Receiver Operating Characteristic curve concave (if it was non-concave under other detection schemes). This effect improves the system's performance under a Neyman-Pearson criterion by realizing a higher probability of detection for the same upper bound on the probability of false alarm. Dependent randomization requires that the DFC and the LDs be synchronized, guided by a coordinated randomization scheme. The DFC and the LDs switch simultaneously together, back and forth, between two set of rules, viz., γ_0^A (for the DFC) and $\gamma_{LD}^A = \{\gamma_1^A, \ldots, \gamma_n^A\}$ (for the LDs); and γ_0^B (for the DFC) and $\gamma_{LD}^B = \{\gamma_1^B, \ldots, \gamma_n^B\}$ (for the LDs). However, if the synchronization between all decision makers in the system is lost, the system may exceed the permitted probability of false alarm. This dissertation revealed the consequences of synchronization loss in the following two sets of circumstances: (a) the DFC is not synchronized with the LDs group; and (b) some LDs are not synchronized with other LDs and with the DFC. Corrective action was devised in order to restore the detection system to compliance with the probability of false alarm constraint, at a cost of reduced probability of detection.

This dissertation also reviewed several design techniques for parallel decentralized binary decision fusion architectures, with and without feedback. The designs vary in performance and complexity, depending on the selection of objective functions and on compromises made between global optimality and computability. Several suboptimal designs exhibit relatively small loss in performance but significant computational advantage when compared to the optimal design. Finally, scenarios were studied where some parameters required by a design are not immediately available. These parameters were then estimated from observation data, using adaptive fusion techniques. The results of five adaptive decision fusion methods that do not assume knowledge of these probabilities are combined, to create a decision that appears superior performance compared to the performance of each of the five adaptive algorithms operating alone.

APPENDIX A

LOCATING A' AND B' (CHAPTER 6)

Section A.1 proves a result used in Section 6.4: $P_d^{C'}$, the probability of detection at the redesigned operating point, is the maximum probability of detection when either (i) $A' \in \Omega^A$ or (ii) $B' \in \Omega^B$ or both ($A' \in \Omega^A$ and $B' \in \Omega^B$). Section A.2 provides an efficient way to locate A' if $A' \in \Omega^A$ and B' if $B' \in \Omega^B$ (per Section 6.5) and shows the flowchart of the proposed corrective action in Chapter 6. Section A.3 presents the complete algorithm of the corrective action for partial loss of synchronization among the LDs when dependent randomization is employed (Chapter 6) and applies the algorithm to two examples.

When the DFC only synchronizes with the m LDs in Y, the system operates at some point on *ROC curve A* with probability p and some point on *ROC curve B* with probability $1-p$. *ROC curve A* can be drawn by connecting points in $\Omega^A = \{w_1^A = (0,0), w_2^A, \ldots, w_{mA-1}^A, w_{mA}^A = (1,1)\}$ sequentially and *ROC curve B* can be drawn by connecting points in $\Omega^B = \{w_1^B = (0,0), w_2^B, \ldots, w_{mB-1}^B, w_{mB}^B = (1,1)\}$ sequentially. The target to find a specific point on *ROC curve A*, denoted as A', and a specific point on *ROC curve B*, denoted as B' that allow the system to maximize the probability of detection while satisfying the probability of false alarm constraint. The optimal resulting system operating point $C' = (P_f^{C'}, P_d^{C'})$ is on the line segment connecting A' and B'.

A.1 Proof: $P_d^{C'}$ (6.4) is the Maximum Probability of Detection when either (i) $A' \in \Omega^A$ or (ii) $B' \in \Omega^B$ or both ($A' \in \Omega^A$ and $B' \in \Omega^B$)

Section A.1 shows that for $P_d^{C'}$ in (6.4) to be the maximum probability of detection either (i) $A' \in \Omega^A$ or (ii) $B' \in \Omega^B$ or both ($A' \in \Omega^A$ and $B' \in \Omega^B$).

Point $a = (P_f^a, P_d^a)$ is on *ROC curve A*, which is a concave linear ROC curve. P_d^a can be expressed as

$$P_d^a = f_A(P_f^a)P_f^a + b_A(P_f^a). \tag{A.1}$$

$f_A(P_f^a)$ and $b_A(P_f^a)$ are respectively the slope and the P_d-axis intercept of the line segment on *ROC curve A* that passes through point a. $f_A(P_f^a)$ is a decreasing piecewise-constant function of P_f^a and $b_A(P_f^a)$ is an increasing piecewise-constant function of P_f^a.

Similarly, point $b = (P_f^b, P_d^b)$ is on *ROC curve B*, which is a concave linear ROC curve. P_d^b can be expressed as

$$P_d^b = f_B(P_f^b)P_f^b + b_B(P_f^b). \tag{A.2}$$

$f_B(P_f^b)$ and $b_B(P_f^b)$ are respectively the slope and the P_d-axis intercept of the line segment on *ROC curve B* that passes through point b. $f_B(P_f^b)$ is a decreasing piecewise-constant function of P_f^b and $b_B(P_f^b)$ is an increasing piecewise-constant function of P_f^b.

Figure A.1 shows the relation between $a = (P_f^a, P_d^a)$ (cyan circle) on *ROC curve A*, $b = (P_f^b, P_d^b)$ (purple triangle) on *ROC curve B*, and the resulting operating point $c = (P_f^c, P_d^c) = (pP_f^a + (1-p)P_f^b = \alpha, pP_d^a + (1-p)P_d^b)$ (purple square), calculated by (6.1) and (6.2), which is the intersection of $P_f = \alpha$ and line ab.

From (6.1), when the probability of false alarm constraint is met, P_f^a is a decreasing function of P_f^b (and P_f^b is a decreasing function of P_f^a):

$$P_f^a = \frac{\alpha - (1-p)P_f^b}{p}, \text{ and,} \tag{A.3}$$

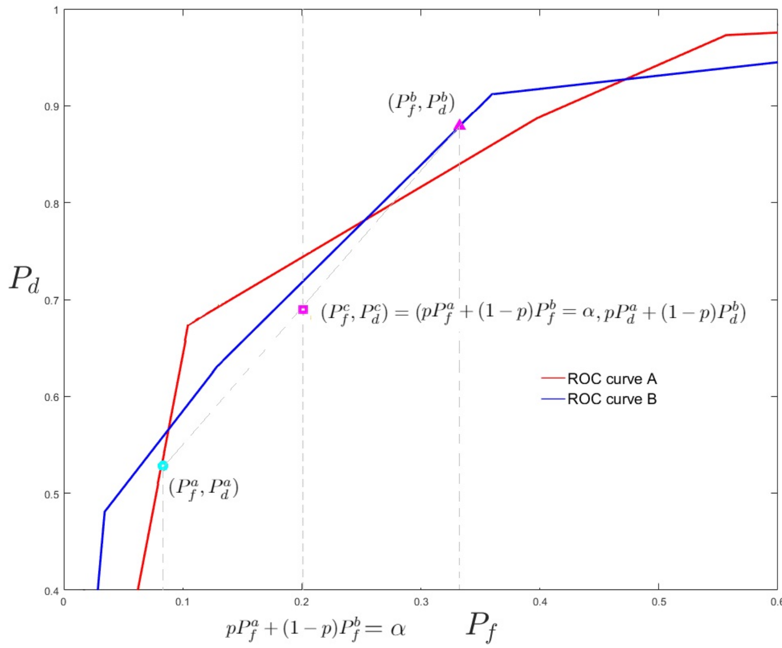

Figure A.1 The system operates at $a = (P_f^a, P_d^a)$ (cyan circle) with probability p. The system operates at $b = (P_f^b, P_d^b)$ (purple triangle) with probability $1-p$. The resulting operating point is $c = (P_f^c, P_d^c) = (pP_f^a + (1-p)P_f^b = \alpha, pP_d^a + (1-p)P_d^b)$, shown by the purple square.

$$P_f^b = \frac{\alpha - pP_f^a}{1-p}. \tag{A.4}$$

Combining (6.2), (A.1), and (A.2), P_d^c can be expressed as

$$\begin{aligned} P_d^c &\overset{\text{from (6.2)}}{=} pP_d^a + (1-p)P_d^b \\ &\overset{\text{from (A.1),(A.2)}}{=} p(f_A(P_f^a)P_f^a + b_A(P_f^a)) + (1-p)(f_B(P_f^b)P_f^b + b_B(P_f^b)). \end{aligned} \tag{A.5}$$

From (A.4), P_f^b is a decreasing function of P_f^a (from (A.3), P_f^a is also a decreasing function of P_f^b). Substitute (A.4) into (A.5), P_d^c can be expressed as a function of P_f^a:

$$\begin{aligned}
P_d^c &= \boldsymbol{s}P_f^a + \boldsymbol{l}, \text{where} \\
\boldsymbol{s} &= p[f_A(P_f^a) - f_B(P_f^b)], \\
&\overset{\text{from }(A.4)}{=} p[f_A(P_f^a) - f_B(\frac{\alpha - pP_f^a}{1-p})], \text{and} \\
\boldsymbol{l} &= f_B(P_f^b)\alpha + pb_A(P_f^a) + (1-p)b_B(\frac{\alpha - pP_f^a}{1-p})
\end{aligned} \tag{A.6}$$

which have the following properties:

Property 1: *P_d^c is a continuous function of P_f^a.*

P_d^a is a continuous function of P_f^a and P_d^b is a continuous function of P_f^b (since a and b are points on continuous ROC curves). Meanwhile, since P_f^b is a continuous function of P_f^a (from (A.4)), P_d^b is a continuous function of P_f^a. P_d^c is a weighted sum of P_d^a and P_d^b (from 6.2), therefore it is a continuous function of P_f^a.

Property 2: *P_d^c is a piecewise-linear function of P_f^a.*

Since both *ROC curve A* and *ROC curve B* are composed of finite line segments, in (A.6), $f_A(P_f^a), f_B(\frac{\alpha-pP_f^a}{1-p}), b_A(P_f^a),$ and $b_B(\frac{\alpha-pP_f^a}{1-p})$ are piecewise-constant functions of P_f^a. Therefore, P_d^c is a piecewise-linear function of P_f^a. The graph of P_d^c consists of finite number of line segments on the $P_f^a - P_d^c$ plane. The slope of each line segment is $s = f_A(P_f^a) - f_B(\frac{\alpha-pP_f^a}{1-p})$ and the P_d^c-axis intercept of each line segment is $l = f_B(P_f^b)\alpha + pb_A(P_f^a) + (1-p)b_B(\frac{\alpha-pP_f^a}{1-p})$.

Property 3: *P_d^c is a concave function of P_f^a.*

From properties 1 and 2, P_d^c is a continuous piecewise-linear function of P_f^a. The slope of each line segment is $s = f_A(P_f^a) - f_B(P_f^b)$. $f_A(P_f^a)$ is a decreasing function of P_f^a since *ROC curve A* is piecewise-linear concave. $f_B(P_f^b) = f_B(\frac{\alpha-pP_f^a}{1-p})$ is an increasing function of P_f^a since $f_B(P_f^b)$ is a decreasing function of P_f^b and P_f^b is a decreasing function of P_f^a. In (A.6), $s = f_A(P_f^a) - f_B(P_f^b)$ is a decreasing function of P_f^a. In this circumstance, P_d^c is a concave function of P_f^a.

Property 4: The range of P_f^a is $P_f^a \in [max(0, \frac{\alpha+p-1}{p}), min(1, \frac{\alpha}{p})]$ when the probability of false alarm constraint is satisfied.

Since points a and b are on ROC curves, $P_f^a \in [0,1]$ and $P_f^b \in [0,1]$. From (A.4), when the probability of false alarm constraint is satisfied, $P_f^b = 0$ indicates $P_f^a = \frac{\alpha}{p}$ and $P_f^b = 1$ indicates $P_f^a = \frac{\alpha+p-1}{p}$. Therefore, $P_f^b \in [0,1]$ indicates that $P_f^a \in [\frac{\alpha+p-1}{p}, \frac{\alpha}{p}]$. Therefore, the range of P_f^a is $P_f^a \in [max(0, \frac{\alpha+p-1}{p}), min(1, \frac{\alpha}{p})]$.

From Properties 1-4, P_d^c is a piecewise-linear concave function of P_f^a and its domain satisfies $P_f^a \in [max(0, \frac{\alpha+p-1}{p}), min(1, \frac{\alpha}{p})]$. Note that a piecewise-linear concave function sometimes can be a monotonic linear function. Three different cases about finding the maximum of P_d^c are discussed: (a) P_d^c is a non-decreasing linear function of P_f^a; (b) P_d^c is a non-increasing linear function of P_f^a; (c) P_d^c is first non-decreasing function and then a non-increasing function of P_f^a. Figure A.2 shows a graphical illustration of these three cases.

Case (a): $s \geq 0$ when $P_f^a = max(0, \frac{\alpha+p-1}{p})$ and when $P_f^a = min(1, \frac{\alpha}{p})$. In this case, P_d^c is a non-decreasing function of P_f^a and the maximum value of P_d^c is achieved at $P_f^a = min(1, \frac{\alpha}{p})$. If $P_f^a = min(1, \frac{\alpha}{p}) = 1$, since point $a = (P_f^a, P_d^a)$ is on *ROC curve* A, when $P_f^a = 1$, $P_d^a = 1$. Therefore, $A' = (1,1) = \omega_{mA}^A \in \Omega^A$. If $P_f^a = min(1, \frac{\alpha}{p}) = \frac{\alpha}{p} = \frac{\alpha-(1-p)0}{p} = \frac{\alpha-(1-p)P_f^{\omega_1^B}}{p} \overset{\text{from (A.3)}}{=} \frac{\alpha-(1-p)P_f^b}{p}$, $P_f^b = 0$. Since point $b = (P_f^b, P_d^b)$ is on *ROC curve* B, when $P_f^b = 0$, $P_d^b = 0$. Therefore, $B' = (0,0) = \omega_1^B \in \Omega^B$

Case (b): $s < 0$ when $P_f^a = max(0, \frac{\alpha+p-1}{p})$ and when $P_f^a = min(1, \frac{\alpha}{p})$. In this case, P_d^c is a non-increasing function of P_f^a and the maximum value of P_d^c is achieved at $P_f^a = max(0, \frac{\alpha+p-1}{p})$. If $P_f^a = max(0, \frac{\alpha+p-1}{p}) = 0$, then $A' = (0,0) = \omega_1^A \in \Omega^A$. If $P_f^a = max(0, \frac{\alpha+p-1}{p}) = \frac{\alpha+p-1}{p} = \frac{\alpha-(1-p)1}{p} = \frac{\alpha-(1-p)P_f^{\omega_{mB}^B}}{p} \overset{\text{from (A.3)}}{=} \frac{\alpha-(1-p)P_f^b}{p}$, $P_f^b = 1$. Then $B' = (1,1) = \omega_{mB}^B \in \Omega^B$.

Case (c): $s \geq 0$ when $P_f^a = max(0, \frac{\alpha+p-1}{p})$ and $s < 0$ when $P_f^a = min(1, \frac{\alpha}{p})$. In this case, when P_f^a increases from $max(0, \frac{\alpha+p-1}{p})$ to $min(1, \frac{\alpha}{p})$, P_d^c is first a non-decreasing function and then a non-increasing function of P_f^a. The intersection of two line segments on a piecewise-linear ROC curve is defined as a *corner point* of that ROC curve. The maximum value of P_d^c is achieved at a *corner point* on the graph of P_d^c where the slope of the left line segment at that *corner point* and the slope of the right line segment at that *corner point* have different sign (the sign of s changes at that *corner point*).

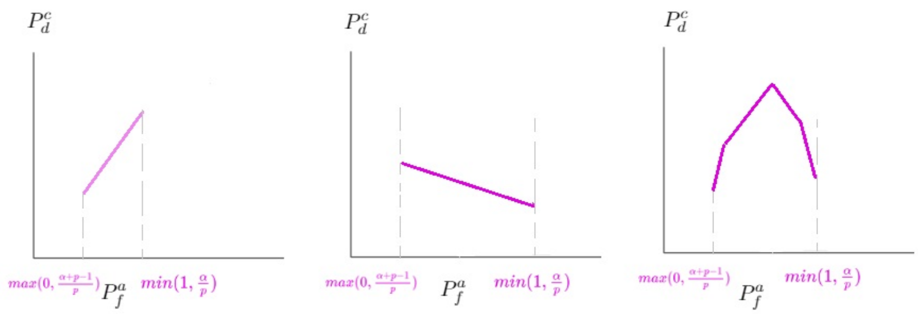

Figure A.2 A graphical illustration of cases (a), (b), and (c) (from left to right).

In cases (a) and (b), P_d^c is a monotonic function of P_f^a, its maximum is achieved when one of the points a and b is at $(0, 0)$ or $(1, 1)$. Since $\omega_1^A = \omega_1^B = (0, 0)$ and $\omega_{mA}^A = \omega_{mA}^B = (1, 1)$, either $A' \in \Omega^A$ or $B' \in \Omega^B$ (or both). In case (c), P_d^c is maximized when the sign of s changes from positive to negative. In the expression of s, $p \in (0, 1)$, $f_A(.)$ changes only when a is a *corner point* of *ROC curve A* ($A' \in \{\omega_2^A \dots \omega_{mA-1}^A\} \subset \Omega^A$), $f_B(.)$ changes only when b is a *corner point* of *ROC curve B* ($B' \in \{\omega_2^B \dots \omega_{mB-1}^B\} \subset \Omega^B$). Therefore, $P_d^{C'}$ is the maximum probability of detection when either (i) $A' \in \Omega^A$ or (ii) $B' \in \Omega^B$ or both ($A' \in \Omega^A$ and $B' \in \Omega^B$).

A.2 Finding A' from Ω^A if $A' \in \Omega^A$ and B' from Ω^B if $B' \in \Omega^B$ (Improved Version)

In Chapter 6, a 2-step procedure to find A' and B' is proposed: Step 1 - Finding A' from Ω^A if $A' \in \Omega^A$ and B' from Ω^B if $B' \in \Omega^B$ (Section 6.5); Step 2 - Finding A' if

$A' \notin \Omega^A$ and B' if $B' \notin \Omega^B$ (Section 6.6). Step 1 requires examining all the points in Ω^A and Ω^B ($mA + mB$ points). In this section, a more efficient way to realize Step 1 is proposed.

The previous section discusses three different cases about finding the maximum of P_d^c, $P_d^{C'}$. The calculation the value of s in (A.6) when $P_f^a = max(0, \frac{\alpha+p-1}{p})$ and when $P_f^a = min(1, \frac{\alpha}{p})$ is required to determine which case is encountered.

Case (a) P_d^c is a non-decreasing function of P_f^a and the maximum of P_d^c achieved when $P_f^a = min(1, \frac{\alpha}{p})$, shown as the first graph in Figure A.2. $P_d^{C'}$ is the maximum of probability of detection indicates that either $A' = (P_f^{A'}, P_d^{A'}) = (1,1)$ or $B' = (P_f^{B'}, P_d^{B'}) = (0,0)$ (or both).

Case (b) P_d^c is non-increasing function of P_f^a and the maximum of P_d^c is achieved at $P_f^a = max(0, \frac{\alpha+p-1}{p})$, shown as the second graph in Figure A.2. $P_d^{C'}$ is the maximum of probability of detection indicates that either $A' = (P_f^{A'}, P_d^{A'}) = (0,0)$ or $B' = (P_f^{B'}, P_d^{B'}) = (1,1)$ (or both).

Case (c) P_d^c is first a non-decreasing function and then a non-increasing function of P_f^a. The slope of each line segment of P_d^c is $s = p[f_A(P_f^a) - f_B(P_f^b)]$ (from (A.6)). The target is to find $a = A' \in \Omega^A$ or $b = B' \in \Omega^B$ such that the sign of $f_A(P_f^a) - f_B(P_f^b)$ changes from positive to negative.

Let $F^A = \{P_f^{\omega_1^A}, .., P_f^{\omega_{mA}^A}\}$ be the probabilities of false alarm of the operating points in $\Omega^A = \{\omega_1^A \ldots \omega_1^{mA}\}$. $A' \in \Omega^A$ when $P_f^{A'} \in F^A$.

Let $F^B = \{P_f^{\omega_1^B}, .., P_f^{\omega_{mB}^B}\}$ be the probabilities of false alarm of the operating points in $\Omega^B = \{\omega_1^B \ldots \omega_1^{mB}\}$. $B' \in \Omega^B$ when $P_f^{B'} \in F^B$.

In order to meet the probability of false alarm constraint α, from (A.4), when $P_f^{B'} \in F^B = \{P_f^{\omega_1^B}, .., P_f^{\omega_{mB}^B}\}$, the probability of false alarm of point A' satisfies $P_f^{A'} \in G^A = \{\frac{\alpha+(p-1)P_f^{\omega_1^B}}{p}, \ldots \frac{\alpha+(p-1)P_f^{\omega_{mB}^B}}{p}\}$.

Let $H = F^A \bigcup G^A$, when $A' \in \Omega^A$ or $B' \in \Omega^B$ (or both), $P_f^{A'} \in H$. Therefore, the target now is to find $P_f^{A'} \in H$ such that the sign of $f_A(P_f^a) - f_B(P_f^b)$ changes from positive to negative at $P_f^a = P_f^{A'} \in H$.

Recall that $f_a(P_f^a)$ represents the slopes of all straight line segments $w_1^A w_2^A$, $w_2^A w_3^A, \ldots, w_{mA-1}^A w_{mA}^A$ composing *ROC curve A*. $f_a(P_f^a)$ can be expressed as a decreasing piecewise-constant function of P_f^a:

$$f_A(P_f^a) = \begin{cases} \dfrac{P_d^{\omega_{j+1}^A} - P_d^{\omega_j^A}}{P_f^{\omega_{j+1}^A} - P_f^{\omega_j^A}}, P_f^a \in [P_f^{\omega_j^A}, P_f^{\omega_{j+1}^A}), j = 1, \ldots, m_A - 1 \\ \dfrac{P_d^{\omega_{m_A}^A} - P_d^{\omega_{m_A-1}^A}}{P_f^{\omega_{m_A}^A} - P_f^{\omega_{m_A-1}^A}}, P_f^a = P_f^{\omega_{m_A}^A} \end{cases}. \tag{A.7}$$

Similarly, $f_b(P_f^b)$ represents the slopes of all straight line segments $w_1^B w_2^B$, $w_2^B w_3^B, \ldots, w_{mB-1}^B w_{mB}^B$ composing *ROC curve B*. $f_b(P_f^b)$ can be expressed as a decreasing piecewise-constant function of P_f^b:

$$f_B(P_f^b) = \begin{cases} \dfrac{P_d^{\omega_{j+1}^B} - P_d^{\omega_j^B}}{P_f^{\omega_{j+1}^B} - P_f^{\omega_j^B}}, P_f^b \in (P_f^{\omega_j^B}, P_f^{\omega_{j+1}^B}], j = 1, \ldots, m_B - 1 \\ \dfrac{P_d^{\omega_2^B} - P_d^{\omega_1^B}}{P_f^{\omega_2^B} - P_f^{\omega_1^B}}, P_f^b = P_f^{\omega_1^B} \end{cases}. \tag{A.8}$$

From (A.4), when the probability of false alarm constraint is met $P_f^c = \alpha$, $P_f^b = \frac{\alpha - pP_f^a}{1-p}$. $f_B(P_f^b)$ can be expressed as a function of P_f^a, where $f_B(P_f^b) = f_B(\frac{\alpha - pP_f^a}{1-p}) = g_A(P_f^a)$. From (A.3), $P_f^a = \frac{\alpha-(1-p)P_f^b}{p}$. When $P_f^b \in (P_f^{\omega_j^B}, P_f^{\omega_{j+1}^B}]$, $P_f^a \in [\frac{\alpha+(p-1)P_f^{\omega_{j+1}^B}}{p}, \frac{\alpha+(p-1)P_f^{\omega_j^B}}{p})$. $g_A(.)$ can be expressed as:

$$g_A(P_f^a) = f_B(\frac{\alpha - pP_f^a}{1-p}) = \begin{cases} \dfrac{P_d^{\omega_{j+1}^B} - P_d^{\omega_j^B}}{P_f^{\omega_{j+1}^B} - P_f^{\omega_j^B}}, P_f^a \in [\dfrac{\alpha + (p-1)P_f^{\omega_{j+1}^B}}{p}, \dfrac{\alpha + (p-1)P_f^{\omega_j^B}}{p}), \\ \qquad j = m_B - 1, \ldots, 1 \\ \dfrac{P_d^{\omega_2^B} - P_d^{\omega_1^B}}{P_f^{\omega_2^B} - P_f^{\omega_1^B}}, P_f^a = \dfrac{\alpha + (p-1)P_f^{\omega_1^B}}{p} \end{cases} \tag{A.9}$$

$g_A(P_f^a)$ calculates the slope of the line segment on *ROC curve B* intersecting the vertical line $P_f = P_f^b = \frac{\alpha - pP_f^a}{1-p}$ (the line segment on *ROC curve B* passing through point $b = (P_f^b = \frac{\alpha - pP_f^a}{1-p}, P_d^b))$. $g_A(P_f^a)$ is a piecewise increasing constant function of P_f^a.

Therefore, in case (c), the target becomes finding $P_f^{A'} \in H$ such that the sign of $f_A(P_f^a) - g_A(P_f^a)$ changes from positive to negative at $P_f^a = P_f^{A'}$.

$f_A(P_f^a) - g_A(P_f^a)$ is a piecewise decreasing constant function of P_f^a and its value only changes when $P_f^{A'} \in H$. Since each one of the constant functions composing $f_A(P_f^a) - g_A(P_f^a)$ is defined on a left-closed right-open interval, when $f_A(P_f^a) - g_A(P_f^a)$ changes from positive to negative, $P_f^{A'}$ can be found as the smallest value of P_f^a in H such that $f_A(P_f^a) - g_A(P_f^a) < 0$.

One way to find $P_f^a = P_f^{A'} \in H$ is using a common binary search algorithm which contains following steps:

(a) Sort the elements in H

(b) Calculate $f_A(P_f^a) - g_A(P_f^a)$ for the middle element in H
(if H has an even number of elements, use the smaller one of the middle two elements)

(c) If the result is negative: eliminate the latter half of H (excluding the middle element); Otherwise: eliminate the former half of H (including the middle element)

(d) Repeat steps b) and c) until H has only one element, which is $P_f^{A'}$

Since $H = F^A \bigcup G^A$ contains at most $mA + mB$ elements (mA elements in F^A and mB elements in G^A), the binary search algorithm performs at most $log(mA + mB)$ iterations.

When $P_f^{A'}$ is found, if $P_f^{A'} \in F^A$, $P_f^{A'}$ can be used to find A' in Ω^A; if $P_f^{A'} \in G^A$, $P_f^{B'}$ can be calculated as $P_f^{B'} = \frac{\alpha - pP_f^{A'}}{1-p}$ (from (A.4)), then $P_f^{B'}$ can be used to find B' in Ω^B.

After finding A' if $A' \in \Omega^A$ and B' if $B' \in \Omega^B$, the procedure in Section 6.6 can be used to find A' if $A' \notin \Omega^A$ and B' if $B' \notin \Omega^B$.

A.3 Complete Algorithm of the Corrective Action

The flowcharts of the complete algorithm of the corrective action for partial loss of synchronization among the LDs when dependent randomization is employed (Chapter 6) are shown as Figures A.3 and A.4. In the flowcharts, Step 1 is the input of the corrective action (Table 6.1). Step 2 calculates the local operating points of *System A* and *System B* (Section 6.2). Step 3 calculates and stores the local operating points in Ω^A and Ω^B and their corresponding global fusion rules (Section 6.3). Steps 4-7 belong to Section A.2, which find A' if $A' \in \Omega^A$ and B' if $B' \in \Omega^B$. Step 8 is used to obtains A' if $A' \notin \Omega^A$ or B' if $B' \notin \Omega^B$ (Section 6.6).

A.3.1 Redesign the 2-LD system shown in Section 4.1 after the 2^{nd} LD lost synchronization

Figure A.5 and Figure A.6 show the detail of applying the proposed algorithm to redesign the 2-LD system shown in Section 4.1.

Before the loss of synchronization, the design output of dependent randomization is shown in Table 4.1. The system operates at $A = (0.1581, 0.7870)$ with probability $p = 0.5$ and at $B = (0.2437, 0.8652)$ with probability $1 - p = 0.5$ in order to operates at $C = (0.2009, 0.8261)$, which satisfies the Neyman-Pearson criterion

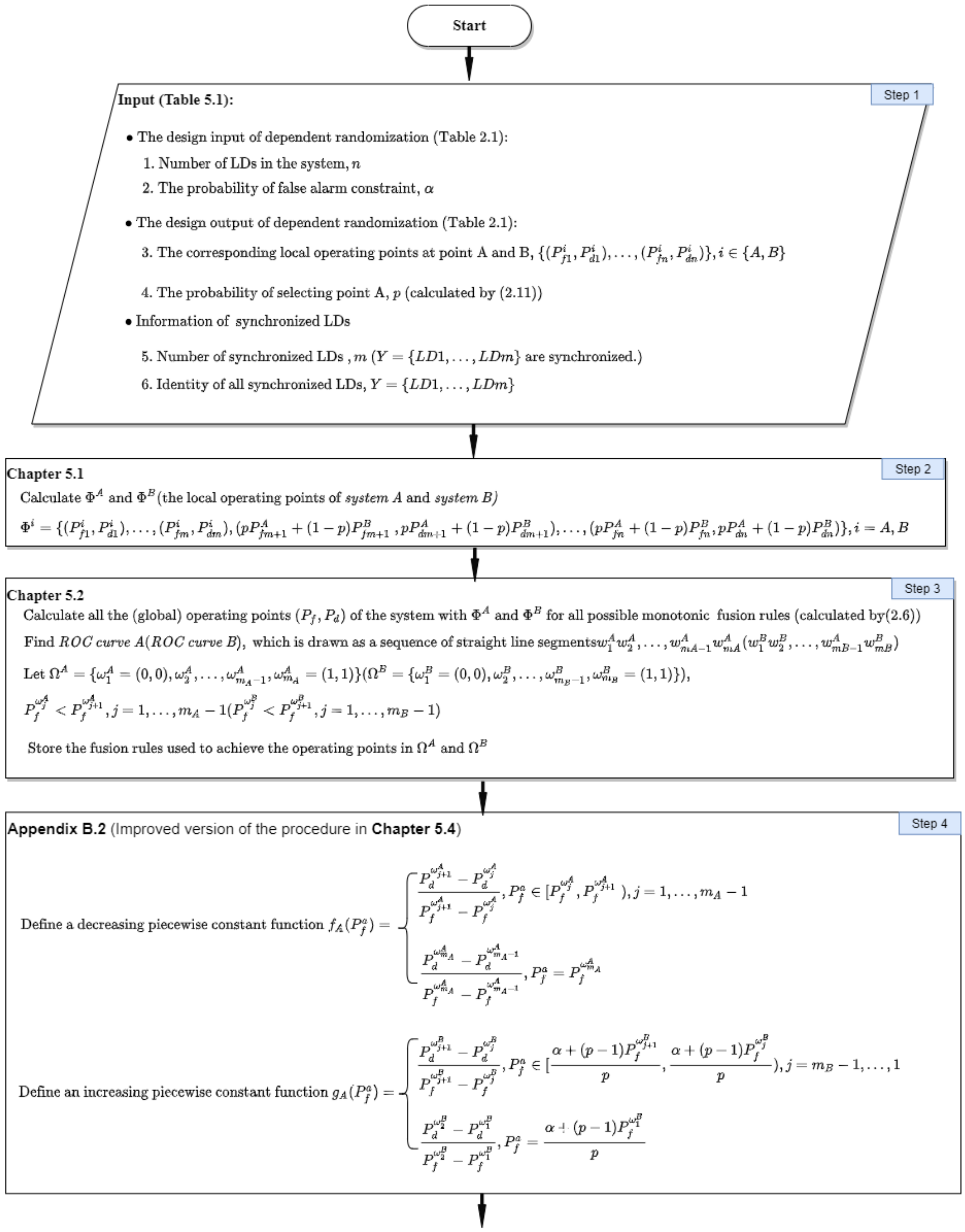

Figure A.3 The preliminary of the algorithm of the corrective action after LDs in $\overline{Y}$ lost synchronization.

with $\alpha = 0.2009$ (Step 1 in Figure A.5). After the 2^{nd} LD loses synchronization ($Y = \{LD1\}, \overline{Y} = \{LD2\}$), when γ_1^A is selected by $LD1$ (the members in Y), the local operating points of the system are $\Phi^A = \{(0.3976, 0.8871), (0.2640, 0.7600)\}$;

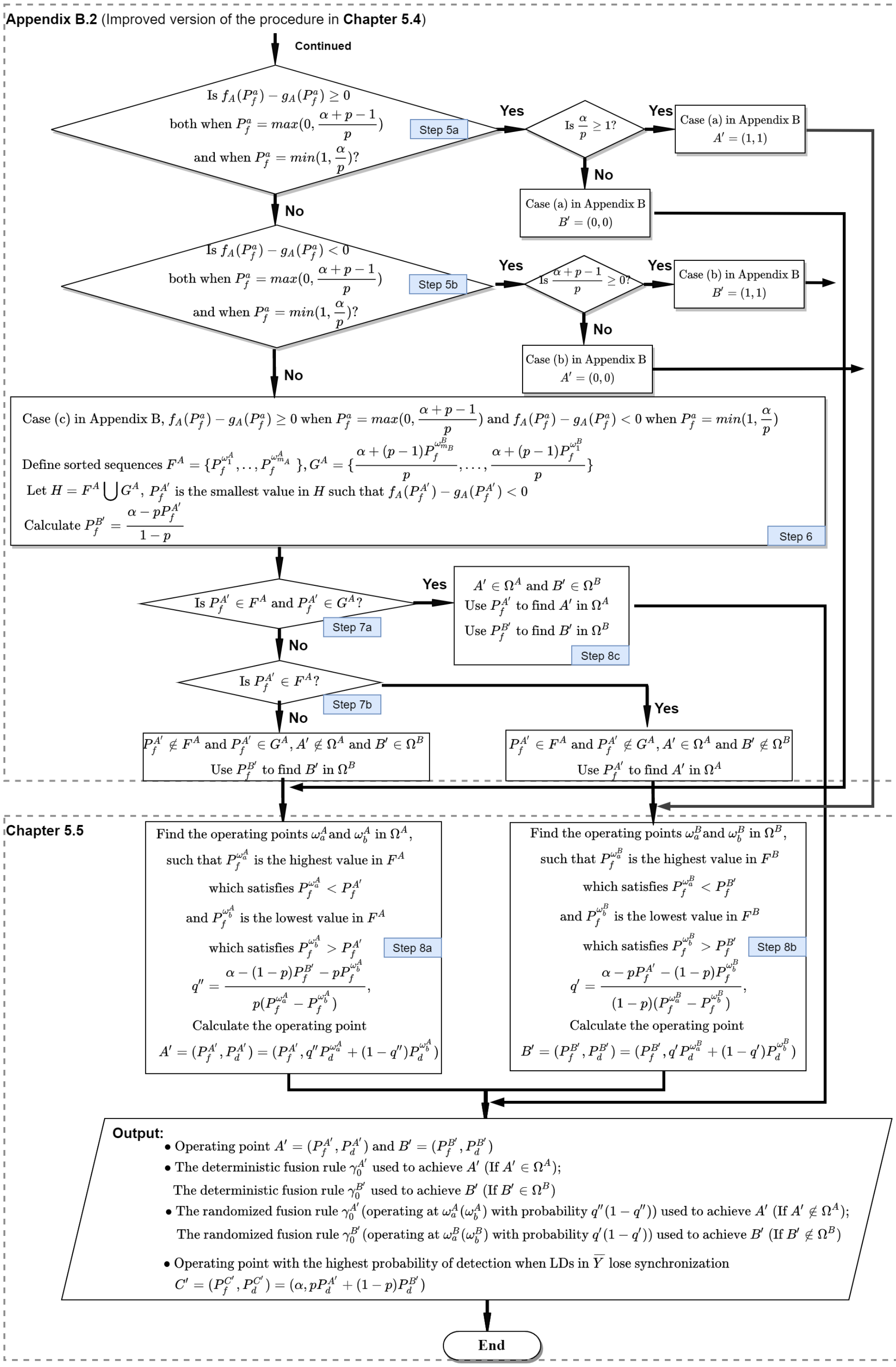

Figure A.4 The algorithm of the corrective action after LDs in $\overline{Y}$ lost synchronization.

when γ_1^B is selected by $LD1$ (the members in Y), the local operating points of the system are $\Phi^B = \{(0.1304, 0.6328), (0.2640, 0.7600)\}$ (Step 2 Figure A.5). For a 2-LD system, there are totally six monotonic fusion rules [8] ($u_0 = u_1, u_0 = u_2, u_0 = 0, u_0 = 1, u_0 = u_1 \& u_2, u_0 = u_1 | u_2$), corresponding to six operating points (some may overlap). In Figure A.7 (Figure A.8), all possible operating points of the system given Φ^A (Φ^B) are shown as the x-marks; *ROC curve A*(*ROC curve B*) is shown by using the red (blue) curve and the operating points Ω^A (Ω^B) are shown as the red (blue) circles (Step 3 in Figure A.5). The slopes of the line segments composing the *ROC curve A*(*ROC curve B*), $f_A(P_f^a)(g_A(P_f^a))$, can be expressed as a piecewise constant function of P_f^a (Step 4 in Figure A.5).

From Property 4 in Section A.1, $P_f^a \in [max(0, \frac{\alpha+p-1}{p}), min(1, \frac{\alpha}{p})] = [0, 0.4018]$. $f_A(P_f^a) - g_A(P_f^a) \geq 0$ at $P_f^a = 0$ and $f_A(P_f^a) - g_A(P_f^a) < 0$ at $P_f^a = 0.4018$ (Steps 5a and 5b in Figure A.6). The sign of $f_A(P_f^a) - g_A(P_f^a)$ changes at $P_f^a = P_f^{A'} = 0.1049$, which is the probability of false alarm of one of the operating points in Ω^A. $P_f^{B'} = \frac{\alpha - pP_f^{A'}}{1-p} = 0.2968$, which is not the probability of false alarm of any one of the operating points in Ω^B (Step 6 in Figure A.6). Therefore, $A' \in \Omega^A$, $B' \in \overline{\Omega^B}$ (Steps 7a and 7b in Figure A.6). $B' = (P_f^{B'}, P_d^{B'}) = (0.2968, 0.8352)$ is generated by two operating points in Ω^B, which are $\omega_a^B = (0.1304, 0.6328), \omega_b^B = (0.3599, 0.9119)$. When the system operates on the *ROC curve B*, ω_a^B is used with probability $q' = \frac{\alpha - pP_f^{A'} - (1-p)P_f^{\omega_b^B}}{(1-p)(P_f^{\omega_a^B} - P_f^{\omega_b^B})} = 0.2748$ while ω_b^B is used with probability $1 - p = 0.7252$. $P_d^{B'} = q'P_d^{\omega_a^B} + (1-q')P_d^{\omega_b^B} = 0.8352$ (Step 8b in the algorithm shown in Figure A.6). The maximal probability of detection can be calculated as $P_d^{C'} = pP_d^{A'} + (1-p)P_d^{B'} = 0.7547$, which is achieved by $C' = (\alpha, P_d^{C'}) = (0.2009, 0.7547)$ (output of the algorithm shown in Figure A.6).

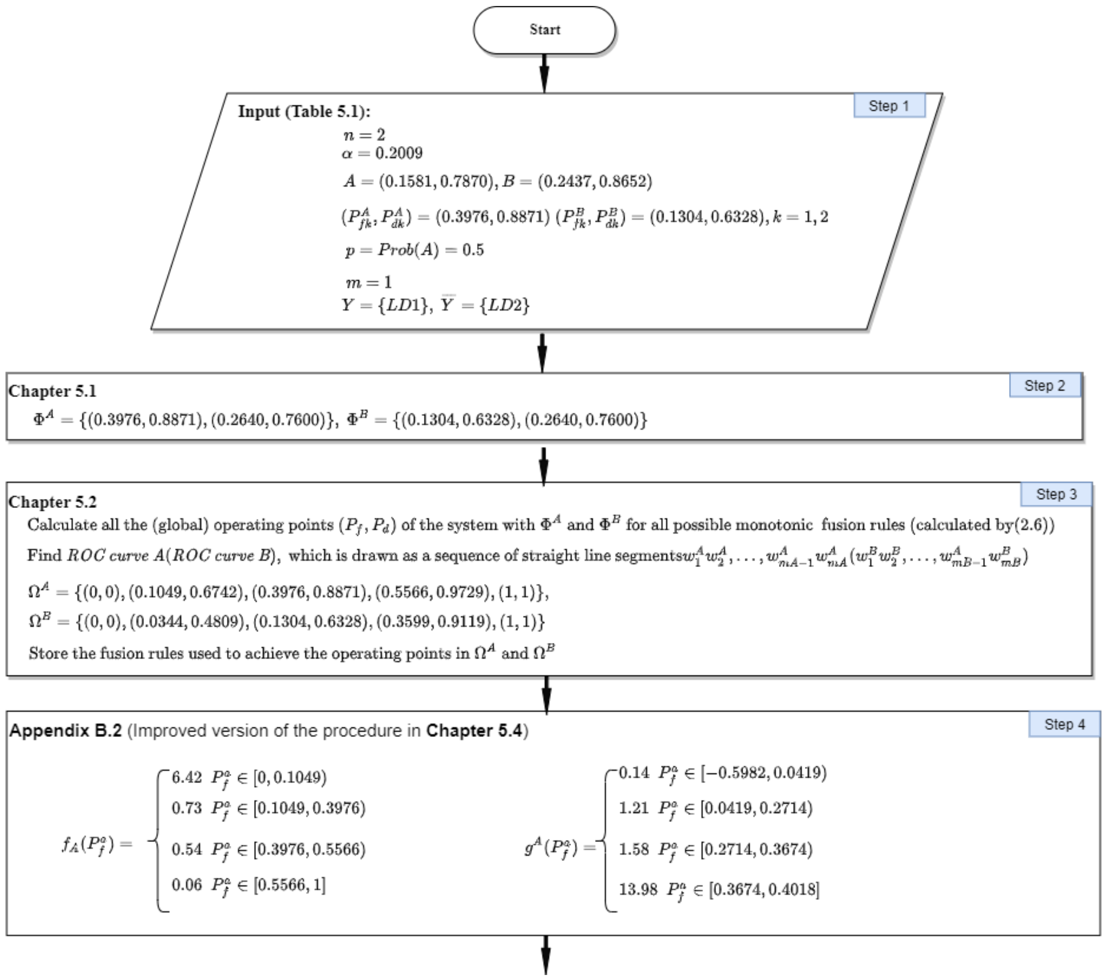

Figure A.5 The preliminary of the proposed algorithm for redesigning the 2-LD system shown in Section 4.1 after the 2^{nd} LD lost synchronization.

A.3.2 Redesign the 3-LD system shown in Section 4.2 after the 3^{rd} LD lost synchronization

Figure A.9 and Figure A.10 show the detail of applying the proposed algorithm to redesign the 3-LD system shown in Section 4.2.

Before the loss of synchronization, the design output of dependent randomization is shown in Table 4.3. The system operates at $A = (0.104, 0.784)$ with probability $p = 0.6$ and at $B = (0.271, 0.936)$ with probability $1 - p = 0.4$ in order to operates at $C = (0.1708, 0.8448)$, which satisfies the Neyman-Pearson criterion with $\alpha = 0.1708$ (Step 1 in Figure A.9). After the 3^{rd} LD lost synchronization ($Y = \{LD1, LD2\}, \overline{Y} = \{LD3\}$), when $\{\gamma^A_1, \gamma^A_2\}$ are selected by $\{LD1, LD2\}$, the local operating points of the system are $\Phi^A = \{(0.2, 0.7), (0.2, 0.7), (0.16, 0.66)\}$; when $\{\gamma_1^B, \gamma_2^B\}$ are selected by $\{LD1, LD2\}$, the local operating points of the system are $\Phi^B = \{(0.1, 0.6), (0.1, 0.6), (0.16, 0.66)\}$ (Step 2 in Figure A.9). For a 3-LD system, there are totally twenty monotonic fusion rules (see Table 4.2), corresponding to twenty operating points (some may overlap). In Figure 6.1 (Figure 6.2), all possible operating points of the system given Φ^A (Φ^B) are shown as the x-marks; *ROC curve* A(*ROC curve* B) is shown by the red (blue) curve and the operating points Ω^A (Ω^B) are shown as the red (blue) circles (Step 3 in Figure A.9). The slopes of the line segments composing the *ROC curve* A(*ROC curve* B), $f_A(P_f^a)(g_A(P_f^a))$, can be expressed as a piecewise constant function of P_f^a (Step 4 in Figure A.9).

From Property 4 in Section A.1, $P_f^a \in [max(0, \frac{\alpha+p-1}{p}), min(1, \frac{\alpha}{p})] = [0, 0.2847]$. $f_A(P_f^a) - g_A(P_f^a) \geq 0$ at $P_f^a = 0$ and $f_A(P_f^a) - g_A(P_f^a) < 0$ at $P_f^a = 0.2847$ (Steps 5a and 5b in Figure A.10). The sign of $f_A(P_f^a) - g_A(P_f^a)$ changes at $P_f^a = P_f^{A'} = 0.0912$, which is the probability of false alarm of one of the operating points in Ω^A. $P_f^{B'} = \frac{\alpha - pP_f^{A'}}{1-p} = 0.2902$, which is not the probability of false alarm of any one of the operating points in Ω^B (Step 6 in Figure A.10). Therefore, $A' = (0.1049, 0.6742) \in \Omega^A$, $B' \in \overline{\Omega^B}$ (Steps 7a and 7b in Figure A.10). $B' = (0.2968, 0.8410)$ is generated by two operating points in Ω^B, which are $\omega_a^B = (0.1900, 0.8400), \omega_b^B = (0.3196, 0.9456)$. When the system operates on the *ROC curve* B, ω_a^B is used with probability $q' = \frac{\alpha - pP_f^{A'} - (1-p)P_f^{\omega_b^B}}{(1-p)(P_f^{\omega_a^B} - P_f^{\omega_b^B})} = 0.2269$ while ω_b^B is used with probability $1 - p = 0.7731$. $P_d^{B'} = q'P_d^{\omega_a^B} + (1-q')P_d^{\omega_b^B} = 0.9216$(Step 8b in Figure A.10). The maximal probability of detection can be calculated as $P_d^{C'} = pP_d^{A'} + (1-p)[q'P_d^{\omega_a^B} + (1-q')P_d^{\omega_b^B}] = 0.8290$, which is achieved by $C' = (\alpha, P_d^{C'}) = (0.1708, 0.8290)$ (output of the algorithm shown in Figure A.10).

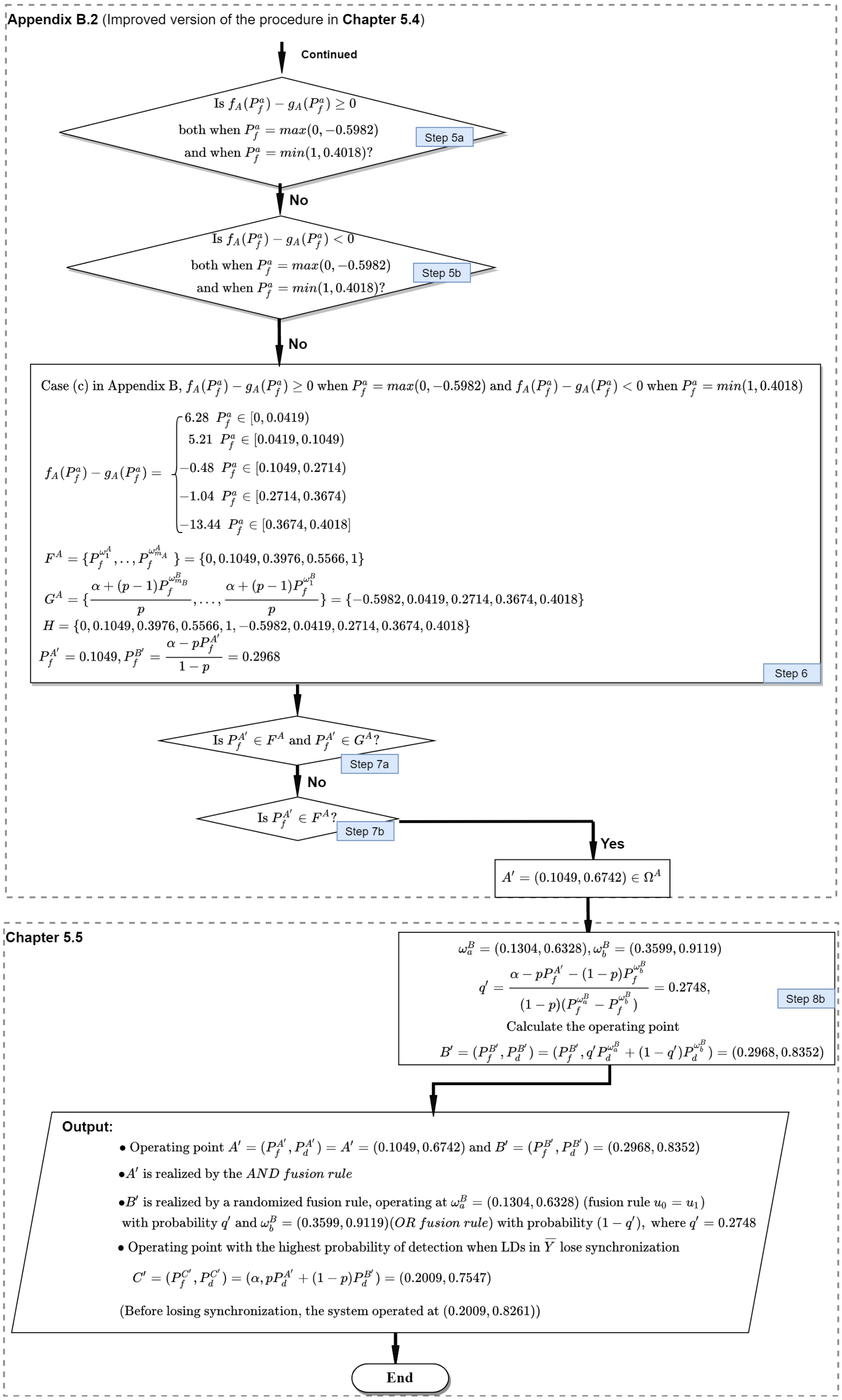

Figure A.6 Applying the proposed algorithm to redesign the 2-LD system shown in Section 4.1 after the 2^{nd} LD lost synchronization.

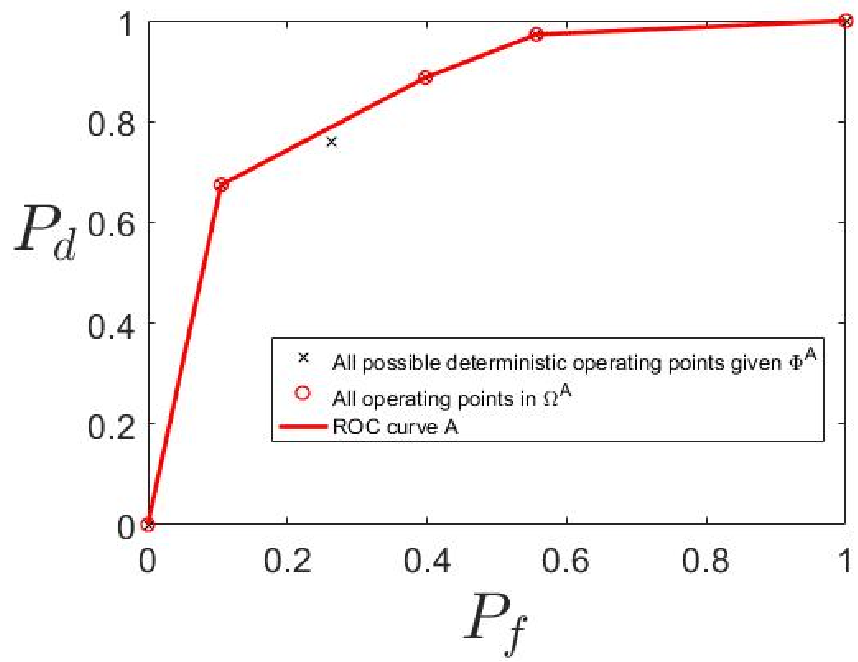

Figure A.7 The 2-LD system with the 2^{nd} LD loses synchronization. x-marks: all possible deterministic operating points given Φ^A; red circles: all the operating points in Ω^A; red curve: *ROC curve A*.

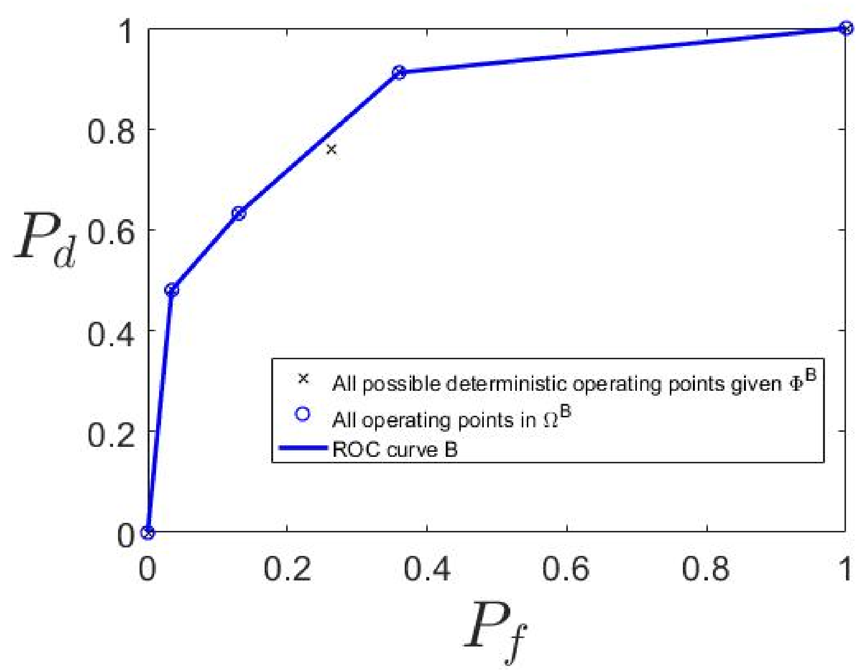

Figure A.8 The 2-LD system with the 2^{nd} LD loses synchronization. x-marks: all possible deterministic operating points given Φ^B; blue circles: all the operating points in Ω^B; blue curve: *ROC curve B*.

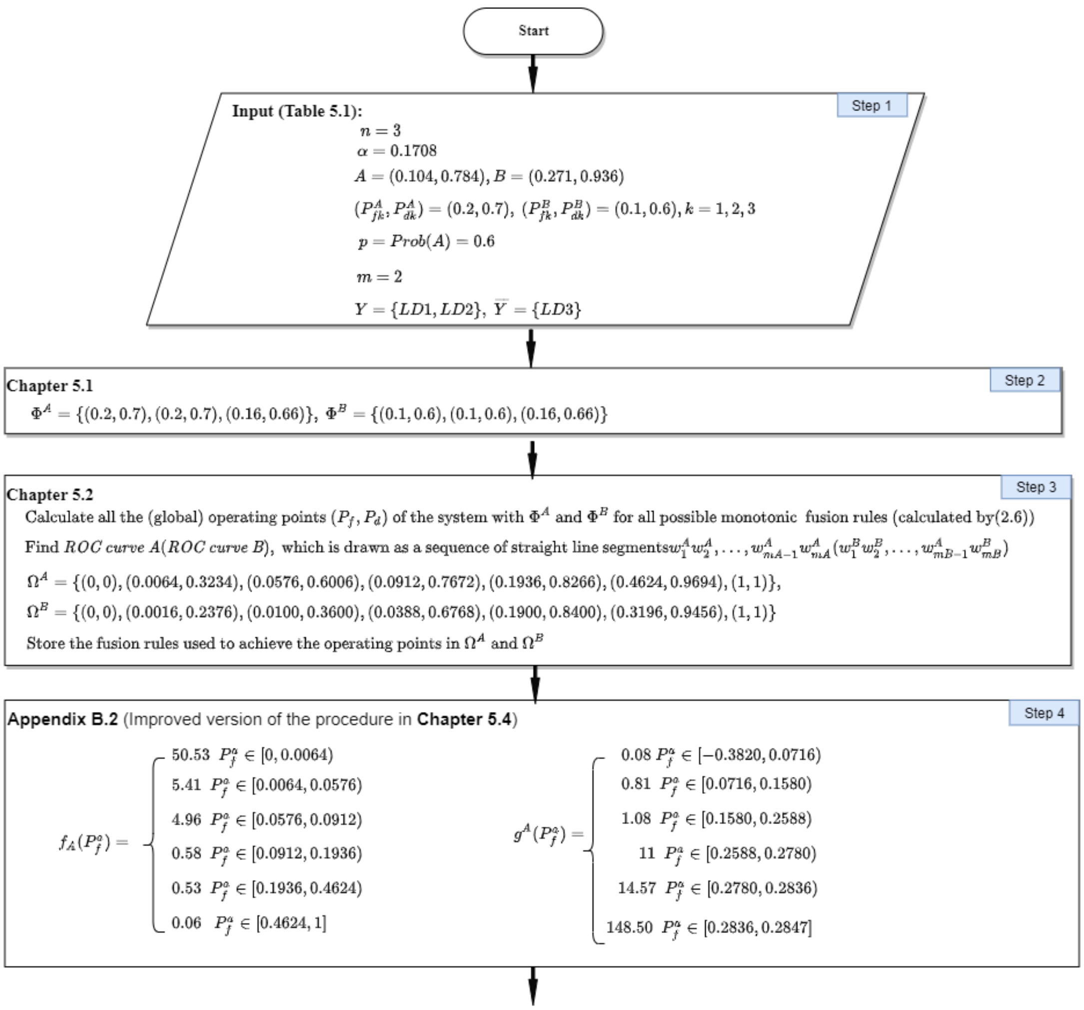

Figure A.9 The preliminary of the proposed algorithm for redesigning the 3-LD system shown in Section 4.2 after the 3^{rd} LD lost synchronization.

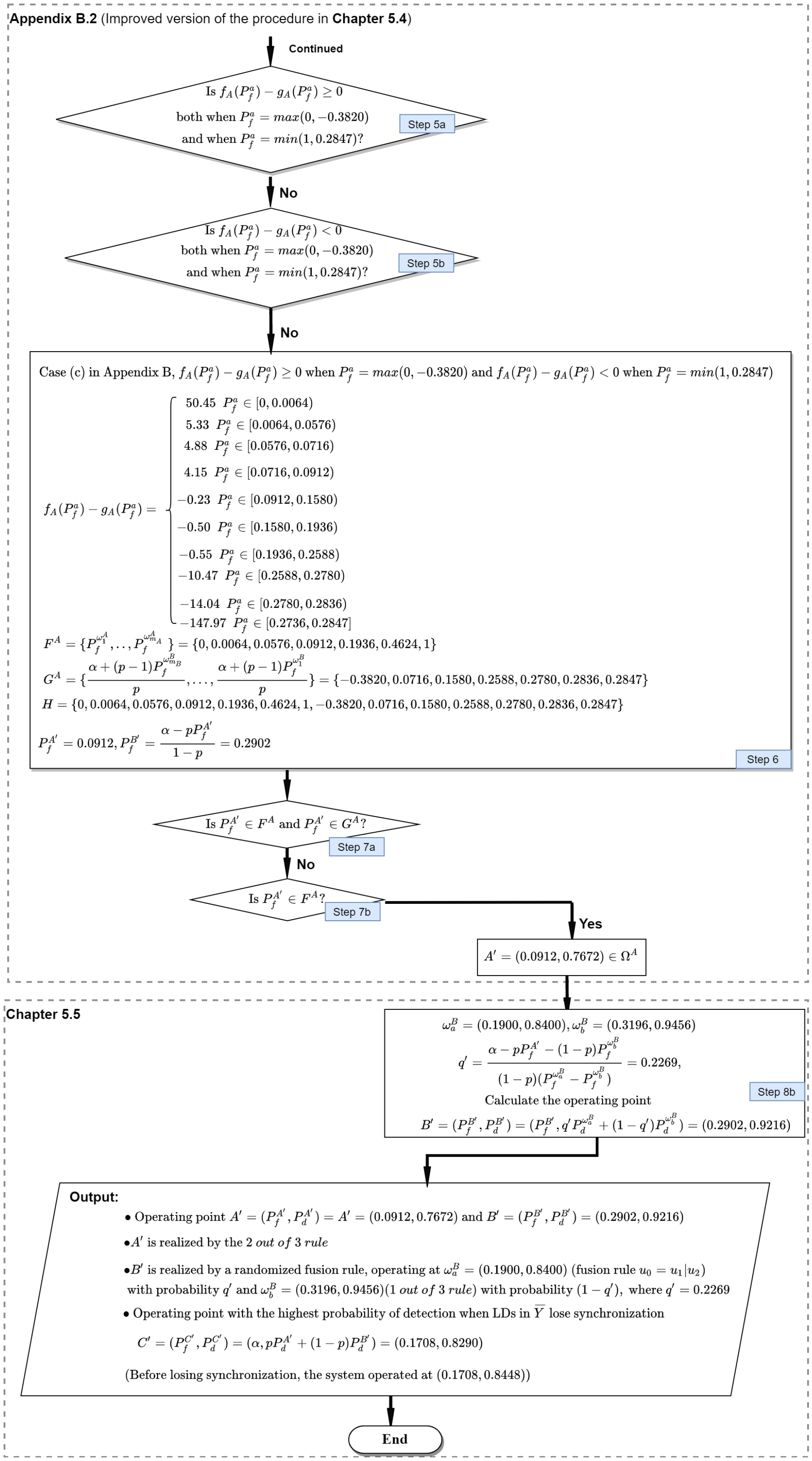

Figure A.10 Applying the proposed algorithm to redesign the 3-LD system shown in Section 4.2 after the 3^{rd} LD lost synchronization.

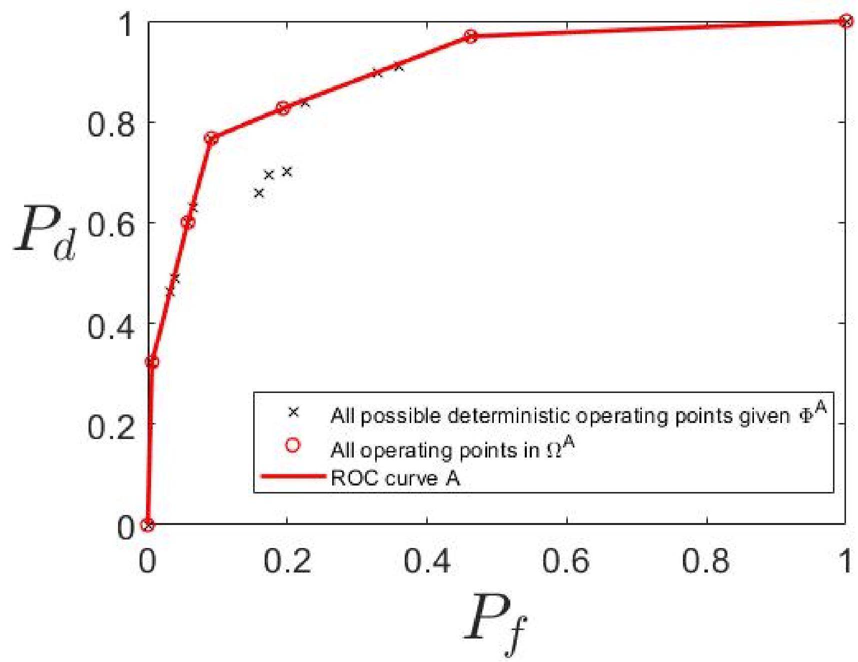

Figure A.11 The 3-LD system with the 3^{rd} LD loses synchronization. x-marks: all possible deterministic operating points given Φ^A; red circles: all the operating points in Ω^A; red curve: *ROC curve A*.

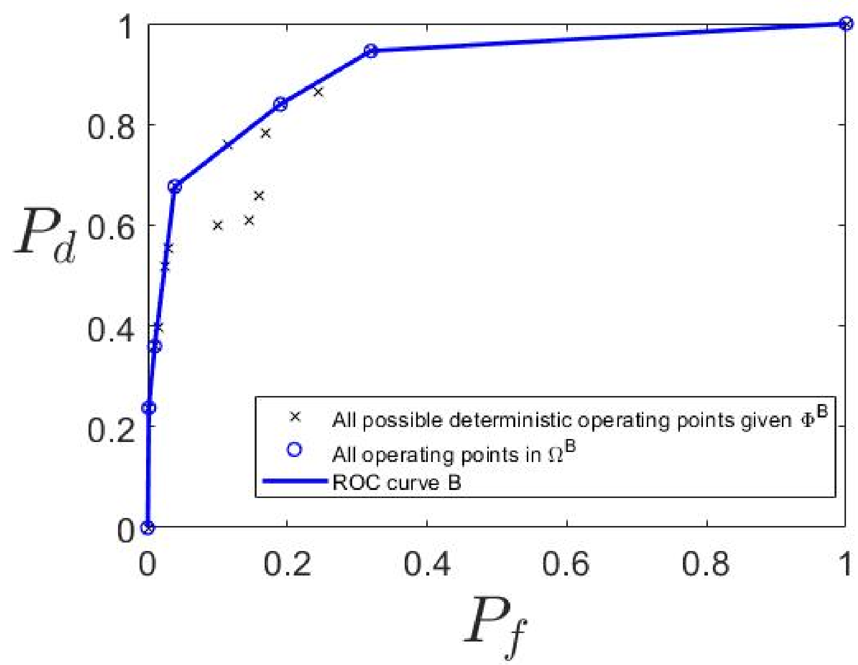

Figure A.12 The 3-LD system with the 3^{rd} LD loses synchronization. x-marks: all possible deterministic operating points given Φ^B; blue circles: all the operating points in Ω^B; blue curve: *ROC curve B*.

REFERENCES

[1] Z. Chair and P. K. Varshney, "Optimal data fusion in multiple sensor detection systems," *IEEE Transactions on Aerospace and Electronic Systems*, vol. AES-22, no. 1, pp. 98–101, 1986.

[2] I. Y. Hoballah and P. K. Varshney, "Distributed Bayesian signal detection," *IEEE Transactions on Information Theory*, vol. 35, no. 5, pp. 995–1000, 1989.

[3] S. Acharya, J. Wang, and M. Kam, "Distributed decision fusion using the Neyman-Pearson criterion," in *17th International Conference on Information Fusion (FUSION)*, pp. 1–7, IEEE, 2014.

[4] M. Kam, C. Rorres, W. Chang, and X. Zhu, "Performance and geometric interpretation for decision fusion with memory," *IEEE Transactions on Systems, Man and Cybernetics, Part A: Systems and Humans*, vol. 29, no. 1, pp. 52–62, 1999.

[5] S. Alhakeem, *Decentralized Bayesian hypothesis testing with feedback, Section 2.* PhD thesis, Syracuse University, 1990.

[6] W. Dong and M. Kam, "A greedy algorithm for decentralized Bayesian detection with feedback," in *37th IEEE Sarnoff Symposium*, pp. 202–207, IEEE, 2016.

[7] I. Y. Hoballah and P. Varshney, "Neyman-Pearson detection with distributed sensors," in *1986 25th Conference on Decision and Control*, vol. 25, pp. 237–241, IEEE, 1986.

[8] S. Thomopoulos, R. Viswanathan, and D. Bougoulias, "Optimal distributed decision fusion," *IEEE Transactions on Aerospace and Alectronic Aystems*, vol. 25, no. 5, pp. 761–765, 1989.

[9] Y. I. Han, "Randomized fusion rules can be optimal in distributed Neyman-Pearson detectors," *IEEE Transactions on Information Theory*, vol. 43, no. 4, pp. 1281–1288, 1997.

[10] J. N. Tsitsiklis *et al.*, "Decentralized detection," *Advances in Statistical Signal Processing*, vol. 2, no. 2, pp. 297–344, 1993.

[11] H. L. Van Trees, *Detection, Estimation, and Modulation theory, Section 2.2.* John Wiley & Sons, 2004.

[12] J. D. Papastavrou and M. Athans, "The team ROC curve in a binary hypothesis testing environment," *IEEE Transactions on Aerospace and Electronic Systems*, vol. 31, no. 1, pp. 96–105, 1995.

[13] A. Naim and M. Kam, "On-line estimation of probabilities for distributed Bayesian detection," *Automatica*, vol. 30, no. 4, pp. 633–642, 1994.

[14] B.-O. Zhu, N. Ansari, and E. S. Hou, "Adaptive fusion model for distributed detection system," in *Applications in Optical Science and Engineering*, pp. 332–341, International Society for Optics and Photonics, 1992.

[15] N. Ansari, J.-G. Chen, and Y.-Z. Zhang, "Adaptive decision fusion for unequiprobable sources," *IEE Proceedings-Radar, Sonar and Navigation*, vol. 144, no. 3, pp. 105–111, 1997.

[16] G. Mirjalily, Z.-Q. Luo, T. N. Davidson, and E. Bosse, "Blind adaptive decision fusion for distributed detection," *IEEE Transactions on Aerospace and Electronic Systems*, vol. 39, no. 1, pp. 34–52, 2003.

[17] W. Dong and M. Kam, "Detection performance vs. complexity in parallel decentralized Bayesian decision fusion," in *51st Annual Conference on Information Sciences and Systems, CISS*, pp. 1–6, IEEE, 2017.

[18] M. Kam, W. Chang, and Q. Zhu, "Hardware complexity of binary distributed detection systems with isolated local Bayesian detectors," *IEEE Transactions on Systems, Man and Cybernetics*, vol. 21, no. 3, pp. 565–571, 1991.

[19] A. T. Zijlstra, *Calculating the 8th Dedekind Number*. PhD thesis, University of Groningen, 2013.

[20] P. Willett and D. Warren, "The suboptimality of randomized tests in distributed and quantized detection systems," *IEEE Transactions on Information Theory*, vol. 38, no. 2, pp. 355–361, 1992.

[21] W. Dong and M. Kam, "Parallel decentralized detection with dependent randomization," in *52nd Annual Conference on Information Sciences and Systems (CISS)*, pp. 1–6, IEEE, 2018.

[22] Q. Yan and R. S. Blum, "On some unresolved issues in finding optimum distributed detection schemes," *IEEE Transactions on Signal Processing*, vol. 48, no. 12, pp. 3280–3288, 2000.

[23] M. Kam, W. Chang, and Q. Zhu, "Hardware complexity of binary distributed detection systems with isolated local Bayesian detectors," *IEEE Transactions on Systems, Man and Cybernetics*, vol. 21, no. 3, pp. 565–571, 1991.

[24] W. Dong and M. Kam, "Integration of multiple adaptive algorithms for parallel decision fusion," in *50th Annual Conference on Information Science and Systems (CISS)*, pp. 355–359, IEEE, 2016.